

**THE FLORIDA STATE UNIVERSITY
COLLEGE OF ARTS AND SCIENCES**

**4-D VARIATIONAL DATA ASSIMILATION AND PARAMETER
ESTIMATION USING THE FSU GLOBAL SPECTRAL MODEL AND
ITS FULL-PHYSICS ADJOINT**

By

Yanqiu Zhu

**A Dissertation submitted to the
Department of Geophysical Fluid Dynamics
in partial fulfillment of the
requirements for the degree of
Doctor of Philosophy**

**Degree Awarded:
Spring Semester, 1998**

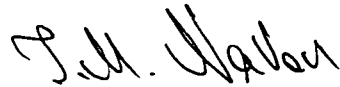
UMI Number: 9827662

**UMI Microform 9827662
Copyright 1998, by UMI Company. All rights reserved.**

**This microform edition is protected against unauthorized
copying under Title 17, United States Code.**

UMI
300 North Zeeb Road
Ann Arbor, MI 48103

The members of the Committee approve the dissertation of Yanqiu Zhu defended on March 4, 1998.



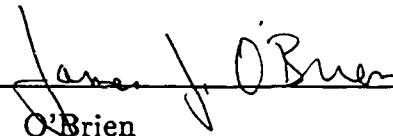
I.M. Navon
Professor Directing Dissertation



T.N. Krishnamurti
Outside Committee Member



S.L. Blumsack
Committee Member



J.J. O'Brien
Committee Member



R.L. Pfeffer
Committee Member

I dedicate this dissertation to my family.

ACKNOWLEDGEMENTS

I would like to express my gratitude and thanks to my major professor, Dr. I.M. Navon, for his support, guidance and encouragement throughout my studies at Florida State University. I have greatly benefited from his thorough knowledge, innovative ideas and deep insight in both numerical analysis and scientific computing.

I wish to thank Drs. S.L. Blumsack, T.N. Krishnamurti, J.J. O'Brien, and R.L. Pfeffer for serving on my committee. Special thanks go to Dr. T.N. Krishnamurti for his encouragement and insightful comments throughout this study. Drs. H.S. Bedi and X-L Zou are thanked for their helpful and stimulating discussions.

I particularly wish to thank my husband Dr. W. Han for his understanding, support and valuable scientific discussions. Special thanks are due to my parents for their support, caring and love, without which the research will not be possible.

I would also like to thank everyone in the Geophysical Fluid Dynamics Institute and Supercomputer Computations Research Institute as well as Dr. Krishnamurti's lab for various help that I received during my study at Florida State University. All the data used in this study were provided by Dr. Krishnamurti's lab.

The support provided by NSF grant ATM-9413050 managed by Dr. Pamela Stephens is gratefully acknowledged. Additional support was provided by Geophysical Fluid Dynamics Institute of Florida State University and Supercomputer Com-

putations Research Institute of Florida State University which is partially funded through contract DE-FC0583ER250000.

The computer facilities were provided by the Special SCD Grant 35111089 in NCAR and National Science Foundation 35111100. Additional computer support was provided by Geophysical Fluid Dynamics Institute and Supercomputer Computations Research Institute at Florida State University.

TABLE OF CONTENTS

List of Tables	ix
List of Figures	x
Abstract	xvi
1 Introduction	1
2 Objectives	8
3 Description of the Tangent-Linear and Adjoint Models of the Radiation and Boundary Layer Parameterization Packages of the FSU Global Spectral Model T42L12	10
3.1 Description of the FSU GSM	10
3.1.1 Description of the radiation processes	13
3.1.2 Description of the boundary layer processes	19
3.2 Modifications in the radiation and PBL processes	25
3.3 Tangent linear model of the radiation and boundary layer processes .	31
3.3.1 Coding the tangent linear model	31
3.3.2 Notational convention for variables and subroutines used in the tangent linear model	33
3.4 Adjoint model of the radiation and boundary layer processes	34
3.4.1 Coding the adjoint model	34
3.4.2 Adjoint correctness check and the gradient check	37

3.4.3	Notational convention for variables and subroutines used in the adjoint model	41
4	Basic Formalism of 4-D VAR	42
4.1	The minimization algorithm	46
4.2	Scaling	49
4.3	The twin experiment	50
5	Impacts of the optimal initial conditions and the optimally identified key parameters on the performance of the FSU GSM	60
5.1	Characteristics of the parameters	60
5.2	The methodology of parameter estimation	65
5.2.1	Adjoint formulation	65
5.2.2	Ill-posedness, identifiability and stability issues	68
5.3	Numerical experiments and results	71
5.3.1	Parameter estimation procedure and the results	71
5.3.2	Forecast experiments using both the retrieved initial conditions and parameter values	76
5.3.3	Impact of the optimal parameters alone on ensuing 24h forecasts	91
5.3.4	A study of the model's "memory" of impacts of optimal initial conditions and identified parameter values	93
6	An application of sensitivity of the model forecast error to the initial conditions	109
6.1	Experimental setup	110
6.2	Results of the numerical experiment	112
7	Summary and future research	127

REFERENCES	144
BIOGRAPHICAL SKETCH	153

LIST OF TABLES

5.1	Experiments designed to assess the impact of optimal parameter estimation.	80
5.2	Experiments carried out by integrating the model for 24h, 48h and 72h from 0000UTC Sept. 3, 1996, respectively.	94

LIST OF FIGURES

3.1	The configuration of the smooth function $F(\mathbf{x})$	30
3.2	The configuration of the smooth function $F(x_1) \cdot F(x_2)$	31
3.3	Variation of $\phi(\alpha)$ with respect to $\log\alpha$	40
4.1	Schematic illustration of the twin experimental design	51
4.2	Variations of the cost function and the gradient norm with respect to the iteration number of the twin experiment.	54
4.3	Difference fields of vorticity (top left), divergence (top right), logarithm of surface pressure (bottom left), temperature (bottom right) between the retrieved and the reference fields at level 8 at the beginning of the assimilation window after the minimization process was performed.	55
4.4	Difference fields of vorticity (top left), divergence (top right), logarithm of surface pressure (bottom left), temperature (bottom right) between the retrieved and the reference fields at level 8 at the beginning of the assimilation window before the minimization process was performed.	56
4.5	RMS errors of the retrieved initial conditions (dot line) and the initial guess (solid line) in the twin experiment.	58
4.6	RMS errors of the analysis fields (dot line) and the initial guess at the end of the assimilation window (solid line) in the twin experiment.	59
5.1	diagram of parameter estimation	69

5.2	The divergence fields at 200 hPa at 0000UTC Sept. 3, 1996: (a) the observation, (b) the initial guess. The contour interval is $5.0 \times 10^{-6} s^{-1}$	74
5.3	The variation of the cost function and the gradient norm with respect to the iteration number when both the optimal initial conditions and the bi-harmonic horizontal diffusion coefficient κ are retrieved. . . .	77
5.4	The evolution of the horizontal diffusion coefficient.	80
5.5	The RMS errors of the vorticity, divergence, virtual temperature and dewpoint depression at the end of the assimilation window. solid line: the control experiment; dashed line: the simulation experiment; dotted line: the optimal experiment.	81
5.6	The divergence fields at 200 hPa at the end of the assimilation window: (a) the observation, (b) the control experiment, (c) the simulation experiment and (d) the optimal experiment, respectively. The contour interval is $8.0 \times 10^{-6} s^{-1}$	82
5.7	The difference fields of specific humidity at 500 hPa between the results of the following three experiments and the observation at the end of the assimilation window: (a) the control experiment, (b) the simulation experiment and (c) the optimal experiment. The contour interval is $0.0005 g/g$	83
5.8	The difference fields of vorticity at 200 hPa between the results of the following three experiments and the observation at the end of the assimilation window: (a) the control experiment, (b) the simulation experiment and (c) the optimal experiment. The contour interval is $10^{-5} s^{-1}$	84

5.9	The difference fields of potential height at 500 hPa between the results of the following three experiments and the observation at the end of the assimilation window: (a) the control experiment, (b) the simulation experiment and (c) the optimal experiment. The contour interval is 5 m^2/s^2	85
5.10	The difference fields of temperature at 850 hPa between the results of the following three experiments and the observation at the end of the assimilation window: (a) the control experiment, (b) the simulation experiment and (c) the optimal experiment. The contour interval is 1K.	86
5.11	The RMS errors of the vorticity, divergence, virtual temperature and dewpoint depression at the end of the 24h forecast. solid line: the control experiment; dotted line: the optimal experiment.	87
5.12	The differences of the RMS errors of the vorticity, divergence, virtual temperature and the dewpoint depression between the three pairs at the end of the forecast. solid line: C2 and C1; dashed line: O2 and O1; dot dashed line: O5 and O4.	90
5.13	The differences of the RMS errors of the 24h forecast vorticity, divergence, virtual temperature and the dewpoint depression between the following pairs. dashed line: experiments (b) and (a); dot dot dashed line: experiments (c) and (a); solid line: experiments (d) and (a). . .	92
5.14	The differences of the RMS errors of the ensuing forecast fields vorticity, divergence, virtual temperature and the dewpoint depression between when the optimally identified parameter values were used and when the estimated parameter values were used. solid line: 24h forecast; long, short dashed line: 48h forecast; dot dot dashed line: 72h forecast.	96

5.15	The percent differences of the RMS errors of the ensuing forecast fields vorticity, divergence, virtual temperature and the dewpoint depression between when the optimally identified parameter values were used and when the estimated parameter values were used. solid line: 24h forecast; long, short dashed line: 48h forecast; dot dot dashed line: 72h forecast.	97
5.16	The differences of the RMS errors of the ensuing forecast fields vorticity, divergence, virtual temperature and the dewpoint depression between when the optimal initial conditions were used and when the initial guesses of initial conditions were used. solid line: 24h forecast; long, short dashed line: 48h forecast; dot dot dashed line: 72h forecast.	98
5.17	The percent differences of the RMS errors of the ensuing forecast fields vorticity, divergence, virtual temperature and the dewpoint depression between when the optimal initial conditions were used and when the initial guesses of initial conditions were used. solid line: 24h forecast; long, short dashed line: 48h forecast; dot dot dashed line: 72h forecast.	99
5.18	The difference fields between experiments (to be enumerated below) and the analysis for the specific humidity at 850 hPa as follows: (a) the control experiment C1, (b) experiment P1. The contour interval is 0.003 <i>g/g</i>	101
5.19	The difference field of specific humidity at 850 hPa between experiments C1 where the estimated parameter values were used and P1 where the optimally identified parameter values were used. The contour interval is 0.0008 <i>g/g</i>	102

5.20	The difference fields between experiments (to be enumerated below) and the analysis for the specific humidity at 500 hPa as follows: (a) the control experiment C1, (b) experiment I1. The contour interval is 0.0008 g/g.	103
5.21	Anomaly correlation of the specific humidity forecasts at 850 hPa for the control experiments (solid line), "optimal parameter" experiments (dot dot dashed line), "optimal initial condition" experiments (dotted line), and the experiments using both the optimal initial conditions and optimally identified parameter values (dashed line). Upper panel: tropical belt; Lower panel: Northern Hemisphere.	106
5.22	Anomaly correlation of the geopotential height forecasts at 500 hPa for the control experiments (solid line), "optimal parameter" experiments (dot dot dashed line), "optimal initial condition" experiments (dotted line), and the experiments using both the optimal initial conditions and optimally identified parameter values (dashed line). Upper panel: tropical belt; Lower panel: Northern Hemisphere.	107
6.1	The geopotential height field at 500 hPa for 12UTC June 7 (upper panel) and June 8 (bottom panel), 1988.	113
6.2	The geopotential height field at 500 hPa of the model 1-day forecast.	114
6.3	The difference field of the geopotential height field at 500 hPa between the model 1-day forecast and the verifying analysis.	114
6.4	The squared sum of sensitivities with respect to the initial analysis of dewpoint depression for each model vertical level.	115
6.5	The sensitivities with respect to the dewpoint depression at the lowest model level. The contour interval is 1 K ⁻¹	115

6.6	The sensitivities with respect to the initial analysis of dewpoint depression at the second lowest model level. The contour interval is $1 K^{-1}$.	116
6.7	The sensitivities with respect to the initial analysis of dewpoint depression at the third lowest model level. The contour interval is $1 K^{-1}$.	116
6.8	The vertical cross-section at 20N for the sensitivity with respect to the dewpoint depression at time t_0 . The contour interval is $2K^{-1}$.	118
6.9	The sensitivity pattern with respect to the initial analysis of virtual temperature at model vertical level 12. The contour interval is $1 K^{-1}$.	118
6.10	The sensitivity pattern with respect to the initial analysis of virtual temperature at model vertical level 10. The contour interval is $2 K^{-1}$.	121
6.11	The vertical cross-section at 20N for the sensitivity pattern with respect to virtual temperature at time t_0 . The contour interval is $2 K^{-1}$.	122
6.12	The sensitivity pattern with respect to the initial analysis of vorticity at model vertical level 11. The contour interval is $200000s$.	123
6.13	The sensitivity pattern with respect to the initial analysis of divergence at model vertical level 11. The contour interval is $200000s$.	123
6.14	The sensitivity pattern with respect to the initial analysis of vorticity at model vertical level 7. The contour interval is $200000s$.	124
6.15	The vertical cross-section at 20N for the sensitivity pattern with respect to vorticity at time t_0 . The contour interval is $200000s$.	124
6.16	The vertical cross-section at 10N for the sensitivity pattern with respect to vorticity at time t_0 . The contour interval is $200000s$.	125
6.17	The sensitivity signal for vorticity at time t_0 .	126
6.18	The sensitivity signal for dewpoint depression at time t_0 .	126

ABSTRACT

Four-Dimensional variational (4-D VAR) data assimilation has become a very active research area during the past two decades. In this dissertation, the full physics adjoint model of the FSU Global Spectral Model (FSU GSM) was completely derived by incorporating the adjoint of radiation and boundary layer parameterization packages into the data assimilation system. The radiation and boundary layer parameterization packages and the derivation of their corresponding tangent linear and adjoint counterparts in the FSU GSM are presented as part of this dissertation. Notational conventions for variables and subroutines used in the tangent linear and adjoint models are also provided.

The full-physics adjoint of the FSU GSM of version T42L12 was applied to carry out 4-D VAR data assimilation and adjoint parameter estimation using initialized analysis data sets. We first presented the formalism of 4-D VAR data assimilation and the methodology of adjoint parameter estimation, and closely examined the feasibility of performing 4-D VAR data assimilation using the FSU GSM and its full-physics adjoint model. Three key parameters (the bi-harmonic horizontal diffusion coefficient, the ratio of the transfer coefficient of moisture to the transfer coefficient of sensible heat, and the Asselin filter coefficient) along with the initial conditions were optimally recovered from the observations using an adjoint optimal parameter estimation approach. Then, we assessed the impacts of optimal initial conditions and key parameters estimation on the performance of the FSU GSM.

The 6h forecast fields starting from the retrieved optimal initial conditions and the optimally identified parameter values, i.e., the forecast fields at the end of the assimilation window, were studied in detail. They were found to successfully capture

the main features of the analysis fields. A number of experiments were conducted to separately assess the effect of carrying out 4-D VAR assimilation when both the initial conditions and key parameters served as control variables versus the case when only the key parameters were optimally estimated. Although the impact of optimal initial conditions dominated that of the optimal parameter values at the early stages of the forecast, a positive impact on the ensuing forecasts due to each optimally identified parameter value was observed with the maximum benefit being obtained due to the combined effect of the three optimal parameter values. The model's "memory" of the impacts of optimal initial conditions and identified parameter values was also investigated. The results show that in the ensuing forecasts the model tended first to "forget" the impact of optimal initial conditions while the impact of the optimally identified parameter values persisted beyond 72 hours. We noticed also that the geographic regions with more pronounced impacts differed depending on whether the results originated from the optimal initial conditions or from the optimally identified parameter values. The performance of the corresponding physical parameterization schemes was improved via tuning the physical parameter values. The best model forecast performance was obtained when both the optimal initial conditions and optimally identified parameter values were used simultaneously.

A preliminary experiment was also performed to calculate the sensitivity of the model 1-day forecast error to the initial conditions. The results were applied to identify regions of large analysis uncertainties.

CHAPTER 1

INTRODUCTION

With the availability of various types of observational data, especially the asynoptic data, the necessity of developing new techniques for using the spatially and/or temporally heterogeneous data to improve the quality of initial conditions in numerical weather prediction (NWP) has become imperious. This is particularly so for the tropics where the coverage of the current observation network is sparse and the geostrophic balance is not a reasonable approximation. Four-Dimensional variational (4-D VAR) data assimilation is one of the most promising methods, whose objective is to fit the model forecasts to the observations over some time and space interval. It can combine the previous data with currently available data using the full model dynamics, and it imposes no restriction on the data type to be used in the variational data assimilation. It is possible, therefore, to utilize the available data, especially asynoptic data, as much as possible, and to retrieve information not only about the variables whose observations are available, but also about the related variables via the full model dynamics.

This technique was first implemented in meteorology by Le Dimet (1980, 1982, 1983a,b), Courtier (1984), Derber (1985), Lewis and Derber (1985), Le Dimet and Talagrand (1986), Talagrand and Courtier (1987), Courtier and Talagrand (1990), etc. on shallow water models and quasi-geostrophic models. Later, this method was applied to more complex models by Thépaut and Courtier (1991), Navon, et al.

(1992c), Rabier and Courtier (1992), Thépaut, et al. (1996), to name just a few. A review of variational and optimization methods in meteorology was presented by Le Dimet and Navon (1988). 4-D VAR data assimilation is able to extract information from the observations in a way consistent with the dynamics of the model. Assuming the model is perfect, 4-D VAR data assimilation is equivalent to the fixed-interval Kalman smoother (Ghil and Malanotte-Rizzoli 1991). The model deficiency was first accounted for in a 4-D VAR method through the definition of a systematic error term by Derber (1989). Later, Zupanski (1997) presented a technique to apply the forecast model as a general weak constraint in the NCEP's regional 4-D VAR data assimilation system in which the model error had a flexible time resolution for the random error term.

Recently, further studies with special emphasis on including the physical processes of the NWP model into 4-D VAR data assimilation system have been carried out. Several groups demonstrated the ability to perform 4-D VAR data assimilation using discontinuous physical processes. Zou et al. (1993b) carried out the variational data assimilation with moist processes using the NMC spectral model. Vukićević and Errico (1993) investigated the impact of high nonlinearity of parameterized scheme on performing linearization. Zupanski (1993c) performed 4-D VAR data assimilation with the Betts-Miller cumulus convection scheme using NMC regional ETA forecast model. Tsuyuki (1996b) carried out a 4-D VAR data assimilation using precipitation data on FSU Global Spectral Model (GSM). Currently, 4-D VAR is the most widely used data assimilation scheme in numerical weather prediction. The National Meteorological Center has implemented a 3-D variational data assimilation (Parrish

and Derber, 1992). The European Center for Medium-Range Weather Forecasts (ECMWF) has put forth a tremendous effort on 3-D VAR and 4-D VAR, and now the 3-D VAR version has become operationally feasible, along with a simplified version of 4-D VAR data assimilation. The more advanced 4-D VAR data assimilation is on the edge of feasibility for operational implementation (Courtier et al. 1994). The HIRLAM project, a joint effort among several weather services in the Nordic countries, the Netherlands and Ireland for research and development in short-range mesoscale numerical weather prediction, has developed a 4-D VAR system in order to better utilize the new sources of data that are becoming available via satellites and radars (Gustafsson and Lönnberg, 1995). However, none of the adjoint models of the above-mentioned models contain the full-physical processes package. Since the radiation and boundary layer processes play important roles in the weather system, especially for the tropics, we developed in this dissertation the tangent linear and adjoint codes for the additional two physical parameterization packages, and incorporated them into the 4-D VAR system, thus obtaining the complete full-physics adjoint model of the FSU GSM.

The optimal model initial conditions retrieved via the 4-D VAR data assimilation decrease the model forecast errors which originate in the errors in the initial conditions. The skill of numerical weather prediction is expected to increase sizably in the near future due to the availability of better initial conditions for numerical weather prediction models. These improved initial conditions result from both the application of the new advanced data assimilation methods and the use of new sources of data, such as satellite data, radar data, profilers, and other remotely sensed data.

Some data assimilation and forecast experiments suggest that large forecast errors usually arise from errors in the initial conditions in the mid-latitude, however, the accurate representations of the physical processes, i.e., parameterization schemes, also play a major role in determining the model forecast skill, at least in the tropics. In this study, we do not focus on the comparison amongst different physical parameterization schemes, rather we study key parameters existing in the schemes currently used in the FSU GSM. By performing adjoint parameter estimation of a few judiciously chosen parameters, we expect to obtain a better understanding of the important roles played by the physical processes in the 4-D VAR data assimilation, and to assess the relative importance of the impacts of the optimal initial conditions and the optimally identified parameter values.

A numerical weather forecast model involves a number of parameters that are determined empirically. Some of these parameters, which are very common in physical parameterization schemes, contain information about the flow's properties and characteristics or originate in the simplification of the physical processes. Other parameters are introduced due to numerical stability considerations. The values of the parameters directly or indirectly impact upon the performance of the model. Generally, the values of the parameters are determined by trial and error, i.e., there is no objective criterion to choose "optimal" values of the parameters. In this study, we focus on the optimal estimation of several key parameters which are known to have an impact on NWP performance. The key parameters to be optimally identified can be chosen either via user's experience or implementing a relative adjoint sensitivity analysis. Such an analysis enables one to rank a subset of chosen parameters

according to their relative sensitivities of adequately chosen model responses. The key parameters studied here are obtained on the basis of meteorological experience. We wish to identify the “optimal” bi-harmonic horizontal diffusion coefficient κ , the ratio, γ , of the transfer coefficient of moisture to the transfer coefficient of sensible heat, and the Asselin filter coefficient FC using adjoint parameter estimation, and study their impacts on the ensuing model forecasts.

Research on adjoint parameter estimation has been carried out in the last twenty years on topics such as aquifer parameter estimation under transient and steady state conditions in the field of hydrology (Carrera and Neumann, 1986a,b,c), bottom drag coefficient identification in a tidal channel (Panchang and O’Brien, 1989), wind stress coefficient estimation along with the estimation of the oceanic eddy viscosity profile (Yu and O’Brien, 1991) and nudging coefficient estimation in the NMC adiabatic version of the spectral model (Zou, et al., 1992), inter alia. The issue of the adjoint parameter estimation was also addressed by Le Dimet and Navon (1988). Wergen (1992) recovered both the initial conditions and a set of parameters from observations using a 1-D shallow-water equation model. His results showed that even with noisy observations the parameters were recovered to an acceptable degree of accuracy. For a detailed survey of the state-of-the-art of parameter estimation in meteorology and oceanography, see Navon (1997).

The parameter estimation procedure is aimed at choosing an “optimal” parameter in an admissible parameter set, so that the model solutions corresponding to this parameter fit the observations in a least-squares sense, i.e., as a minimization problem of an output-error criterion. The full-physics FSU GSM and its adjoint model were

employed to recover the optimal initial conditions and to estimate optimal parameter values from the observations, and their impacts on the performance of the FSU GSM were assessed.

This dissertation is organized as follows. The objectives of this study are presented in chapter 2. The radiation and planetary boundary layer (PBL) parameterization packages and the derivation of their corresponding tangent linear and adjoint counterparts in the FSU GSM are described in chapter 3. The physical processes are usually highly nonlinear and involve numerous on-off switches. However, since we strive to preserve the original physical parameterization characteristics unchanged as much as possible, only function discontinuities which seriously affect the tangent linear approximation and the convergence rate of the minimization algorithm are considered for removal. The modifications of the physical processes are also described in this chapter.

The basic formalism of 4-D VAR data assimilation and a twin experiment are presented in chapter 4. The twin experiment was carried out to ensure that the assimilation system was properly constructed.

The impacts of the optimal initial conditions and the optimally identified key parameters on the performance of the FSU GSM are discussed in chapter 5. First, the characteristics of the three parameters optimally identified in the present study, i.e., bi-harmonic horizontal diffusion coefficient, the ratio γ of the transfer coefficient of moisture to the transfer coefficient of sensible heat and the Asselin filter coefficient, are described. Then, the methodology of adjoint parameter estimation is described in detail. Since some parameters are known to vary between given bounds, two

methods are presented to transform a multivariate constrained optimization problem into an unconstrained one. Ill-posedness, identifiability and stability issues are also addressed in this chapter. Following this, the numerical experiments and results are presented. The optimal initial conditions and the optimal values of the above-mentioned three parameters were retrieved from a set of initialized analysis data, then the model 6h forecasts starting from the retrieved optimal initial conditions and the optimally identified parameter values were compared with the analysis fields at the end of the assimilation window. We also studied the relative importance of the impacts of optimal model initial conditions and optimally identified model parameters on the model performance for both early and late stages of the model forecast. The impact of each optimally identified parameter as well as their combined impact on the ensuing model forecast were also discussed. This was followed by an experimental study of the model's "memory" or retention of the impacts of optimal initial conditions and identified parameter values. Different impact patterns emerged due to the different mechanisms by which optimal initial conditions and the optimally identified parameter values interacted with the model.

A preliminary experiment aimed at studying the sensitivity of the model 1-day forecast error to the initial conditions is described in chapter 6. The results were applied to identify regions where analysis problems lead to large forecast errors. Finally, the summary and directions for future research are presented in chapter 7.

CHAPTER 2

OBJECTIVES

The FSU GSM has been successfully applied for numerical weather forecasting, especially in the tropics. The effort to establish a 4-D VAR data assimilation system for this model has begun in 1993. The adjoint code for the dry adiabatic version of the FSU GSM was developed by Zhi Wang (Wang 1993). Later, Tsuyuki (1996a) incorporated the moisture variable, the smoothed parameterization of moist processes, horizontal diffusion and a simplified surface friction, and carried out experiments using the precipitation data. Our work continues this effort by incorporating the radiation and boundary layer processes into the data assimilation system due to the important roles they play in simulating various large-scale and mesoscale phenomena, especially in the tropical weather system. This study completes the derivation of the full-physics adjoint model of the FSU GSM, and renders the adjoint model consistent with the nonlinear forecast model. If the two models, the forward model and its adjoint, are inconsistent, this may have a negative effect on the process of adjoint optimal parameter estimation. Moreover, the adjoint technique allows to use the variational approach for assimilating various types of observations in meteorology, including satellite observations, and this necessitates availability of the full-physics adjoint.

The main purposes of this study are to complete the full-physics adjoint model of the FSU GSM, carry out 4-D VAR data assimilation and parameter estimation

numerical experiments using the FSU GSM and its full-physics adjoint, and assess the impacts of the optimal model initial conditions and the optimally identified model parameters on the performance of the FSU GSM. A preliminary study for the sensitivity of model 1-day forecast error to the initial conditions is also one of our goals aiming at localizing regions with large analysis uncertainties.

The research work in this dissertation consisted of the following five phases :

- a) Development of the tangent linear and adjoint codes of the radiation processes.
- b) Development of the tangent linear and adjoint codes of the boundary layer processes including vertical diffusion.
- c) Incorporation of the radiation and boundary layer processes into the data assimilation system; A twin experiment was performed to demonstrate the feasibility of carrying out 4-D VAR data assimilation using the FSU GSM and its full-physics adjoint model.
- d) Data assimilation and parameter estimation using initialized ECMWF analysis data, and the assessment of their relative impacts on the performance of the FSU GSM.
- e) An application of sensitivity of the model 1-day forecast error to the model initial conditions.

CHAPTER 3

**DESCRIPTION OF THE TANGENT-LINEAR AND ADJOINT
MODELS OF THE RADIATION AND BOUNDARY LAYER
PARAMETERIZATION PACKAGES OF THE FSU GLOBAL
SPECTRAL MODEL T42L12**

3.1 Description of the FSU GSM

In the FSU GSM, the σ vertical coordinate is defined as

$$\sigma = p/p_s \quad (3.1)$$

where p is the pressure and p_s the surface pressure. Thus, $\sigma = 0$ is at the top of the atmosphere and $\sigma = 1$ at the earth's surface. The boundary conditions are $\dot{\sigma} = 0$ at $\sigma = 1$ and $\sigma = 0$. The original governing equations of the FSU GSM are given as follows:

the vorticity equation:

$$\frac{\partial \zeta}{\partial t} = -\nabla \cdot (\zeta + f)\mathbf{V} - \mathbf{k} \cdot \nabla \times \left(RT\nabla q + \dot{\sigma} \frac{\partial \mathbf{V}}{\partial \sigma} - \mathbf{F} \right), \quad (3.2)$$

the divergence equation:

$$\frac{\partial D}{\partial t} = \mathbf{k} \cdot \nabla \times (\zeta + f)\mathbf{V} - \nabla \cdot \left(RT\nabla q + \dot{\sigma} \frac{\partial \mathbf{V}}{\partial \sigma} - \mathbf{F} \right) - \nabla^2 \left(\phi + \frac{\mathbf{V} \cdot \mathbf{V}}{2} \right), \quad (3.3)$$

the thermodynamic equation:

$$\frac{\partial T_v}{\partial t} = -\nabla \cdot \mathbf{V}T_v + T_v D + \dot{\sigma}\gamma - \frac{RT_v}{C_p} \left(D + \frac{\partial \dot{\sigma}}{\partial \sigma} \right) + H_T, \quad (3.4)$$

the continuity equation:

$$\frac{\partial q}{\partial t} = -D - \frac{\partial \dot{\sigma}}{\partial \sigma} - \mathbf{V} \cdot \nabla q, \quad (3.5)$$

the hydrostatic equation:

$$\sigma \frac{\partial \phi}{\partial \sigma} = -RT_v, \quad (3.6)$$

and the moisture equation:

$$\frac{\partial S}{\partial t} = -\nabla \cdot \mathbf{V}S + SD - \dot{\sigma} \frac{\partial S}{\partial \sigma} + H_T - H_M - \left[\frac{RT}{C_p} - \frac{RT_d^2}{\epsilon L(T_d)} \right] \left[D + \frac{\partial \dot{\sigma}}{\partial \sigma} - \frac{\dot{\sigma}}{\sigma} \right]. \quad (3.7)$$

In the above equations, the terms are defined as follows:

- f = Coriolis parameter,
- \mathbf{V} = horizontal vector wind,
- ζ = vertical component of vorticity = $\mathbf{k} \cdot \nabla \times \mathbf{V}$,
- D = horizontal divergence = $\nabla \cdot \mathbf{V}$,
- T is the absolute temperature,
- T_v is the virtual temperature,
- $q = \ln p_s$,
- γ = static stability = $\frac{RT}{C_p \sigma} - \frac{\partial T}{\partial \sigma}$,

- $\dot{\sigma}$ = vertical velocity in sigma coordinates,

$$= (\sigma - 1) (\hat{D} + \hat{V} \cdot \nabla q) + \hat{D}^\sigma + \hat{V}^\sigma \cdot \nabla q,$$
- ϕ = geopotential height,
- \mathbf{F} is the horizontal frictional force per unit mass,
- H_T = the diabatic heating,
- R is the gas constant for dry air,
- C_p is the specific heat of dry air at constant pressure,
- T_d is the dewpoint temperature,
- $S = T - T_d$ is the dewpoint depression,
- ϵ is the ratio of the molecular weight of water vapor to effective molecular weight of dry air (0.622),
- $L(T_d)$ is the latent heat of vaporization of water or ice,
- H_M represents moisture sources or sinks,
- \hat{F} = integral operator $= \int_0^1 F d\sigma$,
- \hat{F}^σ = integral operator $= \int_\sigma^1 F d\sigma$.

The dependent variables are expanded in triangularly truncated series of spherical harmonics as

$$F = \sum_{m=-J}^J \sum_{l=|m|}^J F_l^m Y_l^m, \quad (3.8)$$

where F_l^m are complex expansion coefficients, functions of σ and t .

In this study, a T42L12 version of the FSU GSM is used, i.e., the horizontal resolution is of a triangular truncation type with total wavenumber of 42 and 12 levels in the vertical. The physical processes include orography, planetary boundary layer processes, vertical diffusion, dry adjustment, large-scale condensation and evaporation, deep cumulus condensation, horizontal diffusion and radiation processes. For a detailed description of the FSU GSM, see T.N. Krishnamurti, et al. (1988). A brief description of the radiation and boundary layer processes is provided in the next two sections.

3.1.1 Description of the radiation processes

In the FSU GSM, the calculation of radiative fluxes is divided into three parts (Chang, C. B., 1980): 1) specification of clouds, 2) long-wave radiation, and 3) short wave radiation.

Long-wave radiation. In this FSU GSM version, the emissivity method proposed by Danard (1969) is used to compute the net longwave radiation at the reference level. The emissivity of a given atmospheric layer is a function of the optical length. For the sake of simplicity, only water vapor is considered in the long-wave radiation flux calculation. The clouds are treated as an infinite isothermal atmosphere which radiates as a blackbody and the earth surface is also treated as a blackbody. Scattering by air molecules is neglected. Moreover, an isotropic hemisphere is assumed in evaluating the upward and downward irradiances at a reference level. Then in a horizontally stratified atmosphere, the upward irradiance at reference level is $F_i \uparrow$

can be expressed as

$$F_i \uparrow = \sigma T_B^4 (1 - E[w_B - w_i]) + \int_{w_i}^{w_B} \sigma T^4 \frac{\partial E[w - w_i]}{\partial w} dw, \quad (3.9)$$

where σ is the Stefan-Boltzmann constant, w is the optical path which includes only the water vapor distribution, T is the temperature, B denotes either ground or cloud top, i refers to the reference level i , $E[w - w_i]$ is the flux emissivity which can be defined as

$$E[w - w_i] = \frac{\pi}{\sigma T^4} \int_0^\infty B_\nu(T) (1 - \tau_\nu[w - w_i]) d\nu. \quad (3.10)$$

Here $B_\nu(T)$ is the Planck blackbody radiance at frequency ν and temperature T , $\tau_\nu[w - w_i]$ is the transmission function evaluated for a path length of $w - w_i$. The optical path w is defined as

$$w = \frac{1}{g} \int_0^p q(p) (p/p_{00})^{0.85} (T_{00}/T)^{0.5} dp, \quad (3.11)$$

where p_{00} and T_{00} denote standard pressure and temperature, respectively.

Similarly, the downward irradiance $F_i \downarrow$ at level i is given by

$$F_i \downarrow = \sigma T_{cb}^4 (1 - E[w_i - w_{cb}]) - \int_{w_{cb}}^{w_i} \sigma T^4 \frac{\partial E[w_i - w]}{\partial w} dw, \quad (3.12)$$

where cb refers to the cloud base. For clear sky, Equation 3.12 is reduced to

$$F_i \downarrow = - \int_0^{w_i} \sigma T^4 \frac{\partial E[w_i - w]}{\partial w} dw + D, \quad (3.13)$$

where

$$D = \sigma T_{top}^4 E[w_{top}]. \quad (3.14)$$

Here D represents the downward infrared irradiance at the top of the model atmosphere, w_{top} and T_{top} denote the optical path and temperature at the top of the model respectively. Here $w_{top} = 4.7 \times 10^{-5}$, $T_{top} = 190K$.

Numerical evaluations of the fluxes make use of tabulations of the emissivity following Kuhn (1963). Kuhn's water vapor flux emissivity was measured directly in the atmosphere.

Solar radiation. Diurnal change in the incoming solar radiation S is affected by computing the zenith angle of the sun as a function of local time of day and its latitude as well as seasonal dependence. The solar radiative fluxes are divided into an absorbed part and a scattered part, which are subject to absorption and reflection at the earth's surface. The absorbed part is important in the generation of heating in the atmosphere, while the scattered part only plays a role in the calculation of the ground temperature. The two parts are expressed as follows:

$$S^a = 0.349S \cos(z) , \quad (3.15)$$

$$S^s = 0.651S \cos(z) , \quad (3.16)$$

where S^a and S^s are absorbed and scattered insolation respectively, S is the solar constant, z is the zenith angle. The cosine of the solar zenith angle is given by:

$$\cos(z) = \sin(\psi) \sin(\delta) + \cos(\psi) \cos(\delta) \cos(hr) , \quad (3.17)$$

where ψ is latitude, δ is the solar declination angle which is a function of day of year, and hr is the hour angle that is zero at solar noon.

The absorptivity due to water vapor with respect to the absorbed part of insolation is expressed by:

$$A[w] = 0.271[w \sec(z)]^{0.303} . \quad (3.18)$$

The diffusivity factor 1.66 was considered for the absorptivity of the diffuse (reflected) radiation to account for the mean diffusive path of the solar ray.

The depletion coefficient of a cloudless atmosphere for the scattered part of solar energy is estimated by

$$\alpha_o = 0.085 - 0.245 \log \left[\frac{p}{p_{sfc}} \cos(z) \right] , \quad (3.19)$$

where p_{sfc} is the surface pressure. The scattering coefficient of the atmosphere with multi-layer clouds is calculated by

$$\beta_n = 1 - (1 - \alpha_o) \Pi^n (1 - \alpha_{cn}) , \quad (3.20)$$

where α_{cn} is the albedo of the cloud with respect to scattered insolation and n is the number of cloud layers.

For clear sky, the downward irradiance of absorbed solar energy at level i is given as

$$S_i^a = S^a \{1 - A[w_i \sec(z)]\} - S^a \{1 - A[w_B \sec(z)]\} \cdot \alpha_s \{1 - A[1.66(w_B - w_i)]\} . \quad (3.21)$$

The downward irradiance of scattered solar energy is given by

$$S_o^s = S^s (1 - \alpha_o) / ((1 - \alpha_o \alpha_s)) , \quad (3.22)$$

where α_s is the albedo of the earth's surface, α_o is the albedo of the atmosphere defined by Equation 3.19.

For the case of the one-layer cloud, the absorbed insolation is calculated as follows:

- Above the cloud:

$$S_i^a = S^a \{1 - A[w_i \sec(z)]\} - S^a \{1 - A[w_{ct} \sec(z)]\} \cdot \alpha_c \{1 - A[1.66(w_{ct} - w_i)]\} ,$$

where ct refers to the cloud top.

- Within the cloud:

$$S_i^a = S^a \{1 - A[w_{ct} \sec(z)]\} (1 - \alpha_c) \{1 - A[w_{ci}]\} ,$$

where $A[w_{ci}]$ is the absorptivity of the cloud and w_{ci} is the equivalent amount of water vapor in the cloud.

- Below the cloud:

$$S_i^a = S^a \{1 - A[w_{ct} \sec(z)]\} (1 - \alpha_c) \left(\{1 - A[w_c + 1.66(w_i - w_{cb})]\} - \{1 - A[w_c + 1.66(w_B - w_{cb})]\} \alpha_s \{1 - A[1.66(w_B - w_i)]\} \right) .$$

The downward flux of scattered insolation below the cloud is given by

$$S_i^s = S^s (1 - \beta_1) / (1 - \beta_1 \alpha_s) .$$

Specification of clouds. Three cloud types (low, middle and high clouds) are defined in this model if the relative humidity in a layer exceeds the threshold values. The corresponding cloud bases are located at 900, 700 and 500 hPa. The cloud amounts were expressed by the empirical formulas:

$$CL = 2.94r_{800} - 1.94 , \quad (3.23)$$

$$CM = 2.0r_{600} - 1.0, \quad (3.24)$$

$$CH = 1.67r_{400} - 0.67, \quad (3.25)$$

where CL , CM and CH are the percentages of low, middle and high clouds estimated using the saturation ratio r at 800, 600 and 400 hPa, respectively. A lower limit $CL, CM, CH = 0$ and an upper limit $CL, CM, CH = 1$ were introduced. It is obvious that the cloud distribution evaluated from the above formulas is horizontally continuous.

Seven different configurations of sky conditions plus a clear-sky condition are possible. They are defined as following:

$$C_1 = (1 - CL)(1 - CM)(1 - CH) \quad \text{Clear sky} \quad (3.26)$$

$$C_2 = CL(1 - CM)(1 - CH) \quad \text{Low cloud only} \quad (3.27)$$

$$C_3 = CL \cdot CM(1 - CH) \quad \text{Low and middle clouds} \quad (3.28)$$

$$C_4 = CL \cdot CM \cdot CH \quad \text{Low, middle and high clouds} \quad (3.29)$$

$$C_5 = CM(1 - CL)(1 - CH) \quad \text{Middle cloud only} \quad (3.30)$$

$$C_6 = CH(1 - CL)(1 - CM) \quad \text{High cloud only} \quad (3.31)$$

$$C_7 = CM \cdot CH(1 - CL) \quad \text{Middle and high clouds} \quad (3.32)$$

$$C_8 = CL \cdot CH(1 - CM) \quad \text{Low and high clouds} \quad (3.33)$$

The sum of C_n ($n = 1, \dots, 8$) must equal to one. Thus, for long wave radiation the upward irradiance at level i can be calculated by

$$F_i \uparrow = \sum_{n=1}^8 C_n F_{in} \uparrow, \quad (3.34)$$

and the downward irradiance at level i is

$$F_i \downarrow = \sum_{n=1}^8 C_n F_{in} \downarrow, \quad (3.35)$$

where n denotes the sky condition.

Similarly, for solar radiation the absorbed insolation is given by

$$S_i^a = \sum_{n=1}^8 C_n S_{in}^a, \quad (3.36)$$

and the scattered insolation is given by

$$S_i^s = \sum_{n=1}^8 C_n S_{in}^s. \quad (3.37)$$

The radiative cooling and warming rates are expressed by the divergence of flux, i.e.,

$$\left(\frac{\partial T}{\partial t}\right)_{\text{infrared cooling}} = -\frac{g}{C_p} \frac{\partial F_i}{\partial p}, \quad (3.38)$$

and

$$\left(\frac{\partial T}{\partial t}\right)_{\text{solar heating}} = -\frac{g}{C_p} \frac{\partial S_i^a}{\partial p}, \quad (3.39)$$

where $F_i = F_i \downarrow + F_i \uparrow$.

3.1.2 Description of the boundary layer processes

Surface fluxes of momentum, heat and moisture. The computation of the surface fluxes of momentum, heat and moisture is based on Monin-Obukhov similarity theory and follows the analysis of Louis (1979). The constant flux layer is defined as the lowest 20–30 m of the atmosphere where the fluxes of momentum, heat and moisture are nearly invariant with height. The frictional velocity u_* , the

characteristic potential temperature θ_* , the characteristic specific humidity q_* and the Monin-Obukhov length L are appropriate scaling parameters for the constant flux layer. A detailed description and derivation can be found in Krishnamurti et al. (1988).

The surface fluxes of momentum, heat and moisture can be expressed in terms of bulk aerodynamic formulae of the form

$$F_M = \rho C_M (\bar{u}_2 - \bar{u}_1)^2, \quad (3.40)$$

$$F_H = \rho C_P C_H (\bar{u}_2 - \bar{u}_1) (\bar{\theta}_2 - \bar{\theta}_1), \quad (3.41)$$

$$F_Q = \rho C_Q (\bar{u}_2 - \bar{u}_1) (\bar{q}_2 - \bar{q}_1) g_w, \quad (3.42)$$

where ρ is the air density, C_P is the specific heat of dry air at constant pressure, g_w the ground wetness, F_M is positive for downward momentum fluxes and F_H and F_Q are positive for upward heat and moisture fluxes. The subscripts 1 and 2 stand for the values on the two levels z_1 and z_2 where both levels are assumed to be within the constant flux layer. C_M , C_H and C_Q are the stability-dependent transfer coefficients that can be computed using the analytical formulae prescribed by Louis (1979) as

$$C_M = \frac{k^2}{[\ln(z_2/z_1)]^2} \frac{1}{(1 + 4.7 Ri_B)^2}, \quad (3.43)$$

$$C_H = C_Q = C_M, \quad (3.44)$$

for stable and neutral conditions ($Ri_B \geq 0$) and

$$C_M = \frac{k^2}{[\ln(z_2/z_1)]^2} \left[1 - \frac{9.4 Ri_B}{1 + c_1 |Ri_B|^{1/2}} \right], \quad (3.45)$$

$$C_H = \frac{k^2}{[\ln(z_2/z_1)]^2} \left[1 - \frac{9.4 Ri_B}{1 + c_2 |Ri_B|^{1/2}} \right], \quad (3.46)$$

$$c_1 = \frac{7.4 \times 9.4 k^2}{[\ln(z_2/z_1)]^2} \left[\frac{z_2}{z_1} \right]^{1/2}, \quad (3.47)$$

$$c_2 = \frac{5.3 \times 9.4 k^2}{[\ln(z_2/z_1)]^2} \left[\frac{z_2}{z_1} \right]^{1/2}, \quad (3.48)$$

for unstable conditions ($Ri_B < 0$). The bulk Richardson number Ri_B for the layer is given as

$$Ri_B = \frac{g \Delta z \Delta \theta}{\bar{\theta} (\Delta u)^2}, \quad (3.49)$$

where $\Delta \theta$ and Δu are the differences of θ_2 , θ_1 and u_2 , u_1 between the levels z_2 and z_1 . Ri_B is capped at 0.212 for stable conditions to prevent the stability-dependent transfer coefficients from becoming very small.

The surface fluxes of momentum, heat and moisture then can be computed from Equations 3.40–3.42 given the values of u_1 , u_2 , θ_1 , θ_2 , q_1 , q_2 and g_w .

The first level z_1 is assumed to be the surface roughness length z_0 , where $\bar{u}_1 = 0$ and $\bar{\theta}_1 = \theta_0$ (the surface temperature). The roughness parameter z_0 over land areas is provided by the input and fixed in the FSU GSM, while z_0 over oceans is determined using Charnock's formula

$$z_0 = \frac{M u_*^2(z_0)}{g},$$

where M is a constant and has a value of 0.04. Since the frictional velocity is a function of z_0 , an iterative process is used to compute z_0 . The minimum value of z_0 is set to be $1.0 \times 10^{-4}m$.

The level z_2 is taken as the first intermediate sigma level $\bar{\sigma}_{12}$ above the earth's surface and is always set to be greater than z_1 . θ_2 and q_2 can be calculated at the level z_2 from the model's prognostic variables. The velocity u_2 is obtained by interpolating

u_{12} at σ_{12} and u_0 at z_0 ($u_0 = 0$) to $\bar{\sigma}_{12}$ as the following logarithmic formula:

$$u_2 = u_{12} \ln(z_2/z_1) / \ln(z_{\sigma_{12}}/z_1) .$$

The computation of the surface temperature (θ_0) is required. Over the ocean, θ_0 is the sea surface temperature that is provided by the input file and is a fixed field. The saturation specific humidity over the ocean (q_1) is computed as a function of the saturation vapor pressure. Over land, the surface temperature T_G (or θ_0) is computed by solving an energy balance equation of the form

$$C_g \frac{\partial T_G}{\partial t} = F \downarrow - (1 - \alpha) S_d + F_H + L F_Q - \sigma T_G^4 , \quad (3.50)$$

where C_g is the soil heat capacity, $F \downarrow$ is the downward longwave flux of radiation at the surface, S_d the downward shortwave flux of radiation at the surface, α the surface albedo, F_H and $L F_Q$ are the sensible and latent heat fluxes respectively, L is the latent heat of water, σT_G^4 is the upward longwave flux of radiation from the surface. Assuming the ground storage of heat is neglected ($C_g = 0$), since the ground temperature T_G is used explicitly in the calculation of the surface fluxes of heat F_H and moisture F_Q , the simplified form of Equation 3.50,

$$f(T_G) = F \downarrow - (1 - \alpha) S_d + F_H + L F_Q - \sigma T_G^4 = 0 , \quad (3.51)$$

is solved using the Newton-Raphson iterative scheme.

A portion of the net radiative flux is used to melt snow over ice-covered oceans or frozen land when $T_G > 273.15K$:

$$f(T_G) = f(T_G) + 15 \cdot (273.15 - T_G) , \quad (3.52)$$

and a portion of $f(T_G)$ is fluxed through the ice over ice-covered oceans only at the initial time

$$f(T_G) = f(T_G) + (273.15 - T_G). \quad (3.53)$$

There are four surface types, namely land, ocean, snow-covered land and ice-covered ocean. The surface types are fixed.

The ground wetness g_w is set to unity over oceans while it is a function of the surface albedo α

$$g_w = 0.85 \left[1 - e^{-200(0.25-\alpha)^2} \right]; \quad (3.54)$$

g_w is set to zero for albedo greater than 25%. g_w is greater than zero but less than unity.

Vertical diffusion. The vertical eddy fluxes of momentum, heat and moisture are given by:

$$\frac{\partial \tau}{\partial t} = \frac{1}{\rho} \frac{\partial}{\partial z} \left[\rho K \frac{\partial \tau}{\partial z} \right], \quad (3.55)$$

where $\tau = u, v, \theta$, and q , ρ is the air density, K is the eddy diffusion coefficients which are determined by

$$K_M = l^2 \left| \frac{\partial \vec{V}}{\partial z} \right| F_1(Ri) \text{ (momentum)}, \quad (3.56)$$

$$K_H = K_Q = l^2 \left| \frac{\partial \vec{V}}{\partial z} \right| F_2(Ri) \text{ (heat, moisture)}. \quad (3.57)$$

The mixing length l is computed as

$$l = kz / (1 + kz/\alpha),$$

where the asymmetric mixing length α is set to 150 m for momentum and 450 m for heat and moisture, k is the Von Karman constant. The stability functions F_1 and F_2 are of the form

$$F_1 = F_2 = 1/(1 + 5Ri)^2 \quad (Ri \geq 0), \quad (3.58)$$

$$F_1 = \frac{1 + 1.746|Ri|^{1/2} - 8Ri}{1 + 1.746|Ri|^{1/2}} \quad (Ri < 0), \quad (3.59)$$

$$F_2 = \frac{1 + 1.286|Ri|^{1/2} - 8Ri}{1 + 1.286|Ri|^{1/2}} \quad (Ri < 0). \quad (3.60)$$

The Richardson number for a given layer is expressed as

$$Ri = \frac{g \frac{\partial \hat{\theta}_v}{\partial z}}{\left| \frac{\partial \bar{V}}{\partial z} \right|^2}, \quad (3.61)$$

where $\hat{\theta}_v$ indicates the virtual potential temperature.

An upper limit on $K_{M,H}$ is set such that

$$K_{M,H} = \Delta z^2 / 86400, \quad (3.62)$$

if the square of the layer thickness Δz divided by the computed value of the eddy diffusivity is less than one day (86400 s).

In the FSU GSM, the boundary conditions on the flux of τ at the top and the bottom of the model atmosphere are set equal to zero. The wind speed between two model levels is constrained to be not less than $1.0ms^{-1}$. The distribution of the surface fluxes within the PBL is parameterized through the use of mixed layer theory. For unstable conditions ($L < 0$), the PBL is assumed to be well-mixed such that the vertical profiles of u, v, θ, q are nearly constant with height, therefore

$$\frac{\partial \tau}{\partial t} = \frac{1}{\rho} \frac{\partial F}{\partial z} = -\frac{F_s}{\rho H_{PBL}}, \quad (3.63)$$

where $\tau = u$ or v for $F_s = F_M$ and $\tau = \theta$ or q for $F_s = F_H$ or F_Q .

However, the assumption of a well mixed layer is not valid in stable conditions. A parabolic profile of fluxes is assumed in stable conditions, hence we get

$$\frac{\partial \tau}{\partial t} = \frac{1}{\rho} \frac{\partial F}{\partial z} = \frac{-2F_s}{\rho H_{PBL}} (1 - z/H_{PBL}). \quad (3.64)$$

H_{PBL} is set equal to 1.0 km for the distribution of F_H and F_Q and 0.75 km for F_M in the unstable regime, while it is set equal to 0.75 km for the distribution of F_M, F_H and F_Q in the stable regime.

3.2 Modifications in the radiation and PBL processes

Generally, physical processes are highly nonlinear and involve many on-off switches in the parameterization schemes that appear in the code as IF statements depending on the values of model state variables. The presence of these on-off switches may introduce discontinuities in the cost function and its derivatives, hence, exaggerate the nonlinearity of the nonlinear model. High nonlinearity of the physical processes also decreases the validity of the tangent linear approximation, especially in the presence of the on-off switches. The high-order nonlinear terms may become important after a certain time integration period. Therefore, the validity period of the tangent linear model including physical processes is shorter than that of the corresponding adiabatic tangent linear model, and the tangent linear approximation of the full physics model is not as good as that of the corresponding adiabatic model version.

For constructing the adjoint model, the forward model is linearized about a basic state. The grid point locations and time levels where the on-off switches occur for the basic state are passed on to the tangent linear model and the adjoint model from the nonlinear forward model and serve as the switching points of the tangent linear model and the adjoint model, i.e., the on-off switching points are retained in the data assimilation process. The basic assumption made here is that a small perturbation $\delta\mathbf{X}_0$ does not change the grid point and time level where the on-off switch occurs. This assumption, however, does not always hold in realistic situation since the on-off switch depends on the model state variables. Once the small perturbation changes the point and time level of the on-off switch occurrence, the forward nonlinear model will be forced to follow a different trajectory, and the cost function and its gradient will be expected to experience a jump due to a sudden change of the basic state. Some studies have been conducted to understand the effect of the on-off switches in the context of data assimilation. Zou, et al. (1993b), carried out variational data assimilation with moist processes using the NMC spectral model directly by ignoring the uncertainties caused by the switch related problems. Their results showed that the impact of nonlinearities might be ignored except in the near vicinity of frontal areas and demonstrated the ability to perform 4-D VAR data assimilation using discontinuous physical processes. Vukićević and Errico (1993) tested the accuracy of the tangent linear model of a mesoscale model against the “true” perturbation obtained by direct nonlinear integration and found that the tangent linear model and associated adjoint model would be more accurate for a nonlinear model that has well-behaved regime transitions. They recommended improving the nonlinear model

prior to performing linearization for high nonlinearity of parameterized regime transitions. Zupanski (1993c) derived the adjoint code of moist processes for NMC/ETA regional forecast model. She demonstrated that discontinuities present in the Betts-Miller cumulus convection scheme increased the linearization errors to a large extent and had adverse effects on 4-D VAR data assimilation. She modified the scheme by applying a vertical smoothing to the layers of transition to render them more continuous before linearization. Tsuyuki(1996a) found a better convergence rate of the minimization algorithm in his study after he removed most of the zeroth-order discontinuities that existed in the moist processes prior to performing the variational assimilation, but he also found that this treatment would introduce another difficulty, i.e., the cost function had a large local gradient, which degraded the efficiency of the minimization process and could even cause the minimization process to fail. Recently, Bao, J-W, et al. (1995) applied the calculus of variations to confirm that variational data assimilation using adjoint method allowed the assimilation model to have a finite number of first-order discontinuous points while the presence of step functions imposed serious difficulties on the data assimilation. Their study provided a better insight into the feasibility of the application of the adjoint method to a model with on-off switches.

Since we aim to keep the original physical parameterization characteristics unchanged as much as possible, only function discontinuities which most impact the tangent linear approximation and the convergence rate of the minimization algorithm were considered as candidates for removal, even though there are numerous on-off switches in the full-physics FSU spectral model.

In the radiation processes, numerical evaluations of the fluxes make use of tabulations of the emissivity following Kuhn (1963). Kuhn's water vapor flux emissivity was measured directly in the atmosphere. Linear interpolation, which is discontinuous in its first derivatives, was applied in the original code. Once an interpolating point falls into a different segment due to a small perturbation, its first derivative will experience a jump in its magnitude. Since there is no analytical expression for the water vapor flux emissivity, and since we want to keep the curvature of the interpolation to be minimum, a cubic spline algorithm proposed by Stephens (1996) is applied to fit the unequally-spaced, presumably errorless observations of the water vapor flux emissivity. It is presumed that ordered data $\{y(x_j), j = 0, J\}$ are given at $(J + 1)$ distinct, but unequally-spaced sample points $\{x_j\}$ in $[x_0, x_J]$, the form of the interpolating cubic adopted is

$$\begin{aligned}
 H_j(x) = & \frac{s_{j-1}}{6} \left[\frac{(x_j - x)^3}{\Delta_j} - \Delta_j (x_j - x) \right] \\
 & + \frac{s_j}{6} \left[\frac{(x - x_{j-1})^3}{\Delta_j} - \Delta_j (x - x_{j-1}) \right] \\
 & + y_{j-1} \left(\frac{x_j - x}{\Delta_j} \right) + y_j \left(\frac{x - x_{j-1}}{\Delta_j} \right) \quad (j = 1, 2, \dots, J). \quad (3.65)
 \end{aligned}$$

The increment Δ_j is defined as

$$\Delta_j = x_j - x_{j-1},$$

where $\{s_j\}$ are the polynomial second derivatives. The integrity of the observations is maintained in this fitting.

Another type of discontinuity is introduced by the definition of the three cloud types that are defined in this model when the relative humidity in a layer exceeded

the threshold values. For the sake of simplicity in calculating the fluxes, the cloud levels are fixed, i.e., they are taken to be identical to the ones of the nonlinear model, only the discontinuities in the saturation ratio r are alleviated as in Tsuyuki (1996a) by using a smooth function

$$F(RH) = 1. - 0.5 \left(\frac{RH - RHC0}{RHC - RHC0} \right)^2 ,$$

where RHC is the threshold value and $RHC0$ is a specified value. In this model, RHC is 0.66, 0.5 and 0.4 for low, middle and high cloud respectively, $RHC0$ is taken as 0.64, 0.48, 0.38 correspondingly. However, our experiments show that the impact of such modification can be neglected.

The boundary layer processes contain many on-off switches, but only the discontinuities in the function itself are considered for removal.

In calculating the eddy diffusivity $K_{M,H}$, an upper limit on $K_{M,H}$ is set. A smooth function,

$$F(x) = \frac{1}{1 + e^x} ,$$

is employed to remove this discontinuity.

Hence, the computed eddy diffusivity $K_{M,H}$ and the upper limit $K0_{M,H}$ can be combined as follows:

$$K_{M,H}/(1 + e^x) + K0_{M,H}/(1 + e^{-x}) , \quad (3.66)$$

where $x = 5(86400 - \Delta z^2/K_{M,H})$. Hence, for the eddy diffusivity, we will adopt the value of $K_{M,H}$ when $\Delta z^2/K_{M,H}$ is larger than 86400, otherwise, it will tend to be $K0_{M,H}$.

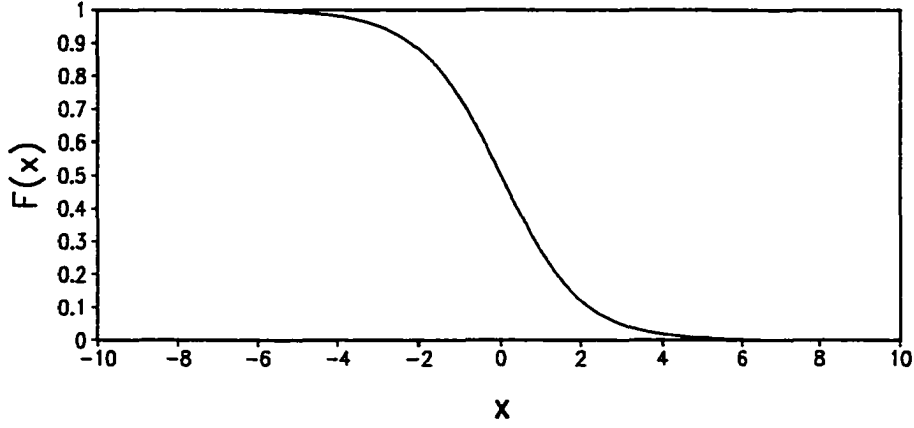


Figure 3.1: The configuration of the smooth function $F(x)$

The distribution of the surface fluxes within the PBL is parameterized through the use of mixed layer theory for unstable conditions ($L < 0$) and through the use of a parabolic profile of fluxes for stable conditions ($L > 0$), i.e.,

$$\frac{\partial \tau}{\partial t} = \begin{cases} \frac{1}{\rho} \frac{\partial F}{\partial z} = -\frac{F_s}{\rho H_{PBL2}} & (z < H_{PBL2} \text{ and } L < 0) , \\ 0 & (\text{otherwise}) \end{cases} , \quad (3.67)$$

and

$$\frac{\partial \tau}{\partial t} = \begin{cases} \frac{1}{\rho} \frac{\partial F}{\partial z} = \frac{-2F_s}{\rho H_{PBL1}} (1 - z/H_{PBL1}) & (z < H_{PBL1} \text{ and } L > 0) \\ 0 & (\text{otherwise}) \end{cases} . \quad (3.68)$$

The same smooth function $F(x)$ is applied to remove the discontinuities in this instance. The modified scheme is given as following:

$$\frac{\partial \tau}{\partial t} = -\frac{F_s}{\rho H_{PBL2}} \cdot F(x_1) \cdot F(x_2) + \frac{-2F_s}{\rho H_{PBL1}} (1 - z/H_{PBL1}) \cdot F(-x_1) \cdot F(x_3) , \quad (3.69)$$

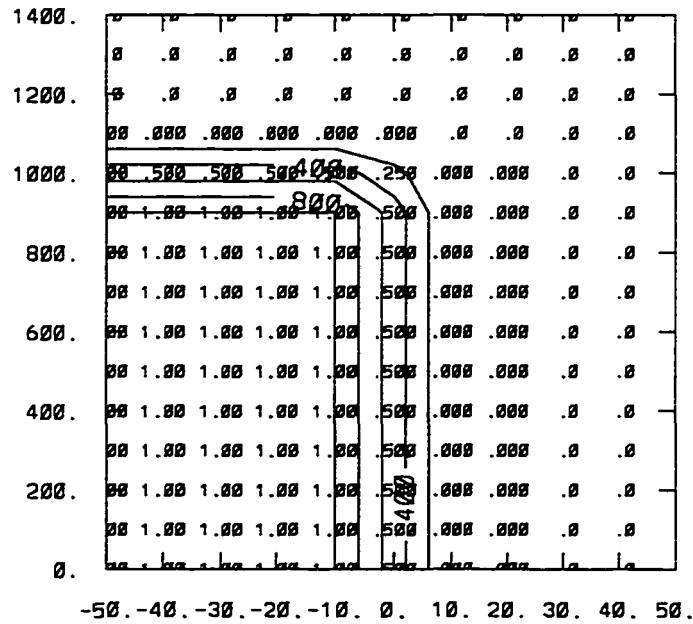


Figure 3.2: The configuration of the smooth function $F(x_1) \cdot F(x_2)$.

where

$$x_1 = 5L, \tag{3.70}$$

$$x_2 = z - H_{PBL2}, \tag{3.71}$$

$$x_3 = z - H_{PBL1}. \tag{3.72}$$

The smooth function of $F(x_1) \cdot F(x_2)$ is shown in Fig. 3.2.

3.3 Tangent linear model of the radiation and boundary layer processes

3.3.1 Coding the tangent linear model

In order to obtain the exact discrete tangent linear model of the nonlinear model, the tangent linear model is developed directly by linearizing the discrete nonlinear

model around a basic trajectory subroutine by subroutine, loop by loop, and line by line.

With a three time level scheme applied, the nonlinear model assumes the following form:

$$\mathbf{X}(t_0 + \delta t) = F_1(\mathbf{X}(t_0)), \quad (3.73)$$

$$\mathbf{X}(t_r + \delta t) = F_2(\mathbf{X}_1, \mathbf{X}_2), \quad (3.74)$$

where F_1 and F_2 are nonlinear operators, \mathbf{X} denotes the model variable vector, δt is the time-step, t_0 is the initial time level, and t_r represents any time level during the integration period, vector $\mathbf{X}_1 = \mathbf{X}(t_r - \delta t)$ and $\mathbf{X}_2 = \mathbf{X}(t_r)$.

Linearizing the nonlinear model in the vicinity of a basic trajectory, we obtain the corresponding tangent linear model for $\delta\mathbf{X}(t_r)$, the perturbation of the state variables at time t_r

$$\delta\mathbf{X}(t_0 + \delta t) = \frac{\partial F_1(\mathbf{X}(t_0))}{\partial \mathbf{X}} \delta\mathbf{X}(t_0), \quad (3.75)$$

$$\delta\mathbf{X}(t_r + \delta t) = \frac{\partial F_2(\mathbf{X}_1, \mathbf{X}_2)}{\partial \mathbf{X}_1} \delta\mathbf{X}_1 + \frac{\partial F_2(\mathbf{X}_1, \mathbf{X}_2)}{\partial \mathbf{X}_2} \delta\mathbf{X}_2. \quad (3.76)$$

The perturbation variable $\delta\mathbf{X}(t_r)$ at time level t_r can be obtained by integrating the tangent linear model from the initial condition $\delta\mathbf{X}(t_0)$. In a compact form, the tangent linear model may be written as in Navon, et al. (1992c).

$$\delta\mathbf{X}(t_r) = P_r \delta\mathbf{X}(t_0), \quad (3.77)$$

where P_r represents the result of the multiplication of all operator matrices to obtain $\delta\mathbf{X}(t_r)$ from $\delta\mathbf{X}(t_0)$.

A basic trajectory (or basic state) and some intermittent variables computed from the nonlinear forward model are required in the tangent linear model. These variables should be stored for the tangent linear model or can be re-calculated in the tangent linear model depending on the memory and computational cost available on the particular computing platform.

3.3.2 Notational convention for variables and subroutines used in the tangent linear model

The same variable name is employed for the model state variable in the nonlinear forward model as the one used for the perturbation variable in the tangent linear model. The same common block name is also used for both the nonlinear forward model and the tangent linear model.

The variable name of the basic trajectory in the tangent linear model is denoted by the same name as in the nonlinear forward model with a suffix “9”. Care should be exercised to a special case when a basic state variable is redefined, usually, a suffix “8” is given to the redefined basic state variable.

The name of the tangent linear subroutine is the corresponding nonlinear subroutine name with a prefix TAN. For instance, the nonlinear subroutine SFLX has a corresponding tangent linear code TANSFLX.

3.4 Adjoint model of the radiation and boundary layer processes

3.4.1 Coding the adjoint model

In time discretized form, the cost function to be minimized is given as following

$$J(\mathbf{X}_0) = \frac{1}{2} \sum_{r=0}^R \left(\mathbf{H}(\mathbf{X})(t_r) - \mathbf{Z}^{obs}(t_r) \right)^T \mathbf{W} \left(\mathbf{H}(\mathbf{X})(t_r) - \mathbf{Z}^{obs}(t_r) \right), \quad (3.78)$$

where \mathbf{X}_0 is the control variable, a vector of dimension N , representing the initial state of the model; \mathbf{X} contains all model variables; \mathbf{Z}^{obs} represents observational data distributed over some space and time interval, which is a vector of dimension M ; \mathbf{H} is a transformation matrix that maps the model variables to the observations; \mathbf{W} is an $M \times M$ diagonal matrix of weighting coefficients. The values of the elements are usually determined by dimensional scaling of various variables, relative importance and quality of the data set and other considerations. Generally, $\mathbf{W}(t)$ may be taken as the inverse covariance matrix of the observation errors. However, since additional studies are required in order to obtain the observation errors, in the following experiments, the diagonal elements of $\mathbf{W}(t)$ are set to be like Navon, et al. (1992c), i.e., the inverse of the square of the maximum difference among each observational variable data to ensure that all terms in the cost function are of approximately the same order of magnitude. The superscript $()^T$ denotes the transpose operator. t_r represents the time when the observation occurs in the assimilation window, R is the total number of time levels when the observations are available.

From section 3.3.1, we see that the tangent linear model can be written in a compact form Equation 3.77, then, the first variation of Equation 3.78 may be written

as follows:

$$J'(\delta\mathbf{X}(t_0)) = \sum_{r=0}^R \left([\nabla_{\mathbf{X}}\mathbf{H}]^T \mathbf{W} \left(\mathbf{H}(\mathbf{X})(t_r) - \mathbf{Z}^{obs}(t_r) \right), P_r \delta\mathbf{X}(t_0) \right), \quad (3.79)$$

i.e.,

$$\nabla J(\mathbf{X}(t_0)) = \sum_{r=0}^R P_r^T [\nabla_{\mathbf{X}}\mathbf{H}]^T \mathbf{W} \left(\mathbf{H}(\mathbf{X})(t_r) - \mathbf{Z}^{obs}(t_r) \right), \quad (3.80)$$

where P_r^T are the corresponding adjoint operator of the linear operator P_r in the tangent linear model.

Therefore, the adjoint code is developed directly from the basic direct code, the tangent linear code. If we view the linear model as the result of the multiplication of a number of operator matrices:

$$P_r = A_1 A_2 \dots A_N,$$

where each A_i represents a subroutine or Do loop. Then the adjoint model can be viewed as

$$P_r^T = A_N^T \dots A_2^T A_1^T,$$

i.e., the adjoint model is written backward from the tangent linear model line by line, subroutine by subroutine (Navon, et al. 1992c).

Some simple examples illustrating how to develop the discrete adjoint code from the tangent linear code were provided by Navon, et al. (1992c), and Yang, et al. (1996). We also provide an example in the APPENDIX for deriving the tangent linear code and the adjoint code from the original nonlinear code. Here we only address some special cases which were encountered in deriving the adjoint for the physical processes in this particular model.

Since an original subroutine might be called several times in a numerical model with different variables being calculated each time, it is very important to distinguish which variable is active and which is inactive in every call. The inactive variable should always be set to zero in the adjoint code. Otherwise an error will be introduced in the adjoint code.

Another particular case is the iterative process. In order to write the adjoint code of an iterative process, one can either develop the adjoint operator directly from the analytic formula if an analytic formula is available, or one has to write an iterative adjoint code. To do the latter, one has to store or calculate the basic state used in every iteration and the total iterative number used in the nonlinear model prior to the adjoint operator being calculated. One should always keep in mind at all times that the basic state used in each stage of the adjoint code should be the same as that used in the corresponding nonlinear code.

The third special case is when a table lookup is used and then an interpolation is applied to obtain the values needed in the nonlinear model. Generally, linear interpolation is sufficient in the nonlinear model, however, since the adjoint code is the adjoint operator of the tangent linear model and the tangent linear model is linearized around a basic state, the first derivatives at the nodes are not continuous when a linear interpolation is used. The smaller the interval between two nodes is, the more serious the problem which the interpolation might introduce into the adjoint model. There are two ways that can be used to resolve this problem. One is to employ the analytic formula that generates the table and write the adjoint code directly from the analytic formula. However, it is usually the case that the direct

calculation from the analytic formula is so time-consuming that a table is constructed precisely to avoid such complex calculation. The other way, which is more practical, is to apply an interpolation with better continuity properties, such as a cubic spline where the function itself and its first derivatives as well as its second derivatives are continuous, hence, its adjoint code will perform very well. Also a further refinement can be obtained by keeping the curvature of the cubic spline to the minimum as we did in the radiation processes (see section 3.2).

The involvement of many nested conditional GO TO statements does not cause trouble for the nonlinear model, however, in the adjoint model, special care must be taken to ensure that every route is included and handled properly. It is recommended to figure out the total number of combinations of all routes the basic state might take, and rewrite the nonlinear code using IF and END IF pairs as much as possible.

A basic trajectory (or basic state) and some intermittent variables computed from the nonlinear forward model are required in the adjoint model. These variables should be stored for the adjoint model or re-calculated in the adjoint model depending on availability of memory and/or computational cost for the given computational platform (see Restrepo, et al. 1997).

3.4.2 Adjoint correctness check and the gradient check

Since a minor error may result in an incorrect gradient of cost function with respect to the control variables, it is necessary to verify the correctness of the adjoint code segment by segment. A final gradient check should also be performed. For a

detailed description of the verification of correctness, see Navon, et al. (1992c). Here we just provide a brief description.

Each of the adjoint operators (either a single DO loop or a subroutine) may be checked by applying the following identity:

$$(AQ)^T(AQ) = Q^T(A^T(AQ)) ,$$

where Q represents the input, A denotes any tangent linear operator and A^T denotes the corresponding adjoint operator. If the above identity holds, the adjoint code is correct for the corresponding tangent linear code.

Care must be exercised when carrying out the adjoint check since the present numerical forecast model is very complicated and detailed, especially when the physical processes are included. For instance, the FSU GSM divides the terrain as land, ocean, land with snow, and ocean with ice, there are many combinations of sky conditions in the radiation processes, and most importantly, a large number of on-off switches specify different trajectories under different conditions. Hence, a complete set of data should be chosen to serve for the purpose of the adjoint check in order to ensure that every route is being examined.

Even though each subroutine passes the adjoint check separately, errors may still be introduced at the stage where the subroutines are linked together. Therefore, the adjoint check should be applied again once all the subroutines are linked together. It is necessary that the adjoint check of the integration of the whole model be carried out. The nonlinear normal mode initialized 18-hour forecast starting from 12UTC June 24, 1994 ECMWF analysis data is utilized to perform the whole model adjoint

check for 1-hour integration (3 time-steps) by using the above identity and the full physics package adjoint check simultaneously by using

$$(X, AY) = (A^T X, Y),$$

where X and Y denote the inputs of the adjoint code and the tangent linear code respectively. The zonal mean value serves as the initial condition of the nonlinear model, while the deviation is used as the initial condition for the tangent linear model. The results we got are accurate to 12 digits on a CRAY J916.

The gradient check is carried out to verify the correctness of the whole adjoint model. Given a small perturbation $\alpha \mathbf{h}$ to the initial conditions \mathbf{X}_0 , where α is a small scalar and \mathbf{h} is a vector, the cost function may then be expanded by using the Taylor expansion

$$J(\mathbf{X}_0 + \alpha \mathbf{h}) = J(\mathbf{X}_0) + \alpha \mathbf{h}^T \nabla J(\mathbf{X}_0) + o(\alpha^2),$$

i.e.,

$$\phi(\alpha) = \frac{J(\mathbf{X}_0 + \alpha \mathbf{h}) - J(\mathbf{X}_0)}{\alpha \mathbf{h}^T \nabla J(\mathbf{X}_0)} = 1 + o(\alpha), \quad (3.81)$$

for small α but not too close to machine accuracy, the value of $\phi(\alpha)$ should be close to unity if the gradient is correct. All terms in the cost function are of approximately the same order of magnitude. Since the gradient components of the cost function with respect to different control variables may differ by several orders of magnitudes from each other, the vector \mathbf{h} here is taken as $\mathbf{h} = \mathbf{S}^2 \nabla J$ as in Tsuyuki (1996b) so that the small perturbation is of the same order of magnitude for each variable. In our case, \mathbf{S} is a diagonal scaling matrix with $\mathbf{S}_\zeta, \mathbf{S}_D, \mathbf{S}_{T-T_d}, \mathbf{S}_{ln(P_s)}$ and \mathbf{S}_{T_v} as

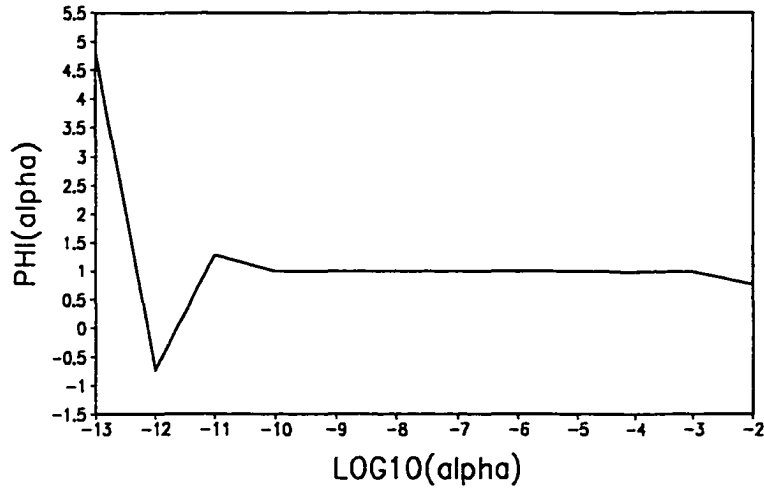


Figure 3.3: Variation of $\phi(\alpha)$ with respect to $\log\alpha$.

submatrices. The diagonal elements are $10^{-5}s^{-1}$, $10^{-5}s^{-1}$, $5K$, 1.5×10^{-2} and $10K$ for \mathbf{S}_ζ , \mathbf{S}_D , \mathbf{S}_{T-T_d} , $\mathbf{S}_{ln(P_s)}$ and \mathbf{S}_{T_v} respectively, so that each component is of order unity.

We present here the result for the gradient check in Figure 3.3. The integration period is six hours from 06UTC June 25, 1994, to 12UTC June 25, 1994 and model generated observations are used. The initial guess \mathbf{X}_0 is set to be the initial condition to which a small random perturbation is added on the Gaussian grids. It is shown that the value of $\phi(\alpha)$ approaches unity when α varies from 10^{-3} to 10^{-10} .

Once the values of cost function J and its gradient with respect to the control variables are available, the minimal value of the cost functional with respect to the

control variables is obtained by applying iteratively an efficient large-scale unconstrained minimization algorithm until a suitable convergence criterion is satisfied (i.e., $\| \nabla J \| \leq \epsilon$).

3.4.3 Notational convention for variables and subroutines used in the adjoint model

The same variable name is employed for the model state variable in the nonlinear forward model as that used for the adjoint variable in the adjoint model. The same common block name is also used for both the nonlinear forward model and the adjoint model.

The variable name of the basic state in the adjoint model is denoted by the same name as in the nonlinear forward model with a suffix "9". Attention should be paid to a special case when a basic state variable is redefined, usually, a suffix "8" is given to the redefined basic state variable.

The name of the adjoint subroutine is the corresponding nonlinear subroutine name with a prefix ADJ. For instance, the nonlinear subroutine SFLX has a corresponding adjoint code ADJSFLX.

CHAPTER 4
BASIC FORMALISM OF 4-D VAR

The mathematical basis of variational data assimilation involves optimizing a cost function subject to a set of constraints, i.e., the governing equations and boundary conditions. In optimal control theory, the optimal values of the control variables (initial conditions, model parameters or boundary conditions) can be found using the large-scale unconstrained minimization algorithm provided information about the cost function and its gradient with respect to the control variables is available.

The 4-D VAR data assimilation determines the model trajectory evolution which minimizes a cost function. The general cost function can be defined as the following functional (Lorenc 1986) where the model serves as a strong/weak constraint:

$$\begin{aligned}
 J(\mathbf{X}_0) = & \frac{1}{2} \sum_{n=1}^N (\mathbf{Z}_n - \mathbf{Z}_n^{obs})^T \mathbf{W} (\mathbf{Z}_n - \mathbf{Z}_n^{obs}) \\
 & + \frac{1}{2} \sum_{k=1}^M \sum_{m=1}^M \phi_m^T \mathbf{Q}_{m,k}^{-1} \phi_k \\
 & + \frac{1}{2} (\mathbf{X}_0 - \mathbf{X}_b)^T \mathbf{B}^{-1} (\mathbf{X}_0 - \mathbf{X}_b) \\
 & + \text{gravity wave penalty}
 \end{aligned} \tag{4.1}$$

with the forecast model \mathbf{G} and a post-processing operator \mathbf{H} that maps the model variables to the observations defined by

$$\mathbf{X}_m = \mathbf{G}(\mathbf{X}_{m-1}) + \phi_m \tag{4.2}$$

$$\mathbf{Z}_n = \mathbf{H}_n(\mathbf{X}_m) + \epsilon_n \tag{4.3}$$

where the superscript T stands for a transpose, obs denotes observations distributed over some space and time interval, b denotes a background value, the index n represents observational times, and indexes m and k are model time steps. \mathbf{X}_0 is the control variable, representing the initial state of the model or other model parameters; $\mathbf{X}(t)$ is a vector containing all model variables. \mathbf{W} is a weighting matrix. Generally, it can be taken as the inverse covariance matrix of the observation errors. Matrices \mathbf{B} and \mathbf{Q} are background and model error covariances, respectively. The model error correction term ϕ_m accounts for the model error growth from time t_{m-1} to time t_m . For simplicity, the observational error ϵ_n can be considered to be stationary and white in space and time, with the mathematical expectation equal to $\langle \epsilon_n \epsilon_k^T \rangle = \mathbf{W}^{-1} \delta_{n,k}$. In our experiments, we neglect ϵ_n in Equation 4.3. That is, the transformation matrix \mathbf{H} is taken as a strong constraint. Moreover, the model is assumed to be perfect, i.e., the forecast model is also applied as a strong constraint, and the background term is neglected. In the following, we present a continuous form of 4-D VAR data assimilation formalism.

Suppose the cost function measures the sum of the discrepancies between the observations and the model forecasts in the following way:

$$J(\mathbf{X}_0) = \frac{1}{2} \int_0^{t_R} (\mathbf{H}(\mathbf{X})(t) - \mathbf{Z}^{obs}(t))^T \mathbf{W} (\mathbf{H}(\mathbf{X})(t) - \mathbf{Z}^{obs}(t)) dt \quad (4.4)$$

Almost all large-scale unconstrained minimization algorithms require the user to supply the values of the cost function J and the gradient of the cost function with respect to the control variables. The value of cost function J can be obtained by integrating the forecast model forward, while the gradient of the cost function can

be calculated most efficiently through the deployment of the adjoint method, i.e., integrating the adjoint model backwards in time. For the purpose of the following discussion, the governing equation of a numerical model will be written as

$$\frac{\partial \mathbf{X}}{\partial t} = \mathbf{F}(\mathbf{X}, t) \quad (4.5)$$

$$\mathbf{X}(0) = \mathbf{X}_0 \quad (4.6)$$

where \mathbf{F} is the nonlinear operator matrix. The values of $\mathbf{X}(t)$ can be obtained by integrating the model from the initial condition \mathbf{X}_0 . The perturbation variables may be obtained as the solution of the tangent linear model:

$$\frac{\partial \delta \mathbf{X}}{\partial t} = \left[\frac{\partial \mathbf{F}}{\partial \mathbf{X}} \right](\mathbf{X}, t) \delta \mathbf{X} \quad (4.7)$$

$$\delta \mathbf{X}(0) = \hat{\mathbf{U}} \quad (4.8)$$

where $\delta \mathbf{X}$ is the perturbation vector, \mathbf{X} is the model state vector, and $\hat{\mathbf{U}}$ is a small perturbation of the initial conditions. For the definition of the adjoint operator, let us consider two Hilbert spaces, E and F , with inner products denoted by $(\cdot, \cdot)_E$ and $(\cdot, \cdot)_F$ respectively. Let $Y \rightarrow AY$ be a continuous linear operator from E into F . There exists a unique continuous linear operator A^* from F into E such that the following equality between inner products holds for any Y belonging to E and any X belonging to F :

$$(X, AY)_F = (A^* X, Y)_E$$

where A^* is called the adjoint operator of A .

In the finite-dimensional case, if (\cdot, \cdot) represents the Euclidean inner product, the matrix associated with A^* is simply A^T the complex conjugate transpose operator of

A. Since a small perturbation $\delta\mathbf{X}(0)$ will result in a change in the cost function, the directional derivative of the cost function J in the $\delta\mathbf{X}(0)$ direction is expressed as,

$$J'(\delta\mathbf{X}(0)) = \int_0^{t_R} \left([\nabla_{\mathbf{X}}\mathbf{H}]^T \mathbf{W}(\mathbf{H}(\mathbf{X})(t_r) - \mathbf{Z}^{obs}(t_r)), \delta\mathbf{X}(t_r) \right) dt \quad (4.9)$$

Introducing the adjoint equation

$$-\frac{\partial \mathbf{S}}{\partial t} - \left[\frac{\partial \mathbf{F}}{\partial \mathbf{X}} \right]^T \mathbf{S} = [\nabla_{\mathbf{X}}\mathbf{H}]^T \mathbf{W}(\mathbf{H}(\mathbf{X})(t_r) - \mathbf{Z}^{obs}(t_r)) \quad (4.10)$$

$$\mathbf{S}(t_R) = 0 \quad (4.11)$$

where the variable \mathbf{S} denotes the adjoint variable, the right hand side of Equation 4.10 is called the forcing term. Then, the gradient of the cost function with respect to the control variables, here taken to be the vector of initial conditions, is given as

$$\nabla_{\mathbf{x}_0} J = \mathbf{S}(0) \quad (4.12)$$

Therefore, the gradient of the cost function can be obtained by integrating the adjoint model backward in time from the final time step to the initial time step with a proper forcing term consisting of the difference between values of forecast and observation (measured at the observation time and space location) when an observation is encountered.

Once the values of cost function J and its gradient with respect to the control variables are available, the optimal initial conditions can be obtained by applying a carefully chosen robust large-scale unconstrained minimization algorithm. Among such algorithms, the limited-memory quasi-Newton and truncated Newton methods were found to be most efficient in atmospheric sciences (see Navon 1992a, 1992b,

Zou et al. 1993a, Wang et al. 1997). The algorithm used in this study is Liu and Nocedal's Limited-memory quasi-Newton algorithm, namely the L-BFGS method (Liu, et al. 1989).

4.1 The minimization algorithm

Part of the 4-D VAR approach consists of minimizing the cost function J directly by an iterative unconstrained minimization algorithm using first-order derivative information of the cost function with respect to the control variables. Two classes of minimization algorithms are most commonly used for large-scale unconstrained minimization problems. The two algorithms are limited-memory quasi-Newton (LMQN) and truncated Newton methods. Limited-memory quasi-Newton methods can be viewed as the extensions of conjugate-gradient methods. They are developed to combine the convergence properties of the quasi-Newton methods and the low requirements of conjugate-gradient methods associated with the evaluation, storage and inversion of the Hessian. Truncated Newton methods on the other hand attempt to preserve the rapid quadratic convergence rate of Newton methods while keeping storage and computational requirements feasible for large-scale applications. Navon and Legler (1987) compared a number of different conjugate-gradient and limited-memory quasi-Newton methods for problems in meteorology and concluded that the Shanno-Phua (1980) limited-memory quasi-Newton algorithm was the most appropriate for their tests. Liu and Nocedal (1989) showed that the L-BFGS method is one of the best limited-memory quasi-Newton methods available to date. Navon (1992a), Navon(1992b) and Zou et al. (1993a) further compared four limited-memory

quasi-Newton methods and two truncated Newton methods. Their results showed that the L-BFGS method of Liu and Nocedal (1989) had the best overall performance. A review of several LMQN methods was presented in their paper. The L-BFGS method of Liu and Nocedal (1989) will be used in our study. For applications of the truncated Newton methods see Wang et al. (1995) and Wang et al. (1997).

The basic procedure of the limited-memory quasi-Newton methods for minimizing $J(\mathbf{X})$, $\mathbf{X} \in \mathfrak{R}^N$ is described below:

- Step 1. Starting with an initial guess of \mathbf{X}_0 and a positive definite initial approximation to the inverse Hessian matrix H_0 (generally the identity matrix I is chosen).
- Step 2. Compute the gradient of J with respect to the control variable \mathbf{X}

$$g_0 = g(\mathbf{X}_0) = \nabla J(\mathbf{X}_0) ,$$

and set the search direction

$$d_0 = -H_0 g_0 .$$

- Step 3. For $k=0,1,2,\dots$, minimize $J(\mathbf{X}_k + \alpha_k d_k)$ with respect to $\alpha \geq 0$ to obtain \mathbf{X}_{k+1} as

$$\mathbf{X}_{k+1} = \mathbf{X}_k + \alpha_k d_k$$

where α_k is a positive scalar, the step-size obtained by a line search to satisfy sufficient decrease.

- Step 4. Compute

$$g_{k+1} = \nabla J(\mathbf{X}_{k+1}) .$$

- Step 5. Compute a new search direction

$$d_{k+1} = -H_{k+1} g_{k+1} .$$

- Step 6. Check whether the solution is convergent. If the convergence criterion

$$\| g_{k+1} \| \leq \epsilon \max (1, \| \mathbf{X}_{k+1} \|)$$

is satisfied, where ϵ is a user supplied small number, then the algorithm terminates with \mathbf{X}_{k+1} as the optimal solution; otherwise the process is repeated from Step 3.

For the line search a unit step length is always tried first. A line search using cubic interpolation is applied only if the Wolfe condition is not satisfied, which is expressed as

$$J(\mathbf{X}_k + \alpha_k d_k) \leq J(\mathbf{X}_k) + \beta' \alpha_k g_k^T d_k$$

$$\left| \frac{\nabla J(\mathbf{X}_k + \alpha_k d_k)^T d_k}{g_k^T d_k} \right| \leq \beta$$

where $\beta' = 0.0001$ and $\beta = 0.9$. A more accurate line search may be performed by using a small value for β . The first inequality is designed to ensure that the function is reduced sufficiently, while the second is used to prevent the step lengths from being too small.

4.2 Scaling

It is well-known that the condition number of the Hessian matrix, which is defined as the ratio of its largest to its smallest eigenvalues, determines the rate of convergence and sensitivity to round-off errors of descent algorithms for computing the minimum of the cost function. When the ratio is large, the matrix is ill-conditioned; when it is close to unity, the matrix is well conditioned. When the Hessian is ill-conditioned, the convergence rate is very slow and sometimes the minimization process might even fail.

Appropriately scaling variables may improve the condition number of the Hessian matrix. In the minimization algorithms, convergence tolerance and other criteria usually are based on the implicit definition of “small” and “large”, hence variables with widely varying orders of magnitude may cause difficulties. There is no general rule to determine the best scaling factors for all minimization problems, and it is problem dependent. A basic rule of scaling is to convert the variables from the physical units to computational units during the minimization process so that the variables of the scaled problem are of similar magnitude and of order unity in the region of interest. A simple transformation commonly used is of the form

$$x = Dy$$

where $\{x_j\}$ are the original variables, $\{y_j\}$ are the transformed variables, and D is the constant diagonal matrix, whose j -th diagonal element may be set to a typical value of the j -th variable. The gradients of the cost function are also scaled. The original gradients g , the transformed gradients g_y , the original Hessian H , and the

transformed Hessian H_y are related by

$$g_y = Dg$$

$$H_y = D^T H D$$

Thus we can see the effect of the transformation on the Hessian. Appropriate scaling can significantly alter the convergence rate of the minimization algorithm. Further refinement can be done by utilizing a preconditioning process (Yang, et al. 1996, Zupanski 1996, Axelsson 1994).

In this study, the scaling constants for different variables are calculated following the method of Navon et al. (1992c):

$$D_{ii} = \frac{1}{2} \max_{i,j,k} |\zeta_{i,j,k}^{obs}(t_0) - \zeta_{i,j,k}^{obs}(t_R)| \quad (4.13)$$

and similarly for the other variables.

4.3 The twin experiment

A twin experiment was carried out using the FSU GSM and its full-physics adjoint model to ensure that the assimilation system is properly constructed. For such an experiment, one knows in advance the exact solution, and the minimum value of the cost function is zero. However, due to the high nonlinearity of the model including the full physical processes, the convergence rate is expected to be much slower than that of the adiabatic version, and the cost function may have multiple minima. This can be seen by studying the convexity of the cost function. For a simplified cost

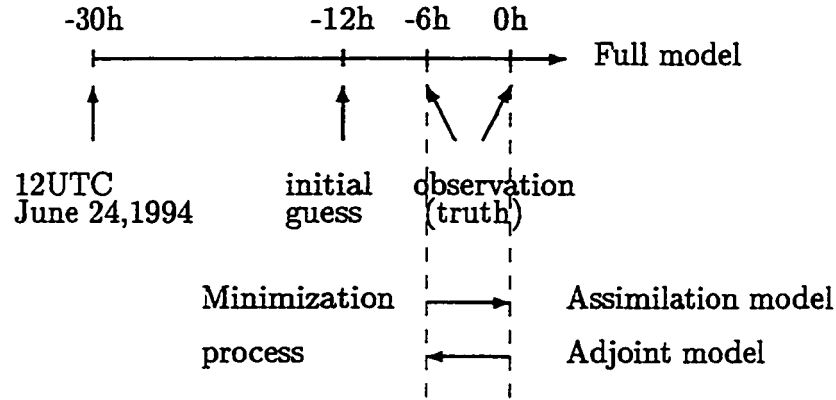


Figure 4.1: Schematic illustration of the twin experimental design

function defined as

$$J = \frac{1}{2} (\mathbf{X} - \mathbf{X}^{obs})^T W (\mathbf{X} - \mathbf{X}^{obs}) \quad (4.14)$$

its Hessian matrix is expressed as,

$$H = (\nabla_{\mathbf{x}_0} F)^T W (\nabla_{\mathbf{x}_0} F) + (\nabla_{\mathbf{x}_0}^2 F)^T W (\mathbf{X} - \mathbf{X}^{obs}) \quad (4.15)$$

where the weighting matrix W is symmetric and semipositive definite, and the second term is due to the nonlinearity of the model F . Due to the existence of the second term the Hessian matrix can not be guaranteed to be positive definite. The cost function may have several relative minima and maxima as well as saddle points. Therefore, the retrieved solution may not be unique. In such cases, a regularization approach may be used (Tichonov, 1977). The quality of the retrieved optimal initial condition depends greatly on the initial guess of the initial condition. More detailed structure of the initial guess will be necessary for obtaining a good result.

The FSU GSM was integrated 24 hours from the initialized ECMWF analysis at 12UTC June 24, 1994, and 12UTC June 25, 1994 was set to be the time level

$t=-6$ h. The assimilation window is set to be 6 hours from 12UTC June 25, 1994 to 18UTC June 25, 1994. The observation fields are generated by the full-physics nonlinear model and are assumed to be available at the beginning and the end of the assimilation window at each Gaussian grid point. The 18h-forecast starting from the initialized ECMWF analysis at 12UTC June 24, 1994, i.e., the forecast at 06UTC June 25, 1994 was taken as the initial guess of the model initial condition. For this T42L12 version of FSU GSM, the control variable vector consists of the initial conditions of vorticity, divergence, dewpoint depression, the logarithm of the surface pressure and the virtual temperature. Its dimension is $128 \times 64 \times (3 \times 12 + 10 + 1) = 385024$. Both the forward nonlinear model and the adjoint model used in the following experiments include the full physical processes.

The cost function used in this experiment is defined to assume the following form

$$J(\mathbf{X}_0) = \frac{1}{2} \sum_{n=0}^2 (\mathbf{X}_n - \mathbf{X}_n^{obs})^T \mathbf{W}_x (\mathbf{X}_n - \mathbf{X}_n^{obs}) \quad (4.16)$$

where *obs* denotes the observational data. The diagonal elements of the weight matrix \mathbf{W} with \mathbf{W}_ζ , \mathbf{W}_D , \mathbf{W}_{T-T_d} , $\mathbf{W}_{\log P_s}$, \mathbf{W}_{T_v} being the block submatrices are taken as the inverse of the square of the maximum difference of each observational variable between the two time level observations.

Fig. 4.2 displays the variations of the cost function and the gradient norm with respect to the number of iterations in the minimization process. The cost function value decreases two orders of magnitude after 60 iterations with 70 function calls, and we observe that it decreases to 22.7% of its original value after 20 iterations with 21 function calls. The gradient norm decreases to 16.8% of its original value in

60 iterations. This pattern corresponds to the fact that most of the decrease in the cost function occurs during the first minimization iterations (see also Navon et al. 1992c).

It is worthwhile to consider the difference fields between the retrieved and the reference (observational) fields before and after the minimization process, since these difference fields measure the ability of the 4-D VAR data assimilation to retrieve the observational fields. Fig. 4.3 shows the difference fields of divergence, vorticity, temperature and the logarithm of the surface pressure between the retrieved and the reference (observational) fields at the beginning of the assimilation window after the minimization process was carried out. Comparing these with the same difference fields (Fig. 4.4) prior to the minimization process, it is observed that after the minimization the maximum difference values are reduced by at least one order of magnitude in all the difference fields, namely, those of divergence, vorticity, temperature and the logarithm of the surface pressure.

The RMS errors of the retrieved initial conditions and the initial guesses of initial conditions are shown in Fig. 4.5. All the control variables are improved throughout the entire range of vertical levels. The RMS error of the surface variable, the logarithm of the surface pressure, decreases from $0.16956\text{E-}02$ to $0.10207\text{E-}03$. Having obtained the optimal initial conditions at $t=0$, we integrate the forecast model for 6 hours from the retrieved initial conditions to obtain the analysis field at the end of the assimilation window. The RMS error results are presented in Fig. 4.6. A similar trend to that found for the control variables is evident and the RMS error of the logarithm of the surface pressure decreases from $0.15543\text{E-}02$ to $0.21654\text{E-}03$. The

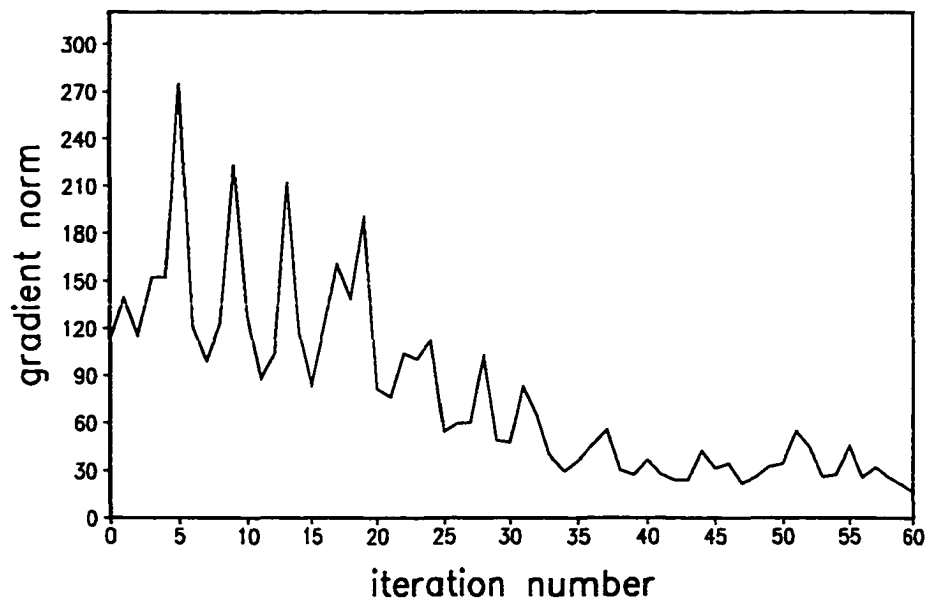
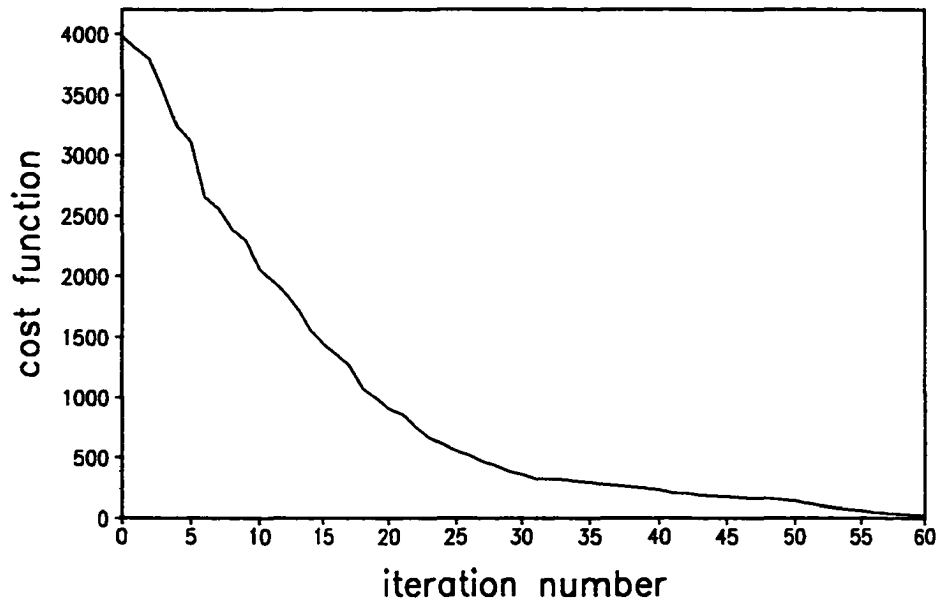


Figure 4.2: Variations of the cost function and the gradient norm with respect to the iteration number of the twin experiment.

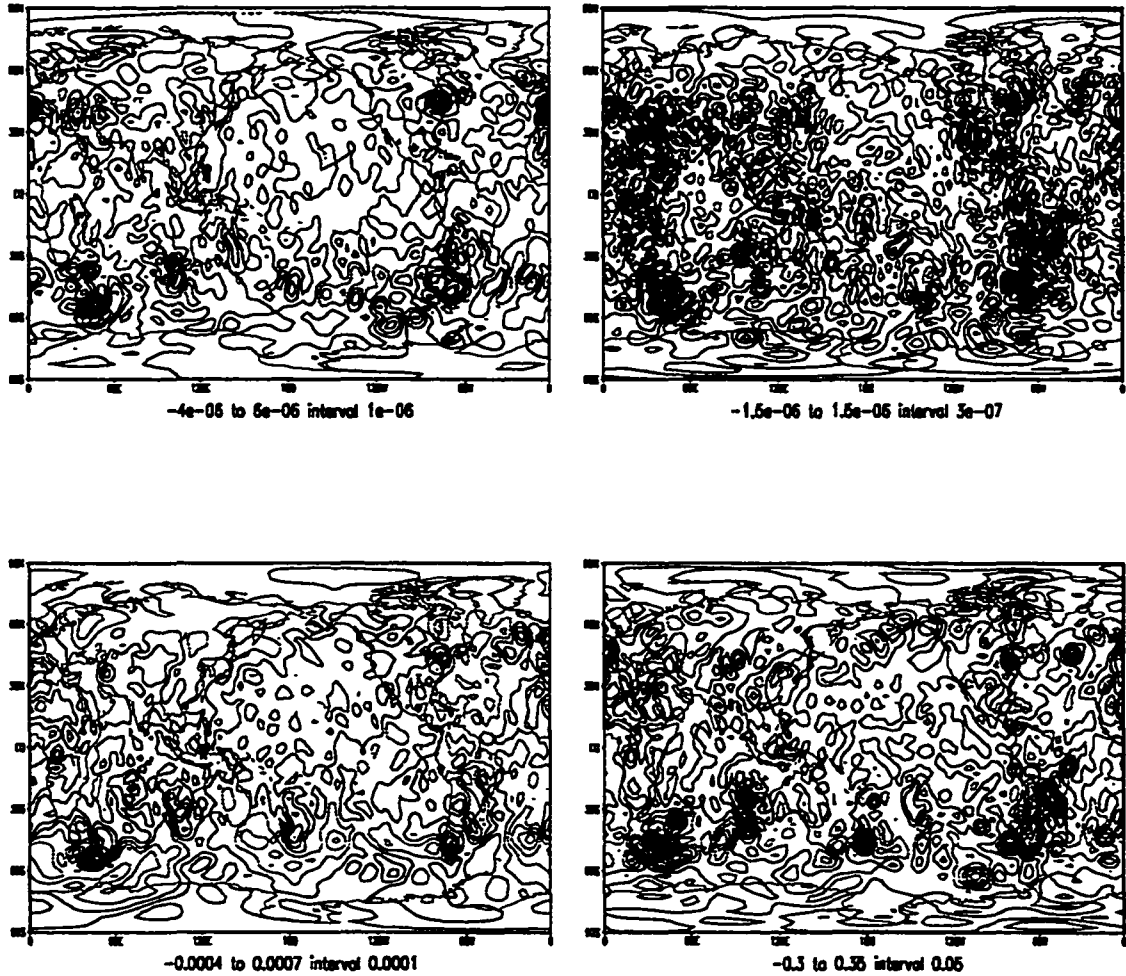


Figure 4.3: Difference fields of vorticity (top left), divergence (top right), logarithm of surface pressure (bottom left), temperature (bottom right) between the retrieved and the reference fields at level 8 at the beginning of the assimilation window after the minimization process was performed.

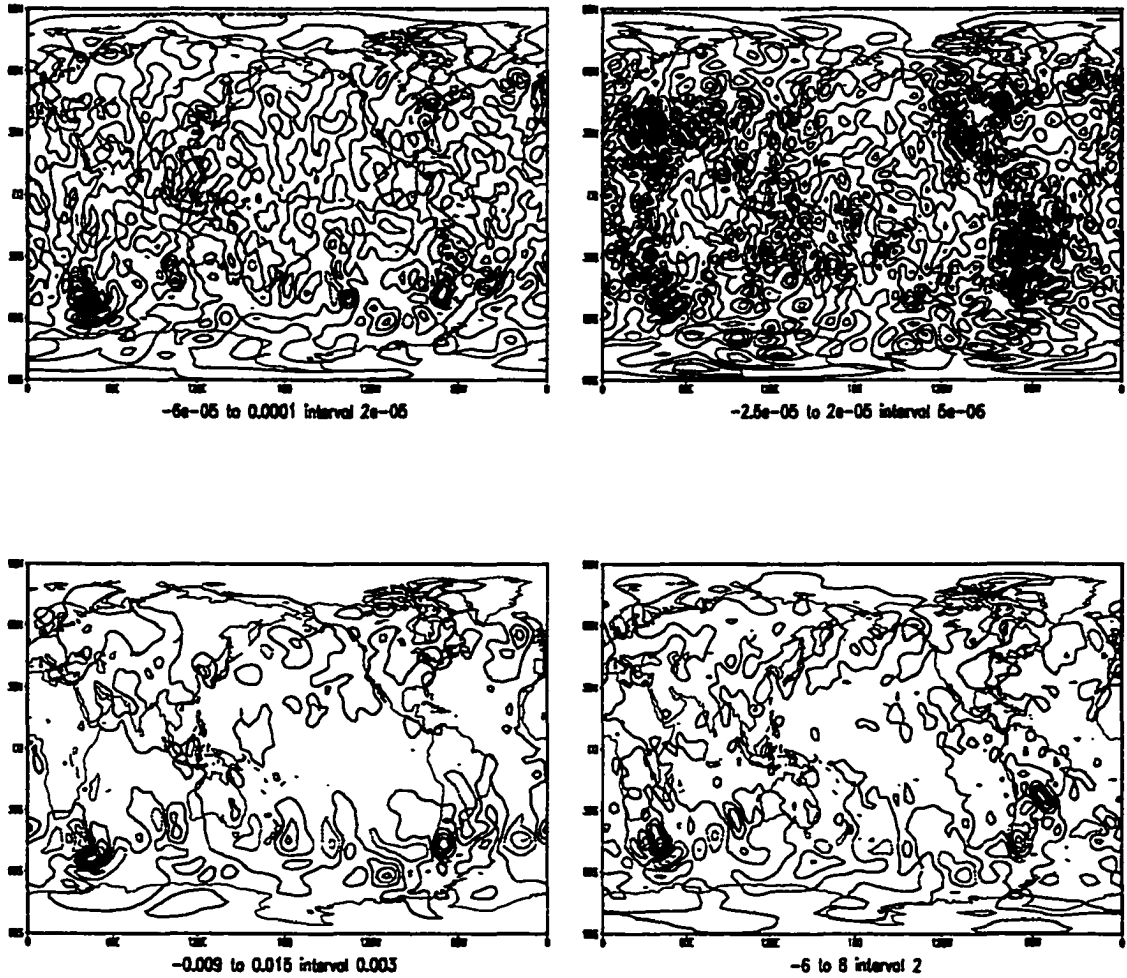


Figure 4.4: Difference fields of vorticity (top left), divergence (top right), logarithm of surface pressure (bottom left), temperature (bottom right) between the retrieved and the reference fields at level 8 at the beginning of the assimilation window before the minimization process was performed.

RMS error of every variable decreases by one order of magnitude at almost all the vertical levels.

In this chapter, we presented the basic formalism of 4-D VAR data assimilation using the full-physics adjoint in a twin experiment. A reasonable reduction in the cost function was achieved, and the quality of the retrieved initial conditions was found to be satisfactory. This experiment demonstrated the numerical feasibility of 4-D VAR data assimilation with the full-physics adjoint model of the FSU GSM to retrieve the initial conditions. Its results indicated that the assimilation system was properly constructed. In the following chapters, the 4-D VAR data assimilation system was applied to carry out numerical experiments on variational data assimilation, adjoint parameter estimation and sensitivity analysis using ECMWF analysis data.

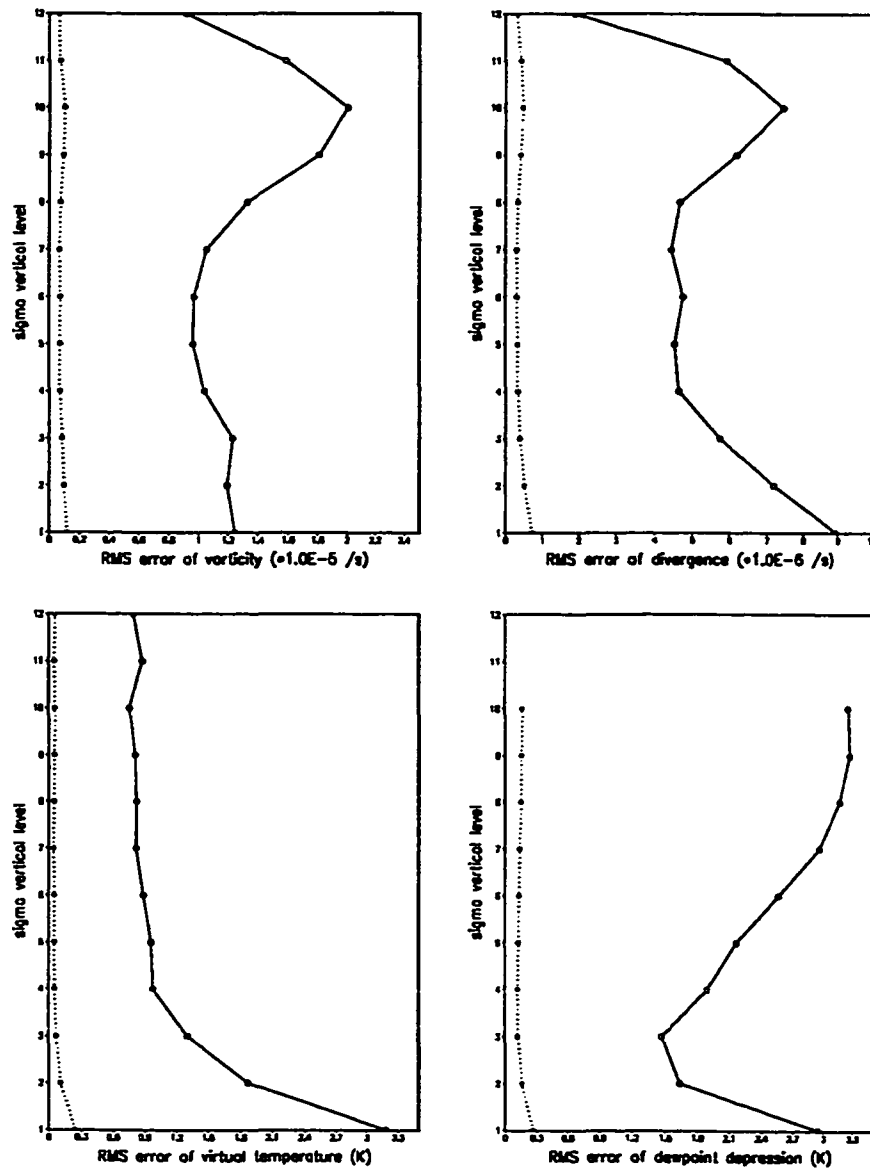


Figure 4.5: RMS errors of the retrieved initial conditions (dot line) and the initial guess (solid line) in the twin experiment.

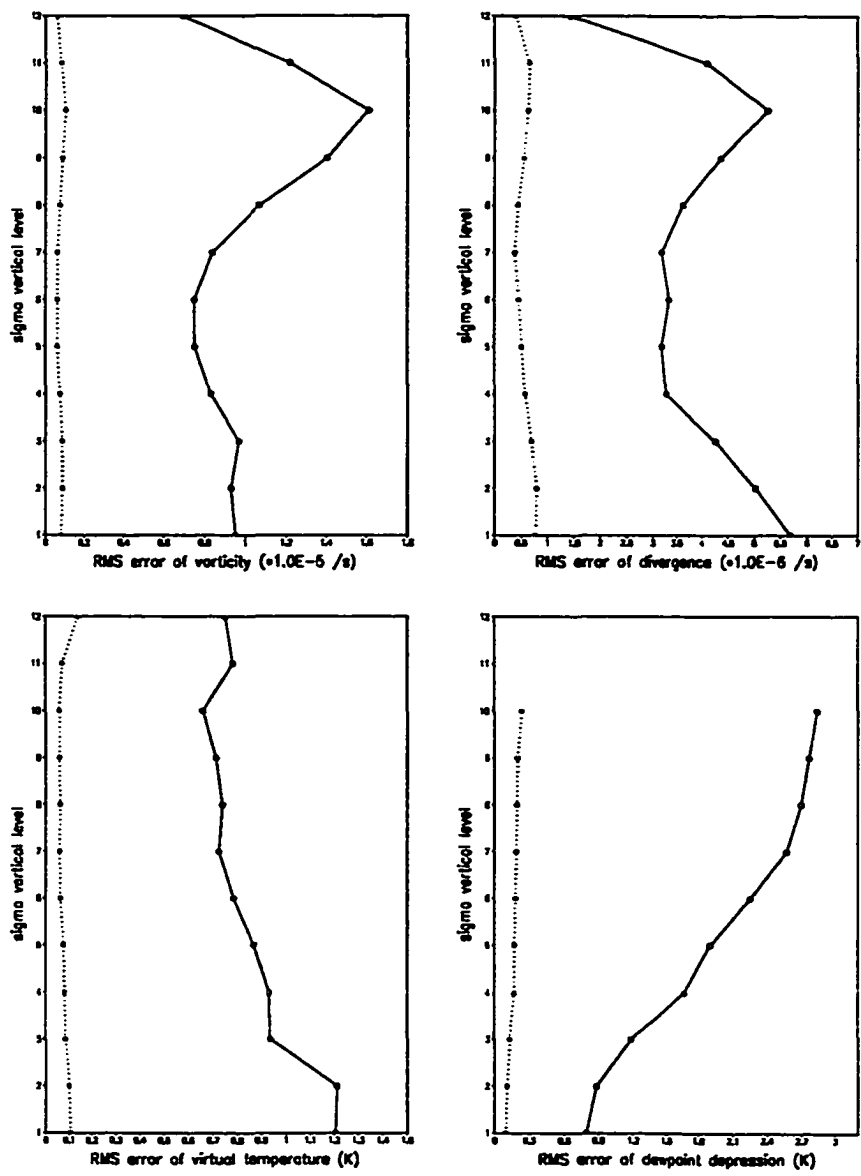


Figure 4.6: RMS errors of the analysis fields (dot line) and the initial guess at the end of the assimilation window (solid line) in the twin experiment.

CHAPTER 5

**IMPACTS OF THE OPTIMAL INITIAL CONDITIONS AND THE
OPTIMALLY IDENTIFIED KEY PARAMETERS ON THE
PERFORMANCE OF THE FSU GSM**

5.1 Characteristics of the parameters

One of the objectives of this dissertation is to optimally identify several parameters of importance in the various physical packages, an endeavor made possible by the availability of the adjoint of the full physics version of the FSU GSM. Parameter estimation refers to the determination of the unknown parameters in the model from observed data such that the predicted response of the model is close in some sense to the process observations. As we know, many parameters in the NWP model are empirically determined. The selection of the set of important parameters to be estimated can be made dependent on experience with the FSU GSM performance, or it can be determined using a relative sensitivity analysis by ranking a set of chosen parameters in the order of their relative sensitivities to selected model responses. This is explained in greater detail in APPENDIX A. In this study, three parameters were chosen to be optimally identified based on numerical experience with the FSU GSM. These three parameters are the bi-harmonic horizontal diffusion coefficient κ , the ratio, γ , of the transfer coefficient of moisture to the transfer coefficient of sensible heat, and the Asselin filter coefficient FC .

The horizontal diffusion term is usually incorporated in a numerical weather prediction model to parameterize the effects of motions on the unresolved scales and to inhibit spectral blocking, the growth of the amplitude at small scales in the dynamic model variables due to the accumulation of energy in the shorter wave range. It is also employed to eliminate the aliasing effect (Phillips 1959). When a solution is obtained on a grid of spacing Δx the smallest wavelength that can be resolved is $2\Delta x$. The energy associated with wavelengths shorter than $2\Delta x$ reappears associated with longer wavelengths. This phenomenon is referred to as *aliasing* (Hamming 1973). Unfortunately, the aliased shortwave contribution to the solution distorts the true longwave solution and may even cause instability (referred to as nonlinear instability) (Phillips 1959) when very long time integrations are made. The presence of any dissipation, physical or computational, can attenuate the amplitude of the short wavelengths very significantly. In this case the errors introduced by aliasing are minimal. MacVEAN (1983) showed that without dissipation, integrations exhibited physically unrealistic features after several days even with very high mesh resolution, indicating the crucial role played by the dissipation in the non-linear baroclinic development. Considerable efforts have been made by various groups in tuning the dissipation parameterizations in their general circulation or forecast models. For instance, Phillips (1956), Smagorinsky (1965), Lilly (1965), Leith (1965) and Richard (1965) applied eddy diffusion terms in their numerical models. Navon (1969) included the lateral viscosity in a two level general circulation model and computed a 62 day integration, comparing its impact to that of using the Matsuno dissipative scheme. Kanamitsu, et al. (1983, 1989) and Gordon, et al. (1982) employed a bi-harmonic

horizontal diffusion in their experiments. Presently, the bi-harmonic horizontal diffusion is used worldwide in NWP models due to its better scale selectivity. One drawback, however, is its lack of a sound physical foundation. Some other horizontal diffusion schemes are also employed, such as the scheme developed by Leith (1971) based on turbulence theory which is now implemented in the NCEP spectral model (Kanamitsu, et al., 1991).

The bi-harmonic horizontal diffusion, $\kappa \nabla^4$, is used for vorticity, divergence, dewpoint depression and virtual temperature in the FSU GSM to selectively control small-scale noise without affecting large scales. The e -folding diffusive decay time at total wavenumber n is given by

$$\tau(n) = \frac{1}{\kappa} \frac{a^4}{n^2(n+1)^2} \quad (5.1)$$

where a is the radius of the earth. The physical significance of the diffusion coefficient κ is not directly intuitive, and its effect may be better understood in terms of the time scale τ at the smallest spatial scale resolved. The model dissipation should remove energy from the end of the spectrum at a rate sufficient to prevent a spurious accumulation of energy there, while not affecting the medium and large scales. In the GFDL spectral model, the coefficients of the eddy diffusion for ∇^4 were determined by trial and error, using the quality of the medium range 500 hPa geopotential height forecast as a criterion (Gordon, et al. 1982). They used values of $1 \times 10^{16} m^4 s^{-1}$ and $2.5 \times 10^{16} m^4 s^{-1}$ for T30 leading to values of τ of about 53 and 21 hours, respectively (based on Equation 5.1). The value used in FSU Global Spectral Model T42 is $6 \times 10^{15} m^4 s^{-1}$, yielding a τ of approximately 23 hours. The effects of a simple second-

order, constant-coefficient diffusion on model initial state variational retrieval was studied by Li and Droegemeier (1993) in the framework of a dry, three-dimensional Boussinesq convection model.

In addition to the horizontal diffusion, filters are also commonly used in numerical models to remove high frequency noise that cannot be resolved at the given model resolution. In the FSU GSM, a supplementary time filter of the form

$$\hat{F}(t) = F(t) + \alpha [\hat{F}(t - 1) - 2F(t) + F(t + 1)]$$

is used. The characteristics of this filter are described in detail by Asselin (1972). The frequency filter is an excellent damper for computational modes arising in leapfrog, centered implicit, and centered semi-implicit time integrations. Also, it discriminates well between frequencies. Therefore, with an adequately chosen coefficient α , this filter damps the spurious computational frequencies and a significant part of the spectrum of the external and internal gravity waves. The Rossby motions of comparable horizontal dimensions are much less affected due to their low frequency. This filter with $\alpha = 0.25$ removes or filters $2\Delta t$ waves and reduces the amplitude of $4\Delta t$ waves by one-half, but has little effect on longer-period waves, i.e. it acts as low-pass filter in time. However, despite the advantage of immediately suppressing the $2\Delta t$ -wave, values of α less than 0.25 are preferable since the stability condition requires a progressively smaller Δt as α increases. Moreover, repeated use of even a weak filter eventually dampens the lower frequencies (Haltiner and Williams 1980). Robert (1966) used this filter in a general circulation primitive-equation spectral model with centered differences to control the instability. The values he used are

$\alpha = 0.02$ and $\Delta t = 20$ min. A number of experiments carried out by Krishnamurti showed that $\alpha = 0.05$ is the best value for the Asselin filter for the model forecast. In this study, we will carry out an optimal parameter estimation experiment to obtain the optimal value of α . The lower bound of α is set to be zero, while its upper bound is set to be 0.1.

The third parameter considered is the ratio, γ , of the transfer coefficient of moisture to the transfer coefficient of sensible heat. This parameter arises from the parameterization of the surface fluxes in the boundary layer. Accurate heat and moisture flux parameterizations are very important since the surface heat flux and surface moisture flux exert a strong influence on the surface energy budget and precipitation rate. Similarity theory has successfully provided a framework for the description of the atmosphere surface layer, namely the lowest 50 m or so of the boundary layer in which the Coriolis force can be ignored and the fluxes can be assumed to be constant with height. The flux profiles and other properties of the flow are reasonably parameterized via this theory. However, certain empirical parameters or constants evolving from the theory need to be experimentally determined. For instance, the von Kármán constant and constants associated with the stability dependence of the flux-profile formulations must be determined empirically. In this study, however, we will not focus on the determination of the constants by fitting to the experimental observations. We will instead attempt to obtain an optimal ratio, γ , of the transfer coefficient of moisture to the transfer coefficient of sensible heat via a variational parameter identification approach in order to improve the model forecast skill. Dyer (1967) found that, over the range $0.02 < |z/L| < 0.6$, both the

transfer coefficient of sensible heat, ϕ_H , and the transfer coefficient of moisture, ϕ_Q , varied approximately as $|z/L|^{-\frac{1}{3}}$; For $|z/L| > 0.2$, ϕ_H was found to be proportional to $|z/L|^{-\frac{1}{2}}$, but insufficient data limited the value of the corresponding analysis for ϕ_Q . Since reasonable agreement was found between the ϕ_H and ϕ_Q data, many numerical weather prediction models adopt a simple relationship of the type $\phi_Q = \phi_H$, i.e., $\gamma = 1.0$. This is also the value used in the original FSU GSM. The specification of the γ value directly impacts upon the moisture flux.

5.2 The methodology of parameter estimation

5.2.1 Adjoint formulation

In this study, we attempt to perform optimal parameter estimation in a variational approach setting, i.e., to obtain an optimal value of the parameter α such that

$$J(\alpha^o) \leq J(\alpha) \quad \text{for all } \alpha$$

where J is a cost function that measures the discrepancy between the observations and the corresponding model forecast variables. Hence, the optimal parameter can be retrieved by fitting the model forecast fields to the observations.

Given bound constrained parameter, i.e., the parameter α satisfies $\alpha \in [a, b]$, where a and b denote the lower and upper bound respectively, the cost function for parameter estimation may assume the following form:

$$J(\mathbf{X}, \alpha) = \frac{1}{2} \int_{t_0}^{t_R} \langle W(\mathbf{X} - \mathbf{X}^{obs}), (\mathbf{X} - \mathbf{X}^{obs}) \rangle dt + \lambda g(\alpha) \quad (5.2)$$

where the vector α denotes the vector of model parameters, λ is the penalty coefficient, \mathbf{X} represents the state variable vector, and \mathbf{X}^{obs} the observation vector. The second term consists of a penalty function, which is defined as:

$$g(\alpha) = \begin{cases} \frac{1}{2} (x - b)^2 & \text{if } x \geq b \\ 0 & \text{if } a < x < b \\ \frac{1}{2} (x - a)^2 & \text{if } x \leq a \end{cases} \quad (5.3)$$

where $g(\alpha)$ is a function only of the violated constraints. The first derivative of this function is:

$$\frac{\partial g}{\partial \alpha} = \begin{cases} x - b & \text{if } x \geq b \\ 0 & \text{if } a < x < b \\ x - a & \text{if } x \leq a \end{cases} \quad (5.4)$$

Another type of penalty effective in transforming a constrained optimization problem into an unconstrained one is the barrier method or interior-point method which imposes a penalty for reaching the boundary of an inequality constraint. Typically, we will use a logarithmic barrier function of the form:

$$J(\mathbf{X}, \alpha) = \frac{1}{2} \int_{t_0}^{t_R} \langle W(\mathbf{X} - \mathbf{X}^{obs}), (\mathbf{X} - \mathbf{X}^{obs}) \rangle dt - \mu \sum_{i=1}^m \log(h_i(\alpha)) \quad (5.5)$$

where μ is the barrier coefficient and h is the constraint function. The barrier methods are strictly feasible methods, i.e., the iterates lie in the interior of the feasible region, and create a “barrier” keeping iterates away from boundaries of the feasible region (Nash and Sofer, 1996). Attention needs to be paid to the case where the Hessian becomes ill-conditioned as well as to the choice of the parameter μ .

There are two different purposes for the inclusion of the second term in Equations 5.2 or 5.5. The first is to ensure that the retrieved parameter lies within the constraint bounds, and a penalty term of the form in Equation 5.2 or a logarithm of the box constraints as in Equation 5.5 is efficient for this problem to transform the constrained minimization problem into a sequence of unconstrained minimization problem. The second purpose is to increase the convexity of the cost function by adding a positive value λ to the Hessian matrix, thereby increasing its positive-definiteness. Here, it is worth mentioning that it is not required that the parameter which is to be estimated appear explicitly in the cost function, i.e., the parameter may only appear implicitly through its dependence on the model independent variables.

Suppose that the forward model is given in the form

$$\frac{\partial \mathbf{X}}{\partial t} = \mathbf{F}(\mathbf{X}, \alpha, t) \quad (5.6)$$

Its corresponding tangent linear model is defined as

$$\frac{\partial \delta \mathbf{X}}{\partial t} = \left(\frac{\partial \mathbf{F}}{\partial \mathbf{X}} \right)_{\|(\mathbf{x}^b, \alpha^b)} \delta \mathbf{X} + \left(\frac{\partial \mathbf{F}}{\partial \alpha} \right)_{\|(\mathbf{x}^b, \alpha^b)} \delta \alpha \quad (5.7)$$

where b denotes the basic state. The adjoint model derived is expressed in the form

$$-\frac{\partial \mathbf{S}}{\partial t} - \left(\frac{\partial \mathbf{F}}{\partial \mathbf{X}} \right)^T \mathbf{S} = \mathbf{W}(\mathbf{X} - \mathbf{X}^{obs}) \quad (5.8)$$

where \mathbf{S} represents the adjoint variables. The gradients of the cost function with respect to the initial conditions and that of the parameter α are assuming the following form,

$$\nabla_{\mathbf{x}_0} J = \mathbf{S}(0) \quad (5.9)$$

$$\nabla_{\alpha} J = \int_{t_0}^{t_R} \left[\left(\frac{\partial F}{\partial \alpha} \right)^T \mathbf{S} \right] dt + \lambda \frac{\partial g}{\partial \alpha} \quad (5.10)$$

respectively. We notice here that the adjoint model where both parameters and initial conditions serve as the control variables assumes the same form as that where only the initial conditions serve as control variables. Hence, the problem of parameter estimation via the adjoint method when the number of parameters to be estimated is small does not result in a significant additional computational burden. We may expect that the parameter estimation process will provide us with both optimally determined parameters and initial conditions simultaneously. The gradient of the cost function with respect to both the initial conditions and the parameter is written as:

$$\nabla J = (\nabla_{\mathbf{x}_0} J, \nabla_{\alpha} J)^T \quad (5.11)$$

5.2.2 Ill-posedness, identifiability and stability issues

An issue of great practical importance in parameter estimation is the ill-posedness problem of parameter estimation (Tichonov et al. 1977). To address this problem, let Q be the set of parameters that guarantee that a chosen model equation has a solution $u(\alpha)$ and let \mathfrak{S} be the observation operator mapping from the solution space of the differential equation to the observation space Z . Composing these mappings we obtain the parameter-to-output mapping

$$\Phi : Q \rightarrow Z,$$

with $\Phi(\alpha) = \mathfrak{S} u(\alpha)$. The parameters are further restricted to a set of admissible parameters $\tilde{Q} \subset Q$ a function space over a domain Ω in R^n . Both Q and \tilde{Q} are

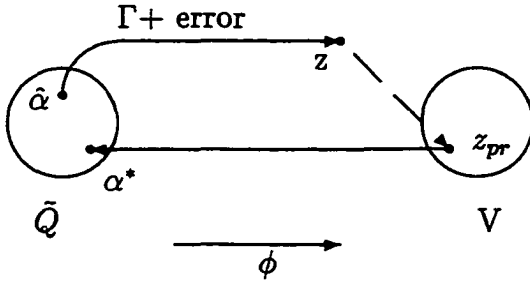


Figure 5.1: diagram of parameter estimation

considered as subsets of a normed linear space Q_1 and Z is a normed space as well. Let $z \in Z$ denote the observation of the process Γ depending on the parameter α which is to be estimated. Due to model and observation error, z may or may not lie in the attainable set V . The output least squares formulation for the determination of the “best” parameter α^* corresponding to the observation z is given by

$$\text{Minimize } |\Phi(\alpha) - z|_Z^2 \text{ over } \tilde{Q} .$$

It is useful to consider the diagram in Fig. 5.1.

Here $\hat{\alpha}$ stands for the actual physical parameter which, when corrupted by various errors leads to the observation z . It is useful to divide the output least squares (OLS) method into two steps, first finding a projection z_{pr} of z in V and second determining a preimage α^* of z_{pr} in \tilde{Q} such that $\Phi(\alpha^*) = z_{pr}$. Uniqueness of the OLS solution thus requires uniqueness of the projection of z onto V as well as injectivity of ϕ at α^* (i.e., $\Phi(\alpha) = \Phi(\alpha^*) = \bar{z}$ for some $\alpha \in \tilde{Q}$ implies $\alpha = \alpha^*$). Continuous dependence of α^* on z will hold if both these inverse operations are continuous.

The parameter α is identifiable with respect to \tilde{Q} if there exists a neighborhood \tilde{V} of the attainable set $V = \Phi(\tilde{Q})$ such that for every $z \in \tilde{V}$ there exists a unique solution $\alpha_z \in \tilde{Q}$ depending continuously on z ; and it is called stable at the local solution $\alpha_{\tilde{z}}$ with respect to \tilde{Q} if there exist neighborhoods $V(\tilde{z})$ of \tilde{z} and $U(\alpha_{\tilde{z}})$ of $\alpha_{\tilde{z}}$ and constants $K, \epsilon > 0$, such that for all $z \in V(\tilde{z})$ there exists at least one local solution $\alpha_z \in U(\alpha_{\tilde{z}})$ and every such local solution α_z satisfies

$$|\alpha_z - \alpha_{\tilde{z}}| \leq K |z - \tilde{z}|^{1/\epsilon}$$

The parameter is called stable if it is stable at every local solution.

Problems that are not identifiable and stable are said to be ill-posed. In case of ill-posedness, the numerically obtained parameter will differ according to the initial guess of the parameter, i.e., it is not stable under small changes in the initial guess, and there will be no reason for the obtained parameter to be close to the "true" parameter value. There is no general rule for uniqueness. It depends on the type of parameter to be estimated (distributed in space, state dependent), on the measurements and on the type of the equation. For constant parameters, there are generally more observations than unknowns so that the general situation is unique. It is possible, however, that some of the parameters are not very sensitive and adjust very slowly to their true values. The problem of identifying spatially-dependent parameters is, in general, both nonlinear and ill-posed, where a regularization approach is recommended (See Tichonov, et al., 1977; Navon 1997). Introducing a reflexive Banach space Q_c with norm $|\cdot|_c$ which is compactly embedded into Q_1 , and assuming $\tilde{Q} \subset Q$ is close and convex, we define $\tilde{Q}_c = \tilde{Q} \cap Q_c$ and assume that \tilde{Q}_c is not empty.

The regularized functional considered is of the form

$$\text{Minimize } |\Phi(\alpha) - z|^2 + \beta|\alpha|_c^2 \text{ over } \tilde{Q}_c$$

with regularization parameter $\beta > 0$. Adding a regularization term can require the solution to satisfy certain additional properties (smoothness) of the solution. The set of regularized solutions is precompact in Q_1 . The effect of convexification is reflected in that it gives a range of values for the regularization parameter β within which a continuous dependence of the solutions on the observation z holds.

5.3 Numerical experiments and results

5.3.1 Parameter estimation procedure and the results

In this study, the FSU Global Spectral Model and its full-physics adjoint model were employed to optimally identify the three parameters, namely, the bi-harmonic horizontal diffusion coefficient, the ratio γ of the transfer coefficient of moisture to the transfer coefficient of sensible heat, and the Asselin filter coefficient separately. A 6h assimilation window was used, from 0000UTC Sept. 3, 1996 to 0600UTC Sept. 3, 1996. The initialized ECMWF analysis data at 0000UTC Sept. 3, 1996 and 0600UTC Sept. 3, 1996 were taken as the observations during the 6h assimilation window period.

The algorithm implementing the parameter estimation procedure is carried out as follows:

- 1. The 6h forecasts starting from the initialized analysis at 1800UTC Sept. 2, 1996 was taken as the initial guess of the initial condition. We integrated

the full-physics FSU GSM 6 hours, then calculated the cost function using Equation 5.2. Since further study needs to be carried out to determine the observational error covariance, we simply took the inverse of the maximum square of the difference between the two time level observations as the weight matrix \mathbf{W} in Equation 5.2 (See Navon, et al., 1992c). The initial guess of α , the penalty coefficient value and the upper and lower bounds where the parameters may vary were specified here.

- 2. Integrate the full-physics adjoint model of the FSU GSM backward in time to obtain the gradient of J with respect to the control variable $\mathbf{Y} = (\mathbf{X}_0, \alpha)^T$,

$$g_0 = g(\mathbf{Y}) = (\nabla_{\mathbf{X}_0} J, \nabla_{\alpha} J)^T ,$$

and the search direction is given by

$$d_0 = -H_0 g_0 .$$

- 3. For $k=0,1,2,\dots$, minimize $J(\mathbf{Y}_k + \beta_k d_k)$ with respect to $\beta \geq 0$ to obtain \mathbf{Y}_{k+1} as

$$\mathbf{Y}_{k+1} = \mathbf{Y}_k + \beta_k d_k$$

where β_k is a positive scalar, the step-size being obtained by a line search so as to satisfy sufficient decrease (See Gill, et al., 1981).

- 4. Compute

$$g_{k+1} = \nabla J(\mathbf{Y}_{k+1}) .$$

- 5. Compute a new search direction

$$d_{k+1} = -H_{k+1} g_{k+1} .$$

- 6. Check whether the solution converges. If the convergence criterion

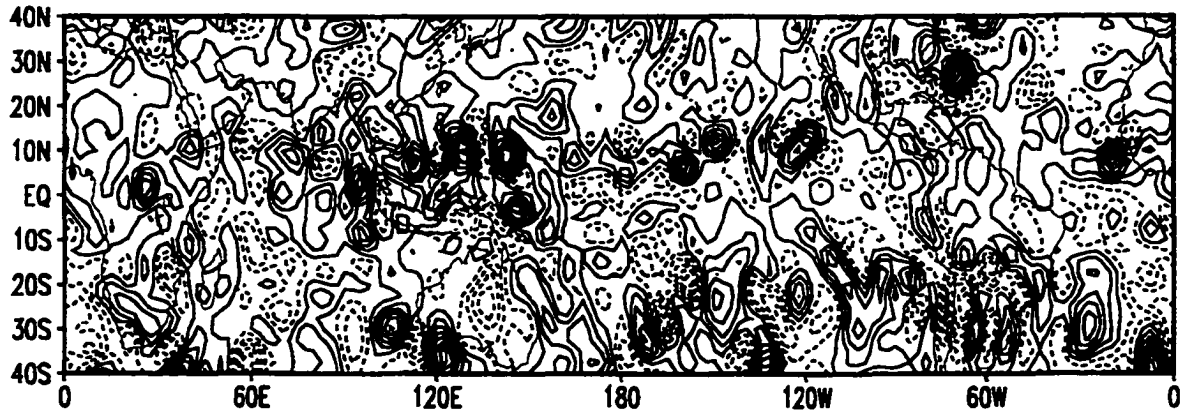
$$\| g_{k+1} \| \leq \epsilon' \max (1, \| Y_{k+1} \|)$$

is satisfied, where ϵ' is a small number supplied by the user, then the algorithm terminates with Y_{k+1} as the optimal solution. Otherwise, go back to Step 3.

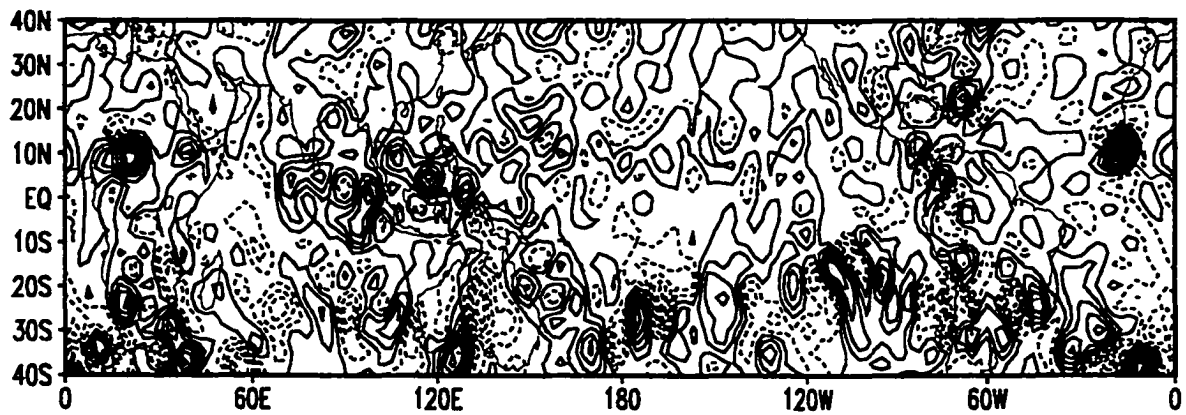
The 6h forecasts from the initialized analysis at 1800UTC Sept. 2, 1996, which serve as the initial guesses of the initial conditions, show important underestimates of the tropical divergence field, particularly in the Pacific (Fig. 5.2). The errors in this field were probably caused by the underestimation of the intensity of tropical convection in the course of the forecast.

The minimization procedure was terminated after 60 iterations, a number of iterations that yielded sufficient decrease in the cost function and its gradient for each experiment. At the end of the minimization procedure, both the optimal initial conditions and optimal value of the parameter were recovered.

The initial guess of the horizontal diffusion coefficient κ was taken to be $6.0 \times 10^{15} m^4 s^{-1}$ as it was used routinely in the T42L12 version of FSU GSM. The penalty parameter λ was taken to be 1.0×10^{-12} , the upper and lower bounds where κ varies were taken to be 3.0×10^{16} , i.e., five times the value used in the original forecast model, and 2.0×10^{15} , respectively. The variations of the cost function and the gradient norm with respect to the number of iterations are presented in Fig. 5.3.



(a)



(b)

Figure 5.2: The divergence fields at 200 hPa at 0000UTC Sept. 3, 1996: (a) the observation, (b) the initial guess. The contour interval is $5.0 \times 10^{-6} s^{-1}$.

We see that the cost function decreased to about 15.8% of its original value, while the norm of the gradient value decreased to 23.6% of its original value. Fig. 5.4 displays the evolution of the horizontal diffusion coefficient during the minimization procedure. This coefficient experienced a rapid increase until the 35th iteration, reaching its peak at the 44th iteration, then experienced a slight decrease. The optimal value obtained for the horizontal diffusion coefficient κ is 1.1124×10^{16} . This value is almost twice the value used in the original forecast model. Since the upper bound of the horizontal diffusion coefficient κ is taken as 3.0×10^{16} , i.e., five times the value used in the original forecast model, the optimally identified parameter value for κ is reasonable.

The initial guess (estimated value) of ratio of the transfer coefficient of moisture to the transfer coefficient of sensible heat, γ , was set to be 1.0 which is the value used in the original T42L12 version of FSU GSM. The penalty parameter λ was set to be 2.0×10^5 , while the upper and lower boundaries where γ may vary were taken to be 5.0 and 0.3, respectively. The initial guess (estimated value) of the Asselin filter coefficient FC was set to be 0.05 which is the value used in the original forecast model. The upper and lower boundaries for the variation of this parameter were taken as 0.1 and 0.0, respectively, and the penalty parameter λ was set to be 1.0×10^8 . Similar variations of the cost function and the gradient norm with respect to the number of iteration were obtained when the ratio γ of the transfer coefficient of moisture to the transfer coefficient of sensible heat and the Asselin filter coefficient FC were retrieved from the observations, respectively. The optimal FC value obtained is 0.0487 which is very close to the initial guess, indicating that the

initial guess was fairly good. The optimal parameter estimation for γ the ratio of the transfer coefficient of moisture to the transfer coefficient of sensible heat yielded a value of 0.4974, which is only half of the initial guess value for this particular parameter.

5.3.2 Forecast experiments using both the retrieved initial conditions and parameter values

Assessing the impact of both the optimal initial conditions and parameter estimation. Three experiments were carried out to integrate the model for 6 hours in order to obtain the analysis fields at the end of the assimilation window for the bi-harmonic horizontal diffusion coefficient κ , namely: 1) a control experiment that was integrated from the initial guess fields, i.e., 6h forecasts from 18UTC Sept. 2, 1996 analysis and the estimated parameter $\kappa = 6 \times 10^{15}$, 2) the “optimal experiment” so called since we were using both the optimal initial conditions and the optimal parameter value κ , and 3) a simulation experiment using the estimated parameter $\kappa = 6 \times 10^{15}$ in which the model was integrated from the initialized 0000UTC Sept. 3, 1996 analysis to serve as the best simulation without using the variational data assimilation. The differences between the control experiment and the optimal experiment reflect the impact of both the optimal initial conditions and the optimal bi-harmonic horizontal diffusion coefficient parameter value.

The RMS errors of the 6h forecast fields at the end of the assimilation window were calculated for the aforementioned experiments and provided in Fig. 5.5. The results obtained show that the optimal experiment yields the best results throughout

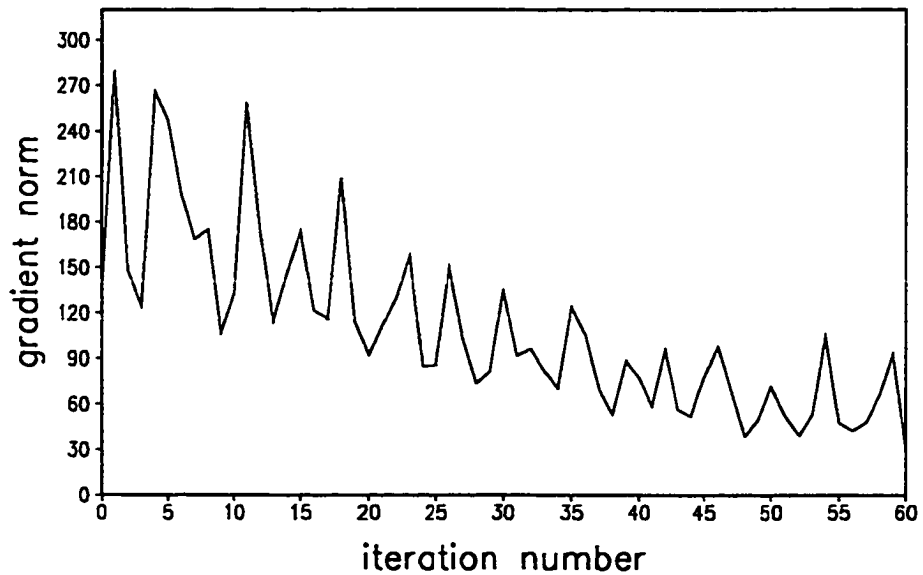
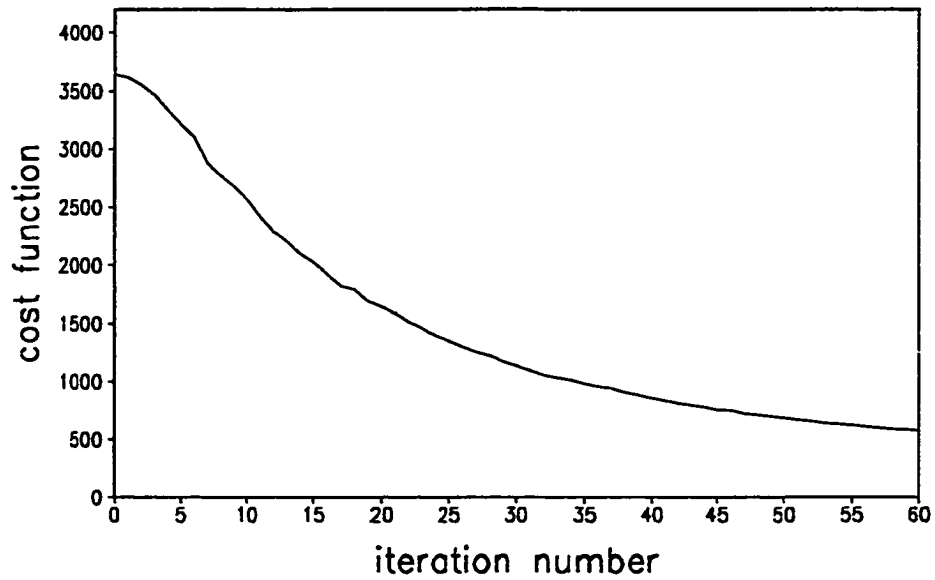


Figure 5.3: The variation of the cost function and the gradient norm with respect to the iteration number when both the optimal initial conditions and the bi-harmonic horizontal diffusion coefficient κ are retrieved.

all of the vertical levels, especially for the divergence field. The RMS errors of the logarithm of the surface pressure are $0.140\text{E-}2$, $0.939\text{E-}3$, and $0.517\text{E-}3$ for the control experiment, the simulation experiment and the optimal experiment, respectively.

Fig. 5.6 presents the divergence analysis field at 200 hPa for the aforementioned experiments and the observation at the end of the assimilation, i.e., 0600UTC Sept. 3, 1996. Only the optimal experiment successfully provided a high quality analysis, capturing the main features of the divergence field. Both the control experiment and the simulation experiment failed to simulate the strong divergence field corresponding to a heavy precipitation event over Indonesia and overestimated the divergence field to the west of Africa. The control experiment also overestimated the divergence field over the northern Africa and underestimated the divergence field around 20W, 35S while the simulation experiment overestimated the divergence field to the east of Australia.

The difference fields of the specific humidity at 500 hPa, the vorticity at 200 hPa, the geopotential height at 500 hPa and the temperature at 850 between the results of the aforementioned experiments and the observation field at the end of the assimilation are displayed in Figures 5.7– 5.10. The improvement obtained due to the optimal experiment over the results obtained by the other experiments is significant, particularly over areas of large errors.

Fig. 5.11 displays the RMS errors of the meteorological variables for the 24h forecast control experiment and optimal experiment for the bi-harmonic horizontal diffusion coefficient κ . The use of the optimal initial conditions and the parameter value improves the 24h forecast fields, however, compared with Fig. 5.5, the differ-

ences between the control experiment and the optimal experiment decrease as the length of the forecast period increases.

Similar results were also obtained for the other two parameters, the ratio of the transfer coefficient of moisture to the transfer coefficient of sensible heat and the Asselin filter coefficient.

Assessing the impact of optimal parameter estimation. In the above section, we recovered three pairs of the optimal initial conditions and optimal values of three model parameters, and discussed their combined impact on the model forecast. An important question remains to be clarified: how much of the improvement obtained is directly attributable to the optimal initial condition, and how much of it originates in the optimal values of the identified parameters? In order to provide a closer look at this issue, three additional experiments were performed to compare with the above-mentioned 6h forecast control experiment (referred to as C1) and the optimal experiment (referred to as O2) as well as with the 24h forecast optimal experiment (referred to as O4) for κ . The additional experiments are: experiment C2 where the initial guesses of the initial conditions and the optimally identified parameter value were used, experiment O1 where the optimal initial conditions and estimated parameter value were used, and experiment O5 where the optimal initial conditions and optimal parameter value were used (Table 5.1).

To assess the impact of the optimal parameter estimation, we use the differences between the RMS errors at all vertical levels for vorticity, divergence, virtual temperature and dewpoint depression fields. If the difference is negative, it means that

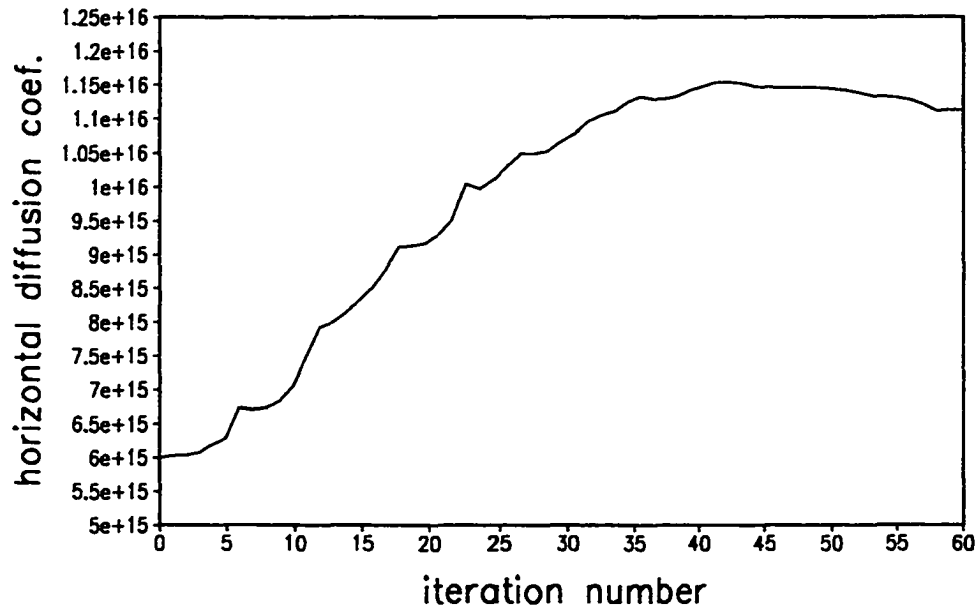


Figure 5.4: The evolution of the horizontal diffusion coefficient.

Table 5.1: Experiments designed to assess the impact of optimal parameter estimation.

Experiment	Initial Conditions	Parameter Value	Integration
C1	initial guesses	estimated value	6 h
C2	initial guesses	optimal value	6 h
O1	optimal initial conditions	estimated value	6 h
O2	optimal initial conditions	optimal value	6 h
O4	optimal initial conditions	estimated value	24 h
O5	optimal initial conditions	optimal value	24 h

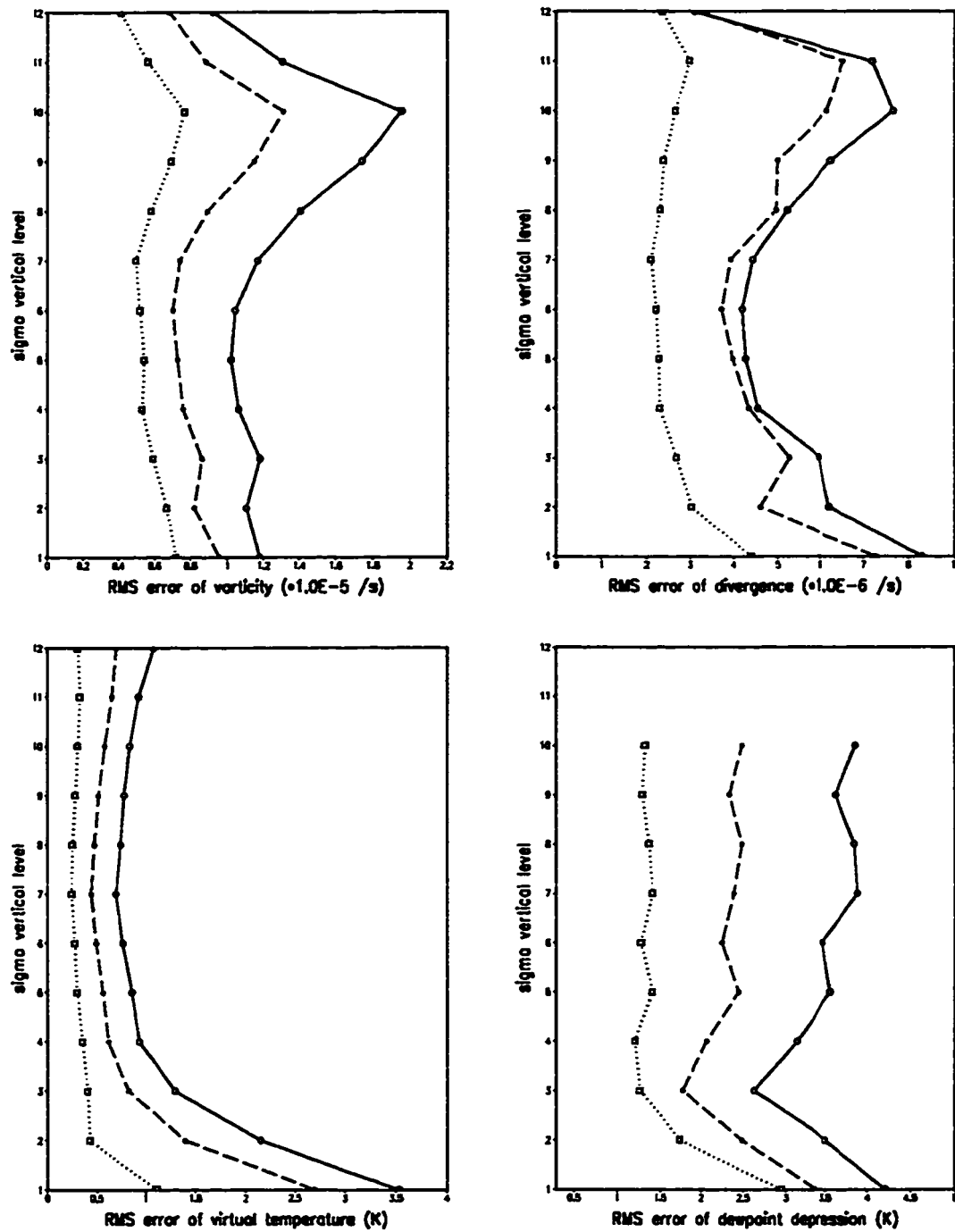


Figure 5.5: The RMS errors of the vorticity, divergence, virtual temperature and dewpoint depression at the end of the assimilation window. solid line: the control experiment; dashed line: the simulation experiment; dotted line: the optimal experiment.

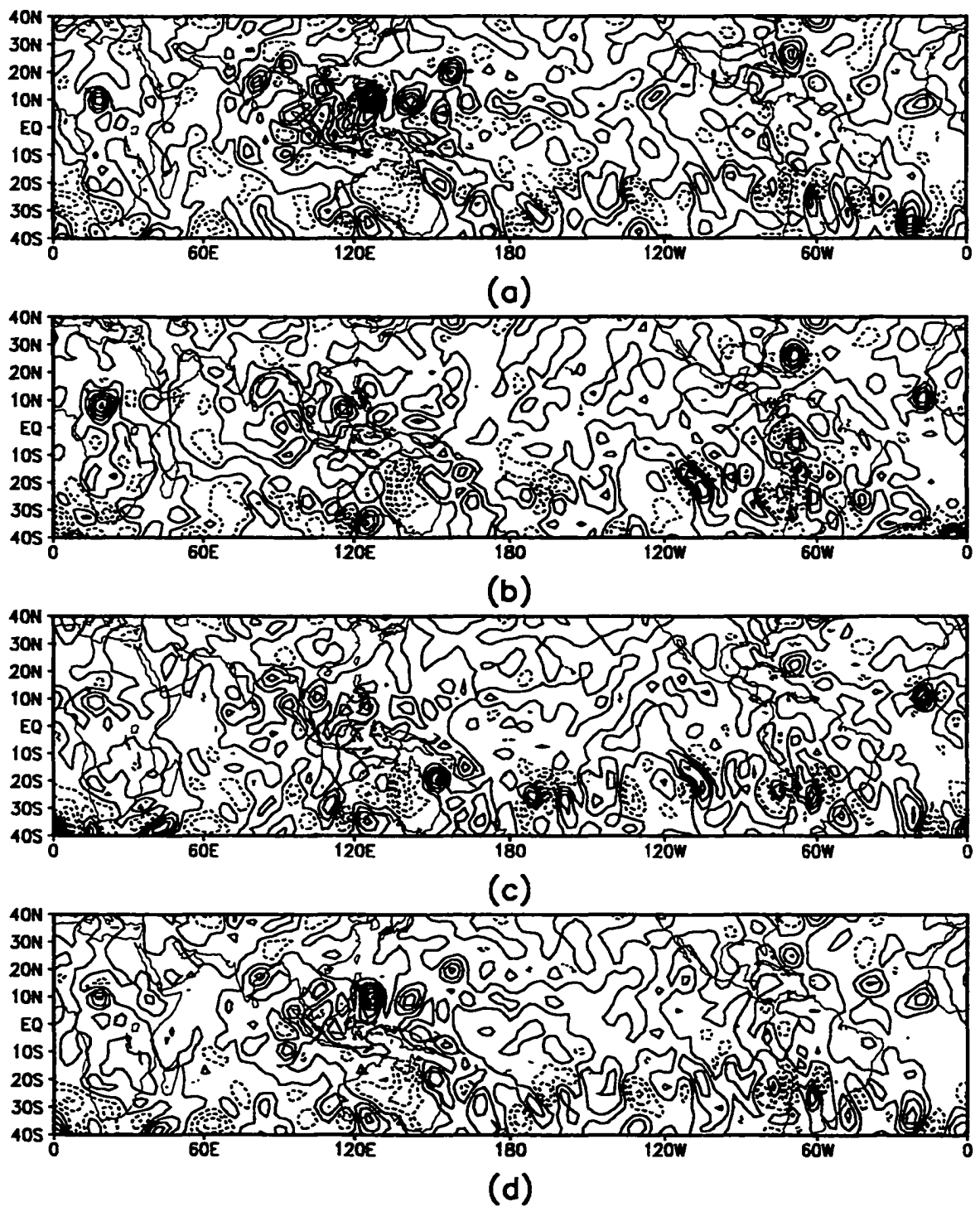
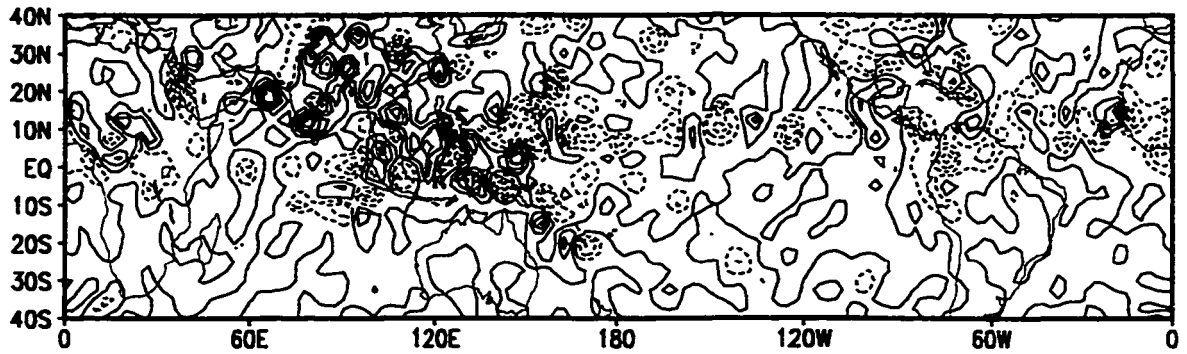
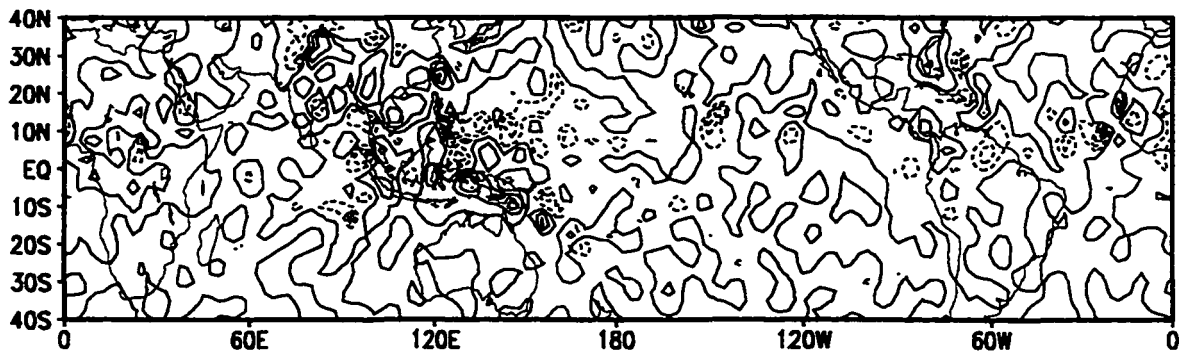


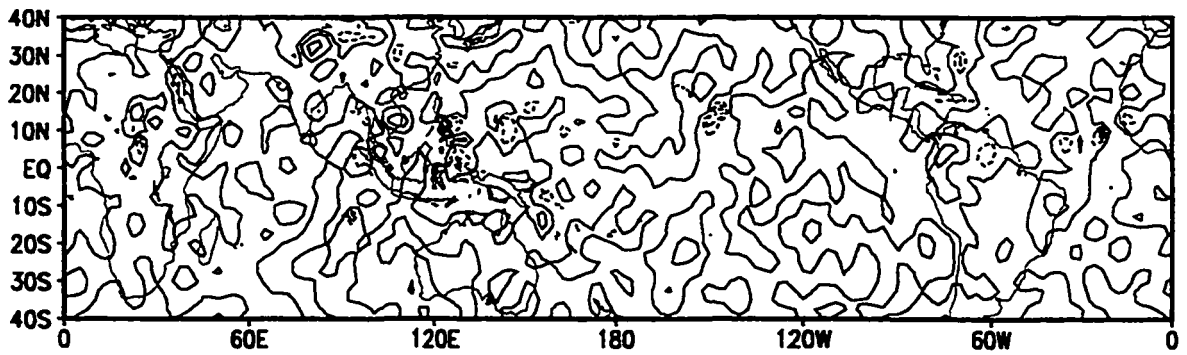
Figure 5.6: The divergence fields at 200 hPa at the end of the assimilation window: (a) the observation, (b) the control experiment, (c) the simulation experiment and (d) the optimal experiment, respectively. The contour interval is $8.0 \times 10^{-6} s^{-1}$.



(a)

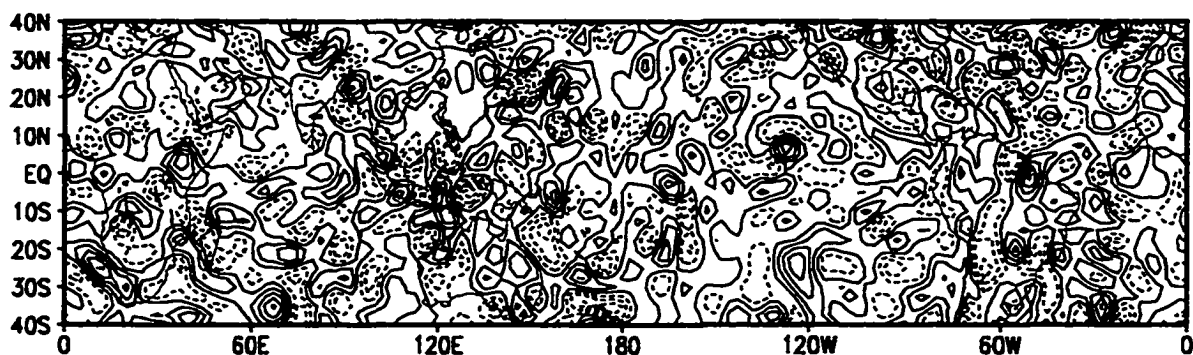


(b)

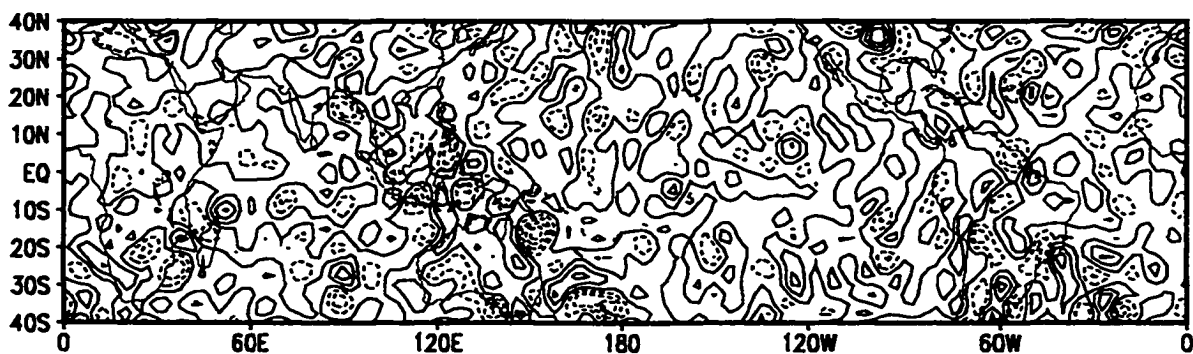


(c)

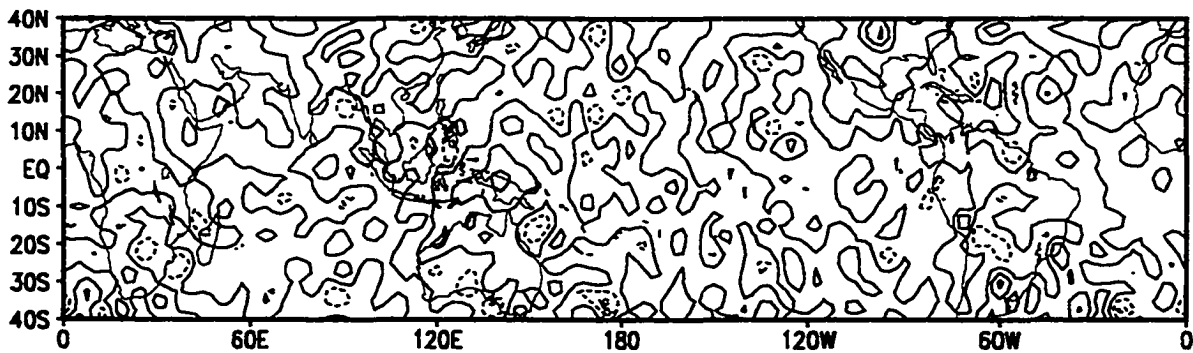
Figure 5.7: The difference fields of specific humidity at 500 hPa between the results of the following three experiments and the observation at the end of the assimilation window: (a) the control experiment, (b) the simulation experiment and (c) the optimal experiment. The contour interval is 0.0005 g/g .



(a)

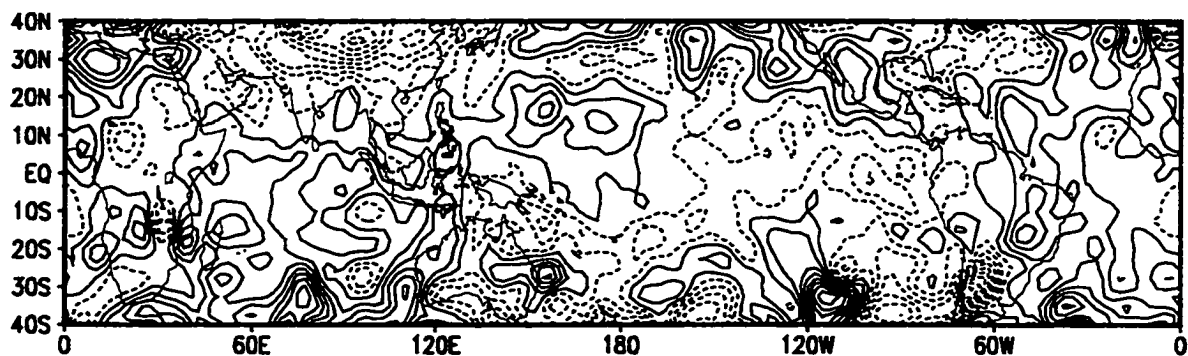


(b)

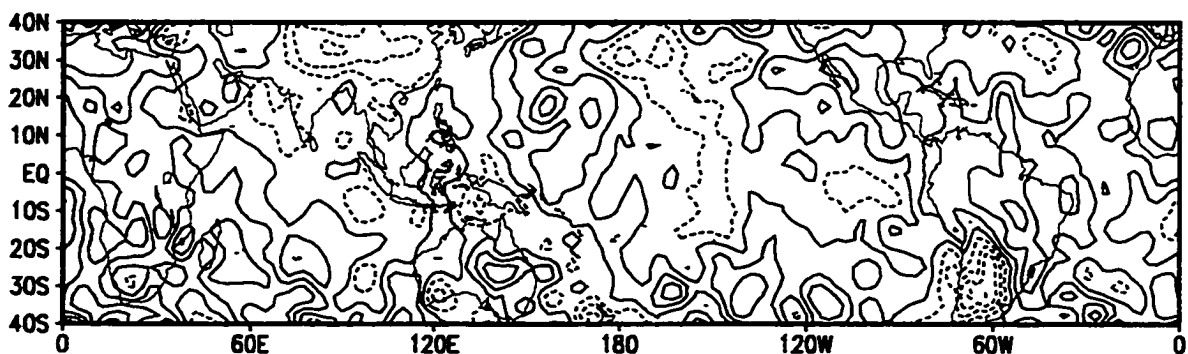


(c)

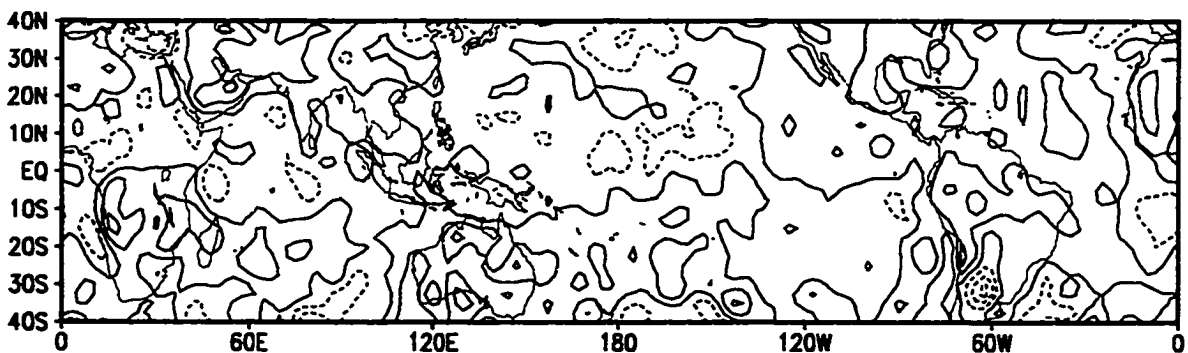
Figure 5.8: The difference fields of vorticity at 200 hPa between the results of the following three experiments and the observation at the end of the assimilation window: (a) the control experiment, (b) the simulation experiment and (c) the optimal experiment. The contour interval is $10^{-5} s^{-1}$.



(a)

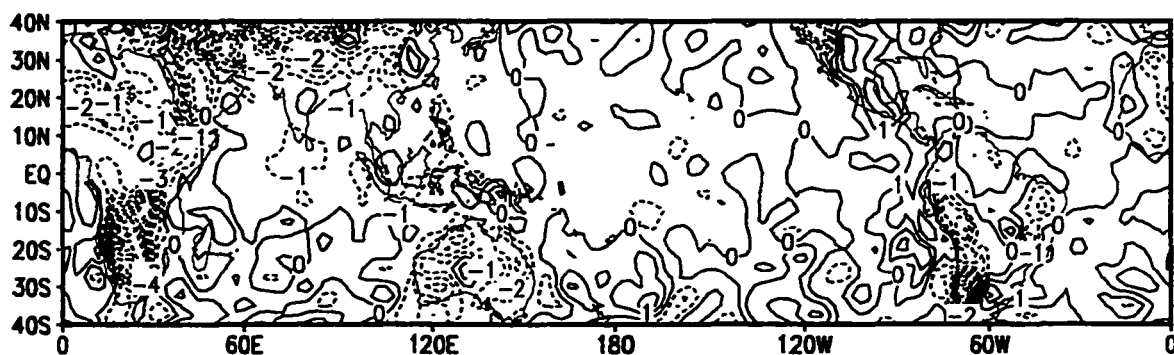


(b)

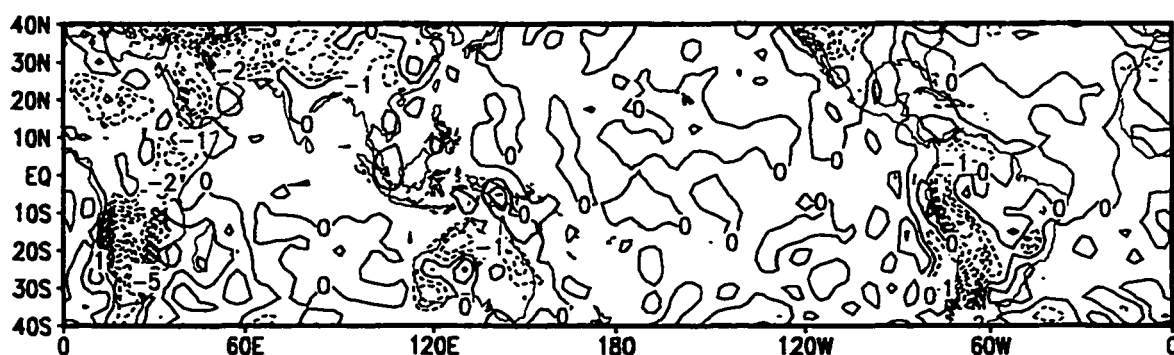


(c)

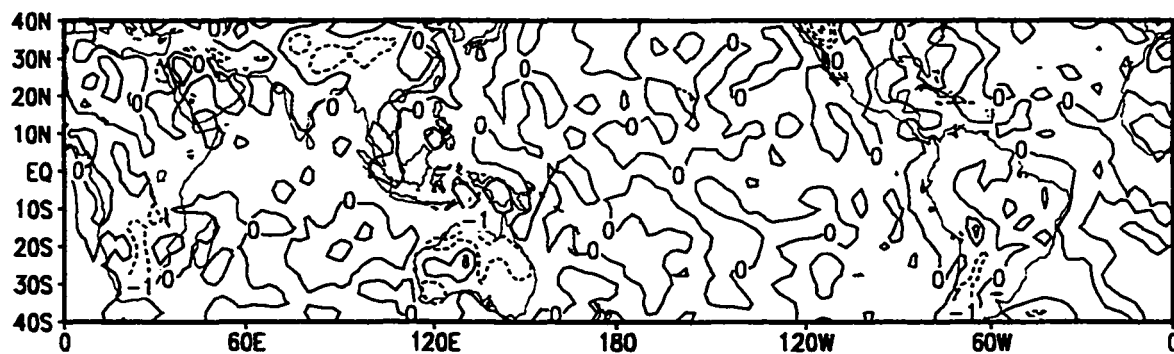
Figure 5.9: The difference fields of potential height at 500 hPa between the results of the following three experiments and the observation at the end of the assimilation window: (a) the control experiment, (b) the simulation experiment and (c) the optimal experiment. The contour interval is $5 \text{ m}^2/\text{s}^2$.



(a)



(b)



(c)

Figure 5.10: The difference fields of temperature at 850 hPa between the results of the following three experiments and the observation at the end of the assimilation window: (a) the control experiment, (b) the simulation experiment and (c) the optimal experiment. The contour interval is 1K.

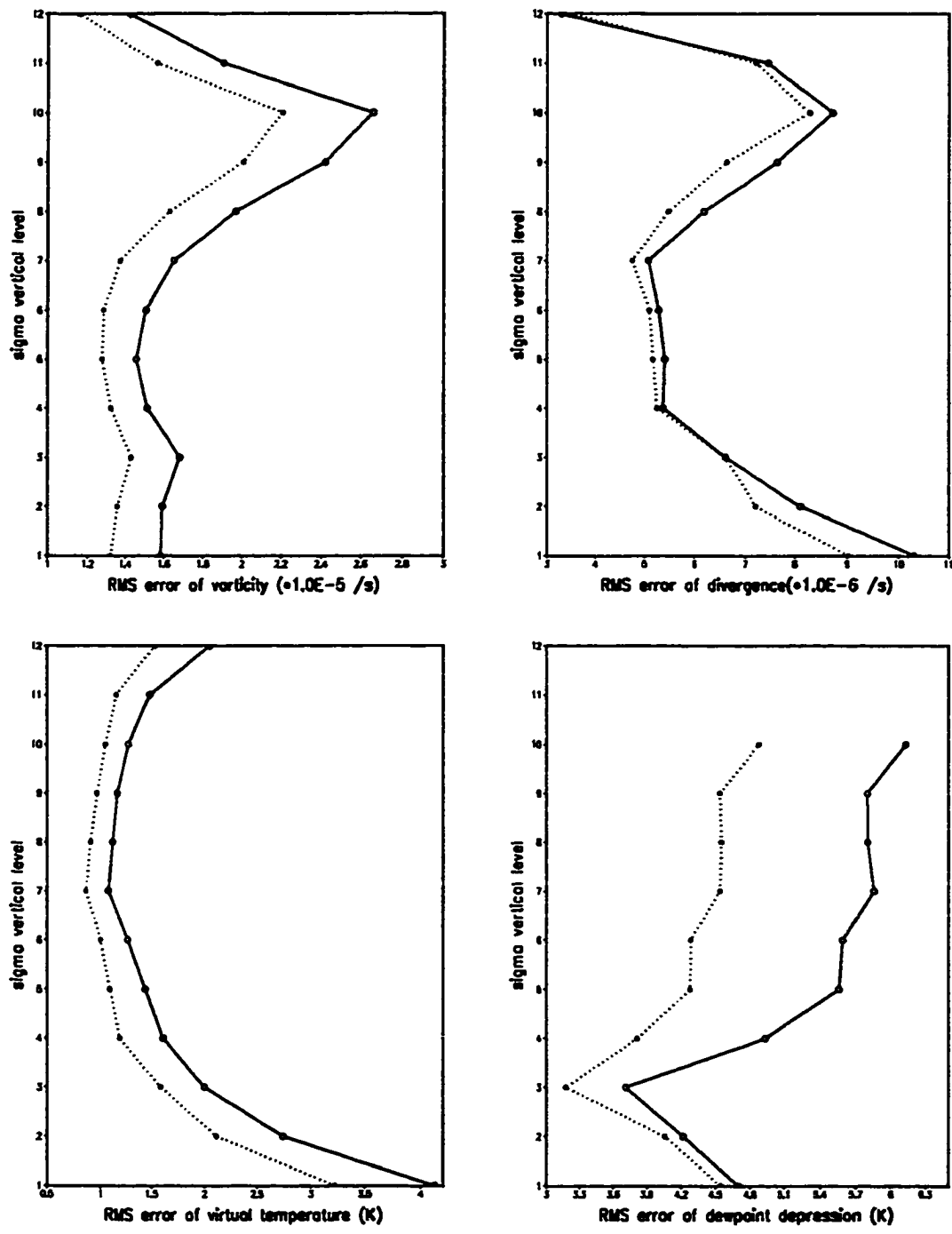


Figure 5.11: The RMS errors of the vorticity, divergence, virtual temperature and dewpoint depression at the end of the 24h forecast. solid line: the control experiment; dotted line: the optimal experiment.

the RMS error of the experiment where the optimally identified parameter value was used is smaller than the RMS error of the experiment where the estimated parameter value was used; otherwise, the RMS error of the experiment where the optimally identified parameter value was used is larger than the RMS error of the experiment where the estimated parameter value was used. The difference between the experiments C1 and C2 reflects the impact of optimal parameter values on the forecast when the optimal initial conditions were not used, while the differences between the experiments O1 and O2, and between the experiments O4 and O5 reflect the impact of the optimal parameter values on the forecast when the optimal initial conditions were applied to the 6-h forecast and 24-h forecast, respectively. The differences of the RMS errors of the vorticity, divergence, virtual temperature and the dewpoint depression fields at the end of the forecast between experiment pairs C2 and C1, O2 and O1, O5 and O4 are displayed in Fig. 5.12. For the pair C2 and C1, the RMS difference values for all of the aforementioned variables are negative except only for the dewpoint depression at the lowest two levels. This indicates a relatively small (compared to the difference of the RMS errors between C1 and O2) but positive impact of the optimal parameter value on the model simulation. The experiment O1 is comparable to O2 in terms of RMS error. The impact of the optimal initial conditions dominates that of the optimal parameter value at the end of the assimilation window. This is very reasonable since in the first few hours of the forecast, the optimal initial conditions may reconstruct the dynamic structure while the optimal bi-harmonic horizontal diffusion coefficient value can only adjust it. However, the lower level divergence fields were largely improved in all of the pairs of experi-

ments conducted when the optimal parameter value κ was used. As the length of the forecast period increased, the impact of the optimal parameter value on the model forecast became more pronounced for the pair O4 and O5. Compared with Fig.5.11, this result implies the known fact that the effect of the optimal initial conditions decays as the forecast period becomes longer.

An additional experiment was conducted with the fixed initial conditions at 0000UTC Sept. 3, 1996 and where only the parameter κ was considered as the sole control variable. An identical cost function and initial parameter value to those used before were employed. The cost function value reached a constant value while the norm of the gradient decreased by three orders of magnitude in five iterations. The optimal bi-harmonic horizontal diffusion coefficient value obtained is 1.1946×10^{16} . This value is very close to that obtained when we recovered both the optimal initial conditions and the optimal parameter value. A similar positive impact was observed when comparing the forecasts using the estimated parameter value and the optimal parameter value, respectively.

Similar experiments (related to the experiments detailed in Table 5.1) were also conducted separately for the parameters FC and γ . Since the optimal value of the Asselin filter coefficient FC is very close to its estimated value, the impact of this parameter on the ensuing forecasts is marginal. A positive impact of the optimal ratio γ on the forecasts was also observed while the impact of the optimal initial conditions was found to be dominant during the first several hours of the forecast.

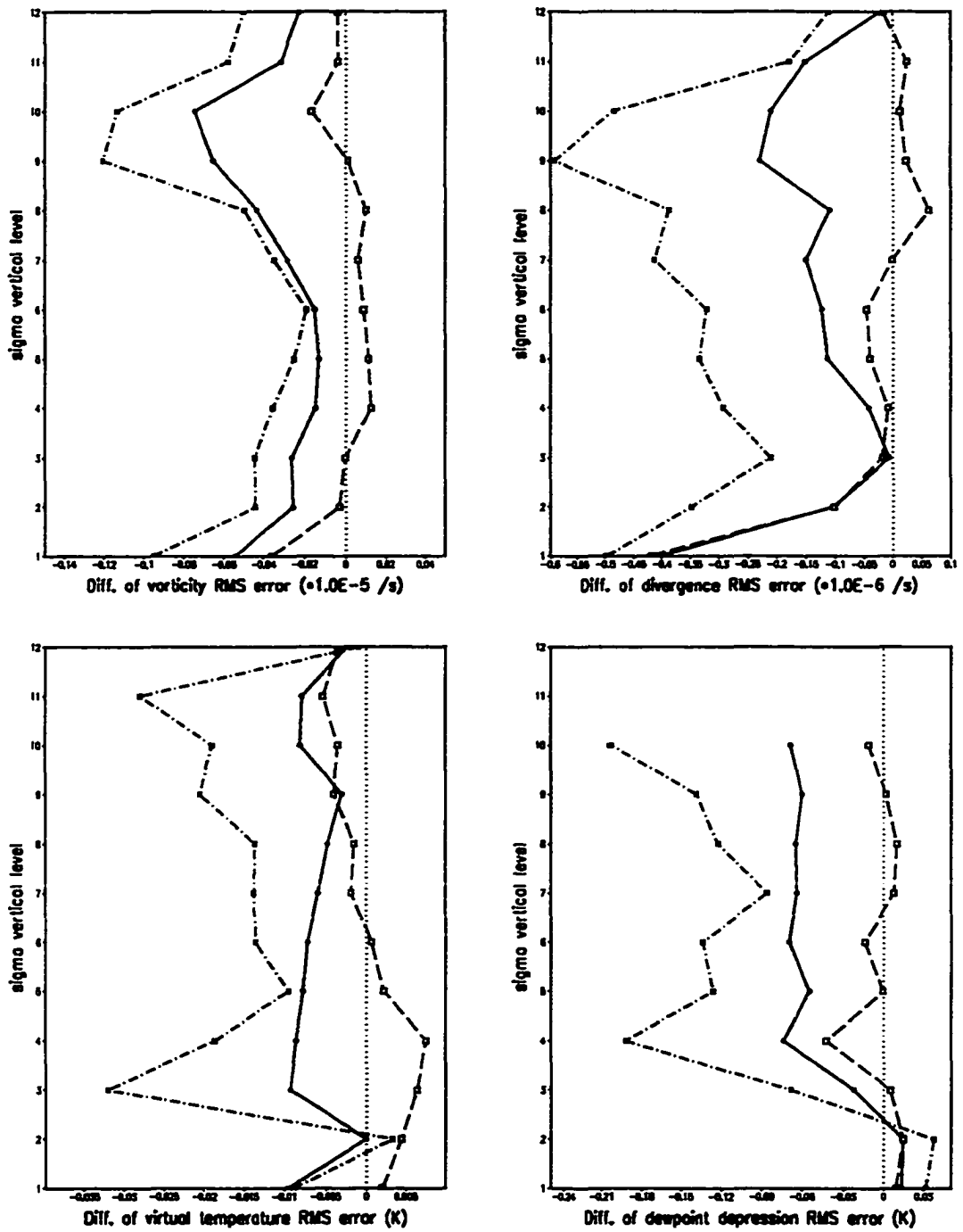


Figure 5.12: The differences of the RMS errors of the vorticity, divergence, virtual temperature and the dewpoint depression between the three pairs at the end of the forecast. solid line: C2 and C1; dashed line: O2 and O1; dot dashed line: O5 and O4.

5.3.3 Impact of the optimal parameters alone on ensuing 24h forecasts

A number of 24h forecast experiments beginning from 0000UTC Sept. 3, 1996 analysis were performed where only the optimal parameter values obtained above were used in order to examine the impact of each parameter separately as well as the combined impact of all the three parameters on the ensuing forecast fields. The experiments are designed as: (a) an experiment with the estimated parameters, i.e., $\kappa = 6.0 \times 10^{15}$, $FC = 0.05$ and $\gamma = 1.0$; (b) an experiment with the estimated FC and γ but the optimally retrieved κ value; (c) an experiment with the estimated FC and κ but the optimally retrieved γ ; (d) an experiment using optimally retrieved κ , FC and γ simultaneously. Since the optimal value of FC is very close to its estimated value, the impact of this parameter is marginal.

The RMS errors of the vorticity, divergence, dewpoint depression and the virtual temperature fields at all vertical levels are calculated between the above experiments and the analysis at 0000UTC Sept. 4, 1996. Fig. 5.13 displays the differences of the RMS errors between the experiments (b) and (a), (c) and (a), (d) and (a). Negative values of the RMS differences indicate that the RMS errors are less than those of the experiment (a) with the estimated parameter values, i.e., the optimal parameter value impacts positively on the forecast.

The results show that the optimal horizontal diffusion coefficient κ mainly impacts on the vorticity and divergence fields. The use of the optimal diffusion coefficient κ also has a positive impact on the upper and middle levels of the virtual temperature and the dewpoint depression fields, but a negative impact on the lower levels of these fields. On the other hand, in experiment (c) when only the optimal value of the ratio

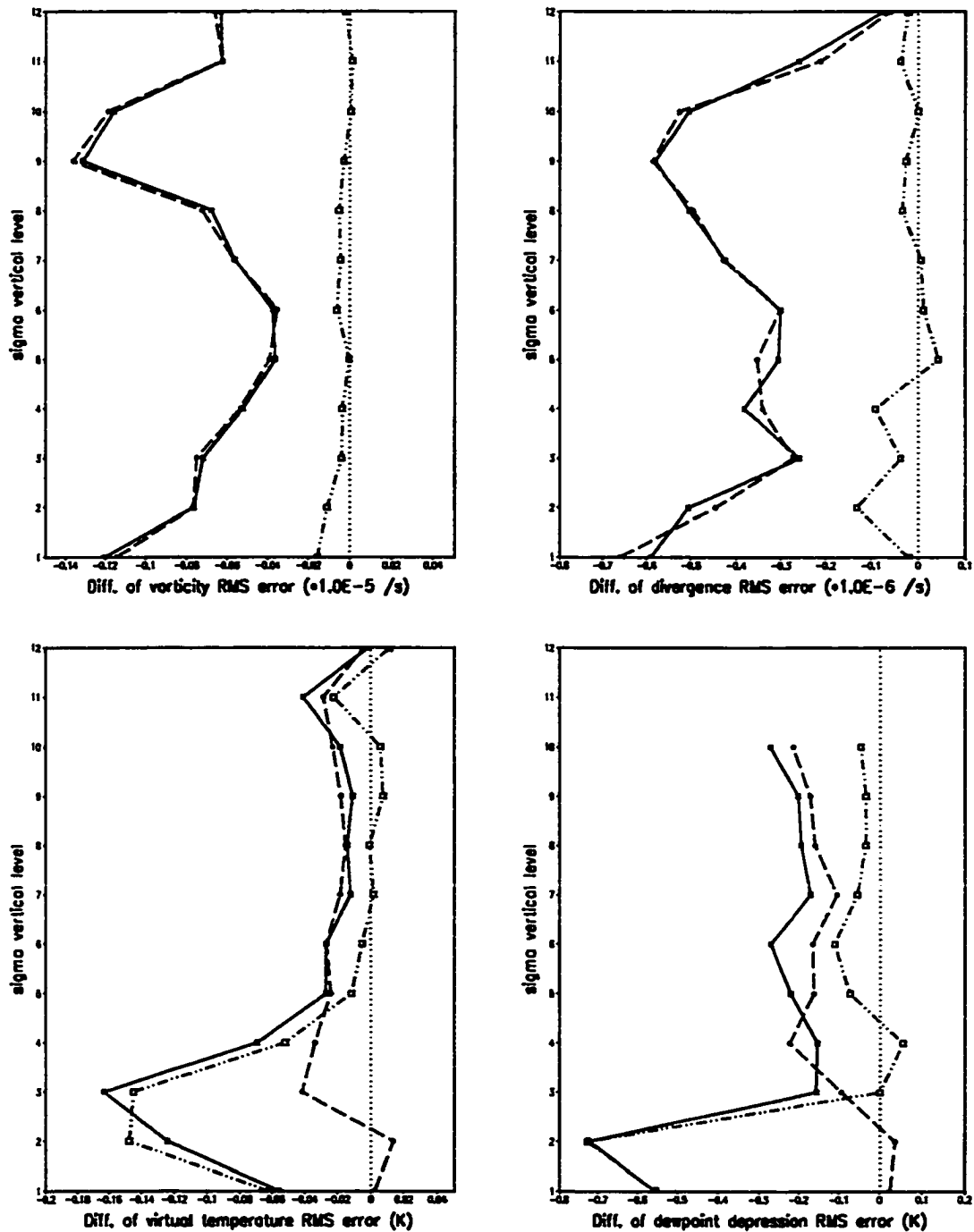


Figure 5.13: The differences of the RMS errors of the 24h forecast vorticity, divergence, virtual temperature and the dewpoint depression between the following pairs. dashed line: experiments (b) and (a); dot dot dashed line: experiments (c) and (a); solid line: experiments (d) and (a).

γ is employed, the vorticity and divergence fields are only slightly improved, but the middle and lower levels of the virtual temperature and the lower levels of the dewpoint depression experienced a large improvement. The effect of γ is mainly confined to the lower vertical levels of the model. As might be expected, the best forecasts were obtained by experiment (d) where all of the optimal parameter values of κ and FC as well as γ were used simultaneously. In this sense, experiment (d) combined all of the advantages of experiments (b) and (c).

5.3.4 A study of the model's "memory" of impacts of optimal initial conditions and identified parameter values

So far we have studied either the combined impact of both the optimal initial conditions and the optimal parameter values or the impact of only the optimally identified parameter values on the ensuing forecast. In this section, we will discuss the persistence (memory) of the combined impact of the above-mentioned three optimally identified parameter values as well as the persistence (memory) of the impact of the optimal initial conditions obtained by variational data assimilation on the ensuing forecast, respectively.

Three sets of experiments were carried out by integrating the model for 24h, 48h and 72h respectively from 0000UTC Sept. 3, 1996. The first set of experiments C1, C2 and C3 are control experiments which were integrated from the initial guesses of the initial conditions (i.e., the 6h forecast from 1800UTC Sept. 2, 1996) using the estimated parameter values. The second set of "optimal parameter" experiments P1, P2 and P3 started from the initial guesses of the initial conditions using the optimally

Table 5.2: Experiments carried out by integrating the model for 24h, 48h and 72h from 0000UTC Sept. 3, 1996, respectively.

Exp.	Initial conditions	Parameter values	Length of forecast
C1	initial guesses	estimated values	24 h
C2	initial guesses	estimated values	48 h
C3	initial guesses	estimated values	72 h
P1	initial guesses	optimal values	24 h
P2	initial guesses	optimal values	48 h
P3	initial guesses	optimal values	72 h
I1	optimal initial conditions	estimated values	24 h
I2	optimal initial conditions	estimated values	48 h
I3	optimal initial conditions	estimated values	72 h

identified values of the above-mentioned three parameters. The third set of “optimal initial condition” experiments I1, I2 and I3 were integrated from the variationally derived optimal initial conditions using estimated parameter values (Table 5.2).

The RMS errors of vorticity, divergence, virtual temperature and dewpoint depression fields were calculated for each experiment. Then, the percentages of the differences of the RMS errors between C1 and P1, C2 and P2, C3 and P3, C1 and I1, C2 and I2 and C3 and I3 were computed. The differences of RMS errors and the percentages of the decrease of RMS errors due to the use of the three optimally identified parameter values are displayed in Figures 5.14 - 5.15. The results show that all the experiments using optimally identified parameter values exhibit smaller RMS errors than those using estimated parameter values through out all of the vertical levels except for the virtual temperature at the top vertical level of the model. This means that the combined impact of the three identified parameter values still persists for the 72h forecast, and probably even further beyond. The largest improvement in the 24h forecast occurred at the low vertical levels of the dewpoint depression field where the RMS error decreased by up to 17%. The overall forecast RMS errors further decreased during the 48h forecast. The impacts of the optimally identified parameter values on the vorticity field and on the middle vertical levels of the divergence, virtual temperature fields as well as the lower levels of the dewpoint depression field decayed for the 72h forecast compared to the results obtained with optimally estimated parameters for the corresponding 48h forecast. The RMS errors, however, still decreased by up to 10% compared to the experiment where estimated parameters were used for the same 72h forecast.

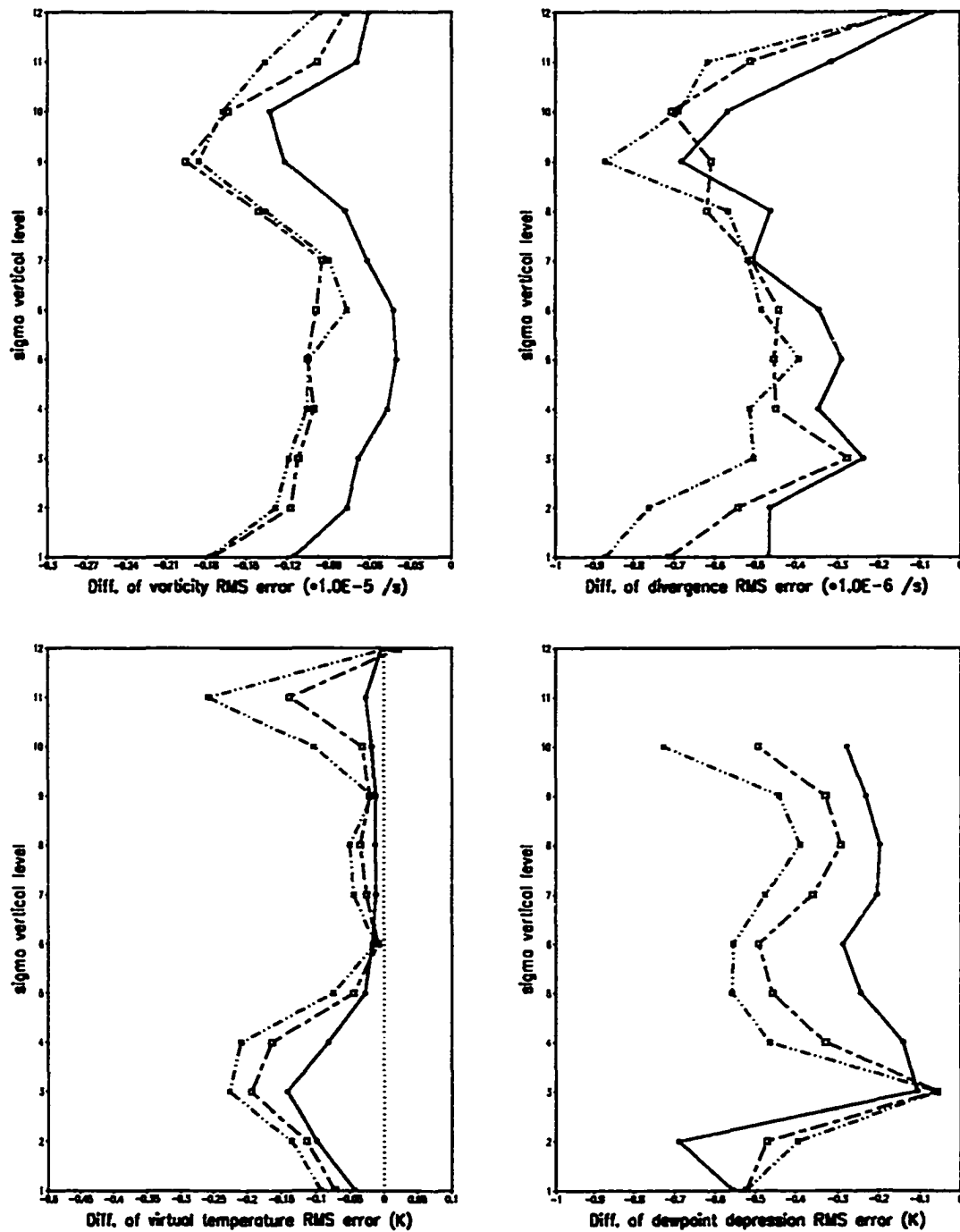


Figure 5.14: The differences of the RMS errors of the ensuing forecast fields vorticity, divergence, virtual temperature and the dewpoint depression between when the optimally identified parameter values were used and when the estimated parameter values were used. solid line: 24h forecast; long, short dashed line: 48h forecast; dot dot dashed line: 72h forecast.

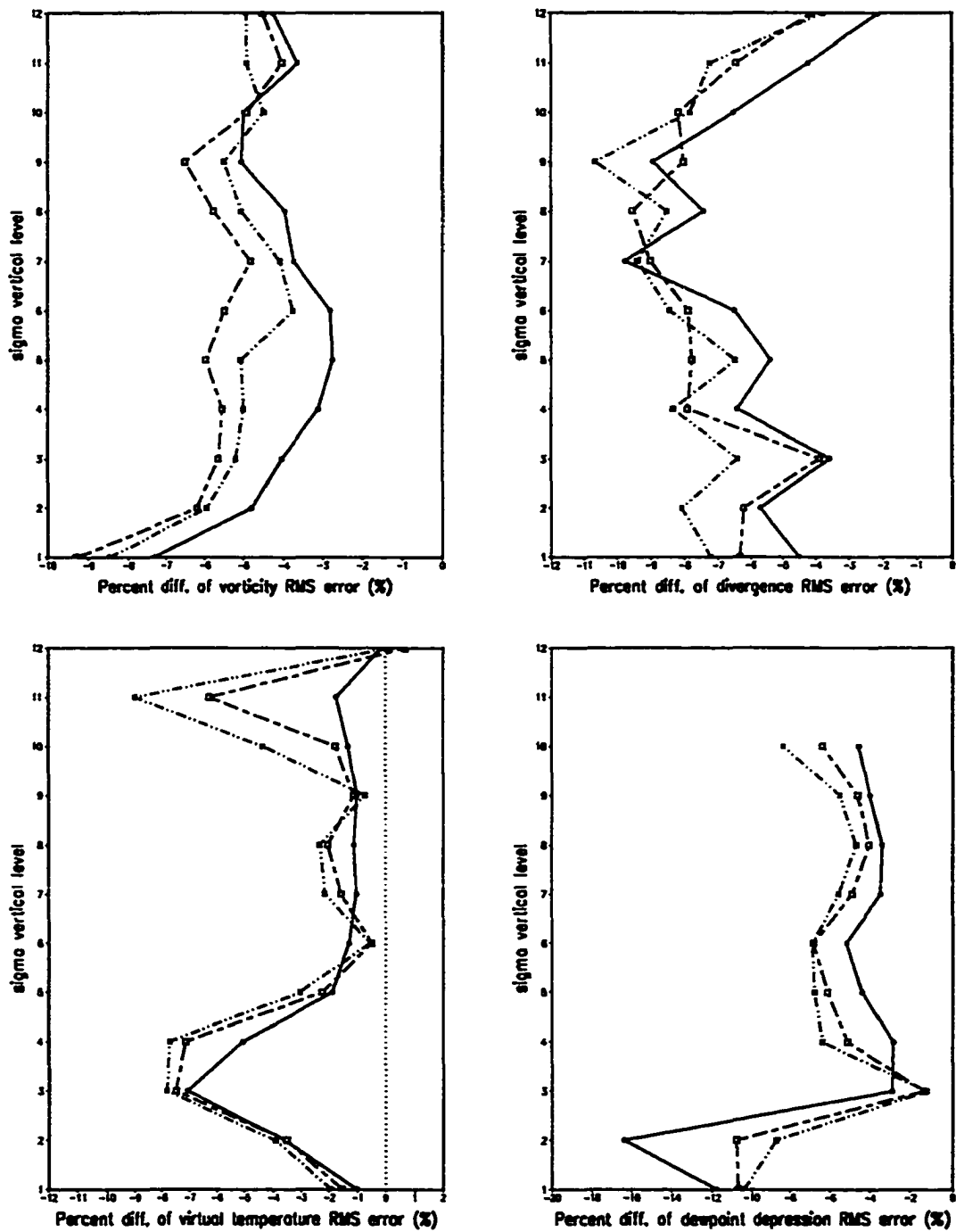


Figure 5.15: The percent differences of the RMS errors of the ensuing forecast fields vorticity, divergence, virtual temperature and the dewpoint depression between when the optimally identified parameter values were used and when the estimated parameter values were used. solid line: 24h forecast; long, short dashed line: 48h forecast; dot dot dashed line: 72h forecast.

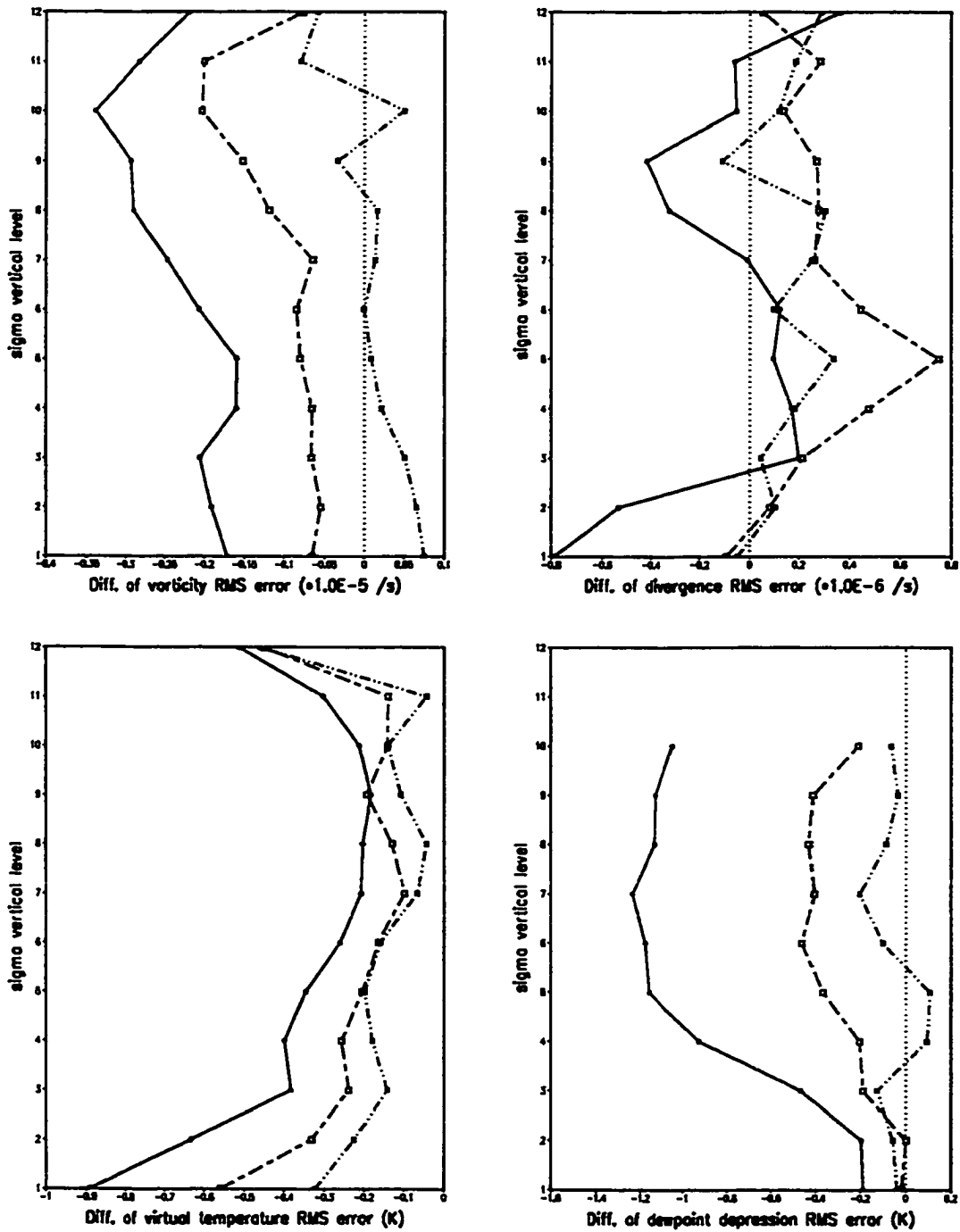


Figure 5.16: The differences of the RMS errors of the ensuing forecast fields vorticity, divergence, virtual temperature and the dewpoint depression between when the optimal initial conditions were used and when the initial guesses of initial conditions were used. solid line: 24h forecast; long, short dashed line: 48h forecast; dot dot dashed line: 72h forecast.

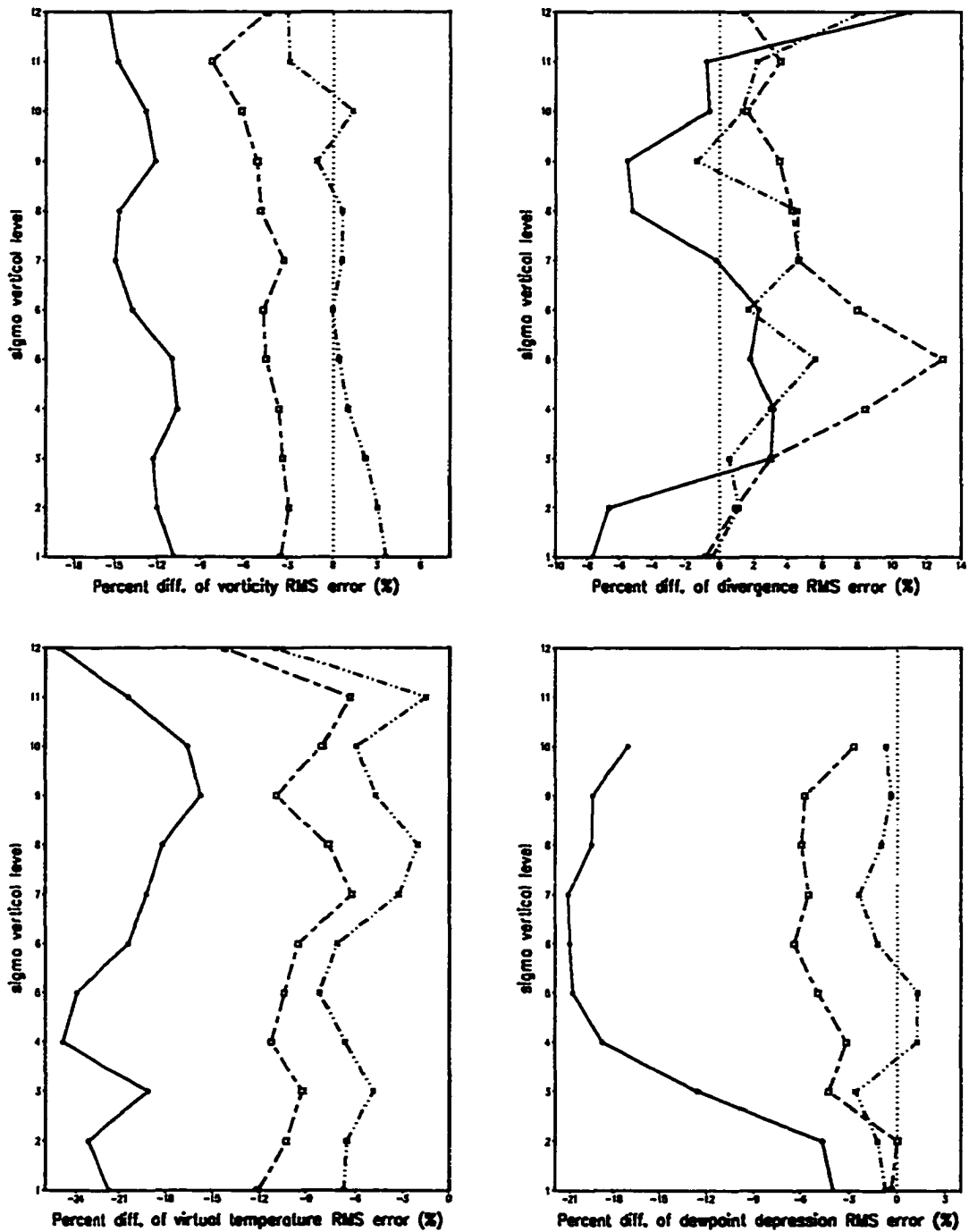


Figure 5.17: The percent differences of the RMS errors of the ensuing forecast fields vorticity, divergence, virtual temperature and the dewpoint depression between when the optimal initial conditions were used and when the initial guesses of initial conditions were used. solid line: 24h forecast; long, short dashed line: 48h forecast; dot dot dashed line: 72h forecast.

The differences of RMS errors and the percentages of the decrease in RMS errors for vorticity, divergence, virtual temperature and dewpoint depression fields by using variationally derived optimal initial conditions are presented in Figures 5.16 and 5.17, respectively. A very clear trend is observed, namely, the impact of the optimal initial conditions decays as the forecast time increases, especially the impact on the divergence field which decays very rapidly. The improvement of the forecast in terms of RMS errors due to the combined impact of the three optimally identified parameter values exceeds that obtained due to the impact of the optimal initial conditions in the ensuing 72h forecast. Even for the 24h forecast, the impact of the three optimally identified parameter values on the lower vertical level of the dewpoint depression exceeds that of the optimal initial condition. This means that the model tends to “forget” first the impact of the optimal initial conditions in the ensuing forecast, while the impact of using optimally estimated parameters on above-mentioned forecast fields persists even after 72 hours.

We would like to point out that the mechanisms of the impacts resulting from variationally derived optimal initial conditions and from the optimally identified parameter values are quite different. The impact of the optimally identified parameter values is effective throughout the entire integration period via the corresponding physical parameterization or numerical schemes, while the impact of the optimal initial conditions obtained via variational data assimilation is to reduce the errors in the initial conditions that might lead to poor forecast, and to provide a more accurate specification of the initial conditions. This explains why their impacts are quite different. Fig. 5.18 displays the difference fields between experiments C1, P1

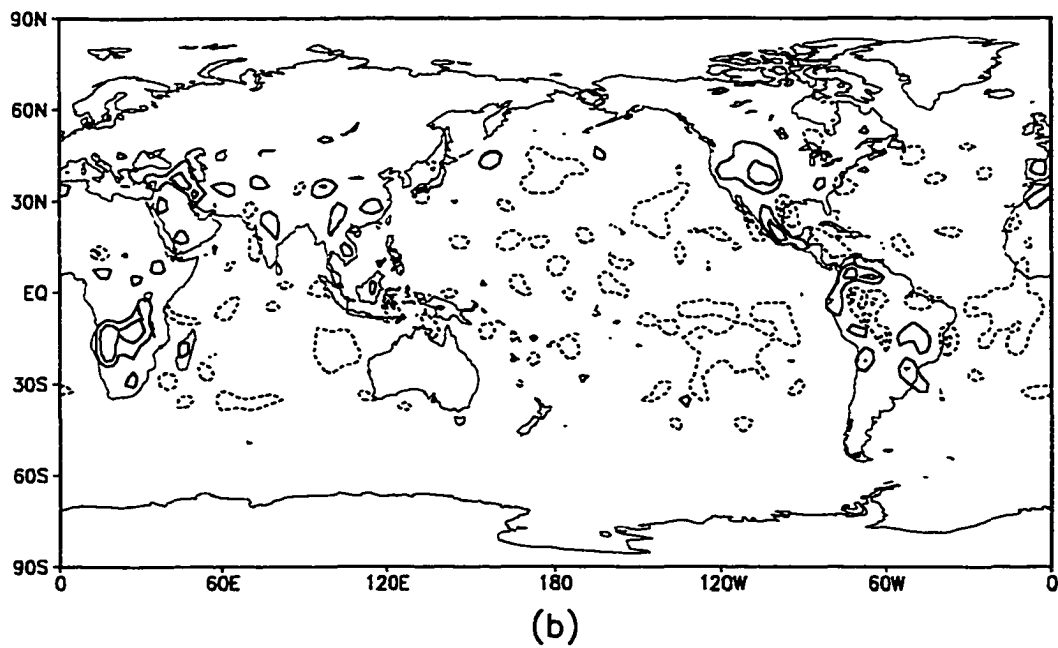
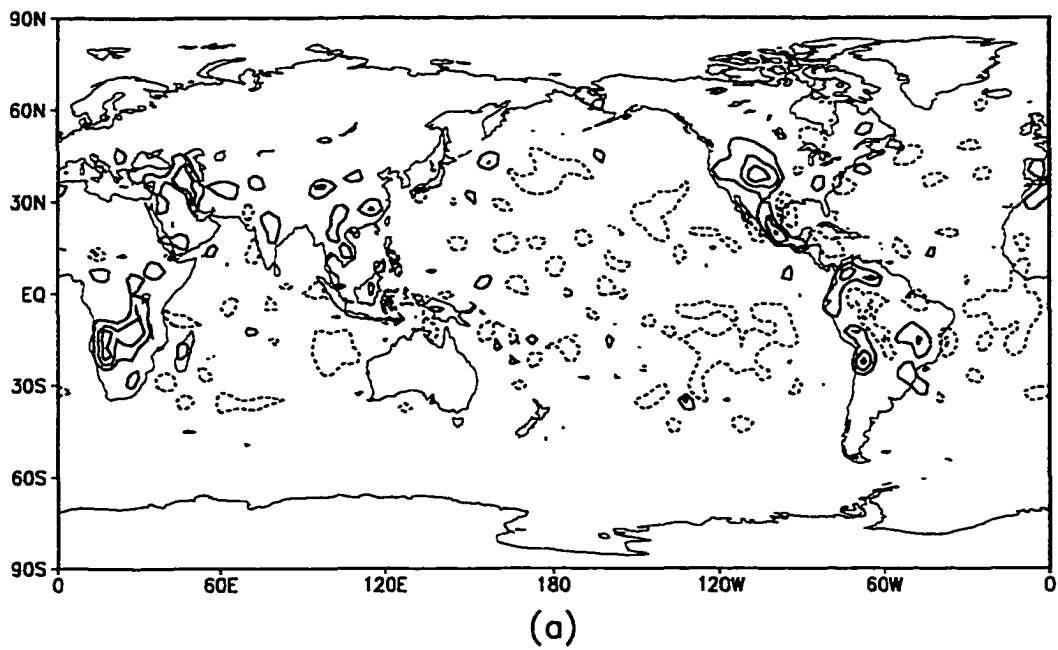


Figure 5.18: The difference fields between experiments (to be enumerated below) and the analysis for the specific humidity at 850 hPa as follows: (a) the control experiment C1, (b) experiment P1. The contour interval is 0.003 g/g .

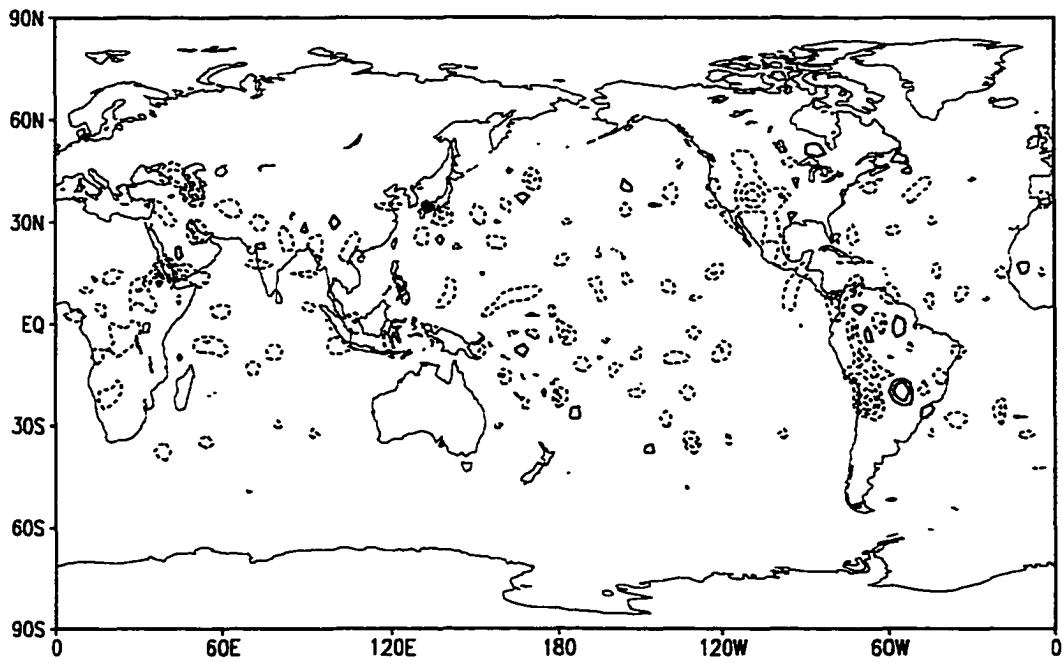


Figure 5.19: The difference field of specific humidity at 850 hPa between experiments C1 where the estimated parameter values were used and P1 where the optimally identified parameter values were used. The contour interval is 0.0008 g/g .

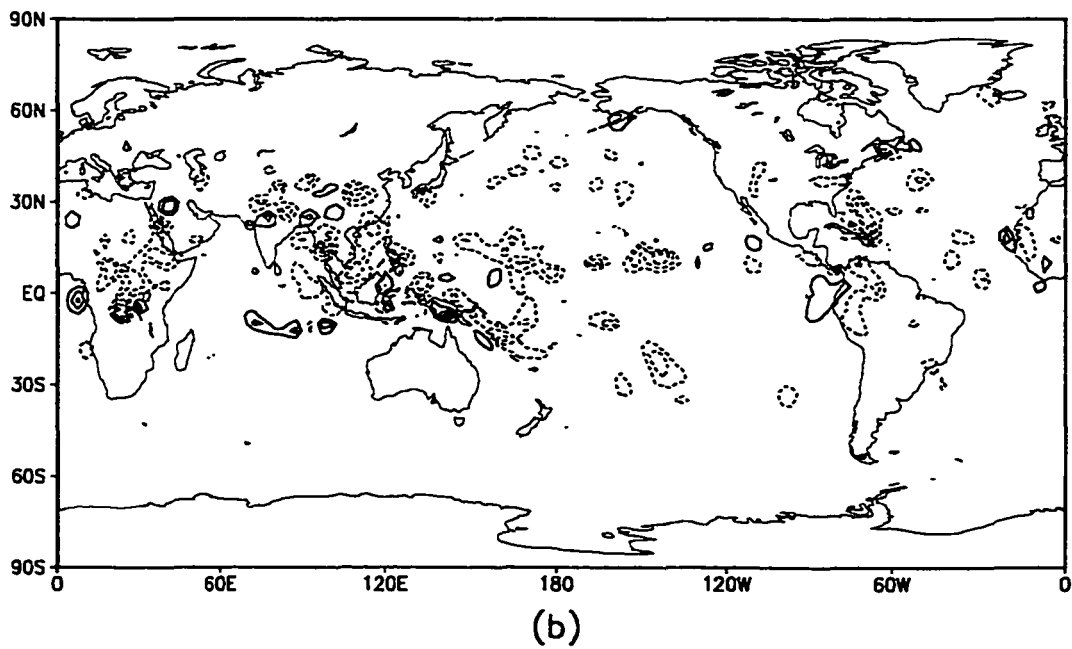
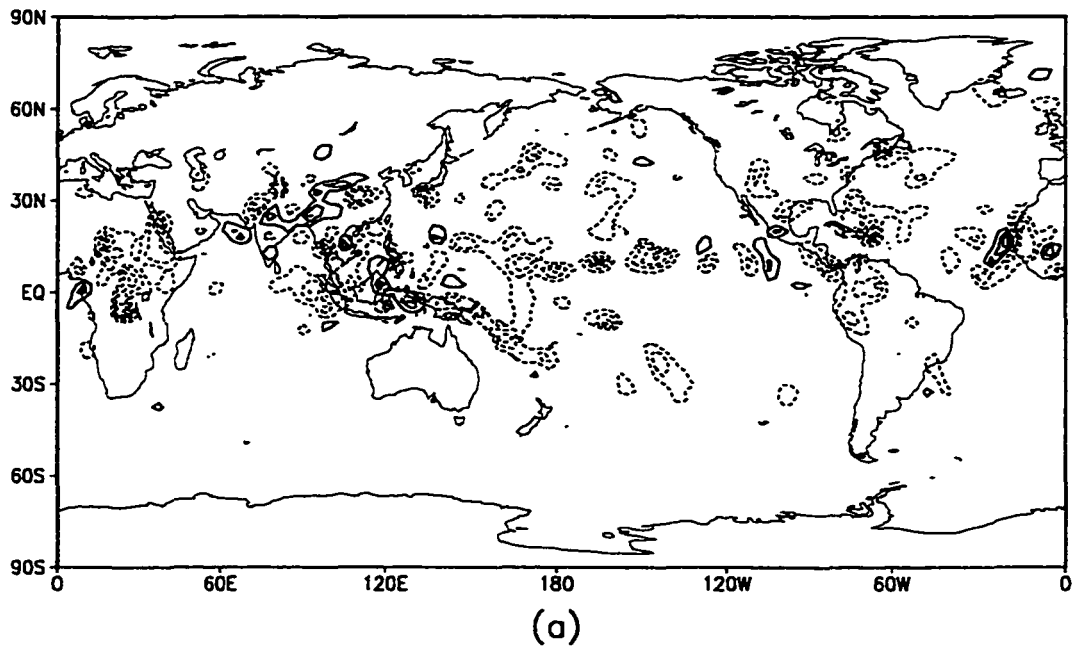


Figure 5.20: The difference fields between experiments (to be enumerated below) and the analysis for the specific humidity at 500 hPa as follows: (a) the control experiment C1, (b) experiment I1. The contour interval is 0.0008 g/g.

and the analysis for specific humidity at 850 hPa, respectively, while the difference field of specific humidity at 850 hPa between experiments C1 and P1 is displayed in Fig. 5.19. Comparing Fig. 5.18 (a) and (b), we notice that the positive differences between the forecast and the analysis became smaller while the negative differences between the forecast and the analysis became larger over most of the forecast area in experiment P1 when optimally identified parameter values were used. That is to say, the use of the optimally identified parameter values tended to produce a smaller specific humidity forecast over most of the global domain since the optimal ratio of the transfer coefficient of the moisture to the transfer coefficient of the sensible heat is only about half of its estimated value. Larger specific humidity forecasts in experiment P1 than those in experiment C1 were observed only in a few regions, such as central South America, which might have been caused by the impact of the optimal bi-harmonic horizontal diffusion coefficient or by interactions between the impacts of the three optimally estimated parameter values. In this case, the improvement due to the use of the optimally identified parameter values was observed mainly over the overestimated areas with respect to the analysis (in experiment C1) which spread over the land. Fig. 5.20 displays the difference fields of the specific humidity at 500 hPa between experiments C1, I1 and the analysis, respectively. Experiment I1 where the optimal initial conditions were used, however, does not exhibit such features as mentioned above, rather the improvement was obtained both in underestimated and overestimated areas compared with the result of experiment C1, especially in areas of large errors.

It is also known that forecasts starting from the variationally derived optimal initial conditions are not as good as the forecasts starting from the latest available analysis (Pu, et al., 1997). However, we compared the forecasts starting from 0600UTC Sept. 3, 1996 analysis (the latest available analysis in this study) using both the estimated values of the three parameters and the previously optimally identified parameter values, respectively. Similar improvements to those shown in Fig. 5.14 were observed. The optimally identified values of the bi-harmonic horizontal diffusion coefficient and the ratio of the transfer coefficient of the moisture to the transfer coefficient of the sensible heat actually improved the performance of the corresponding physical parameterization and/or numerical schemes, so that their impacts on the model forecast persisted under a similar large-scale atmospheric environment.

Finally, we present anomaly correlation results in Figures 5.21 - 5.22 for the specific humidity forecasts at 850 hPa and the geopotential height forecasts at 500 hPa for the control experiments, "optimal parameter" experiments, and "optimal initial condition" experiments as well as the experiments using both optimal initial conditions and optimally identified parameter values, respectively. These anomaly correlations were measured both for the tropical belt (defined here to be 40S - 40N where physical initialization was usually carried out (Krishnamurti, 1991)) and for the Northern Hemisphere (Fig. 5.21). The specific humidity field, which is mainly distributed in the lower troposphere, is very important in the tropical system. Comparing Fig. 5.21 (a) and (b), we see that the anomaly correlation for the Northern Hemisphere is consistently higher than that for the tropical belt for the entire 5-day

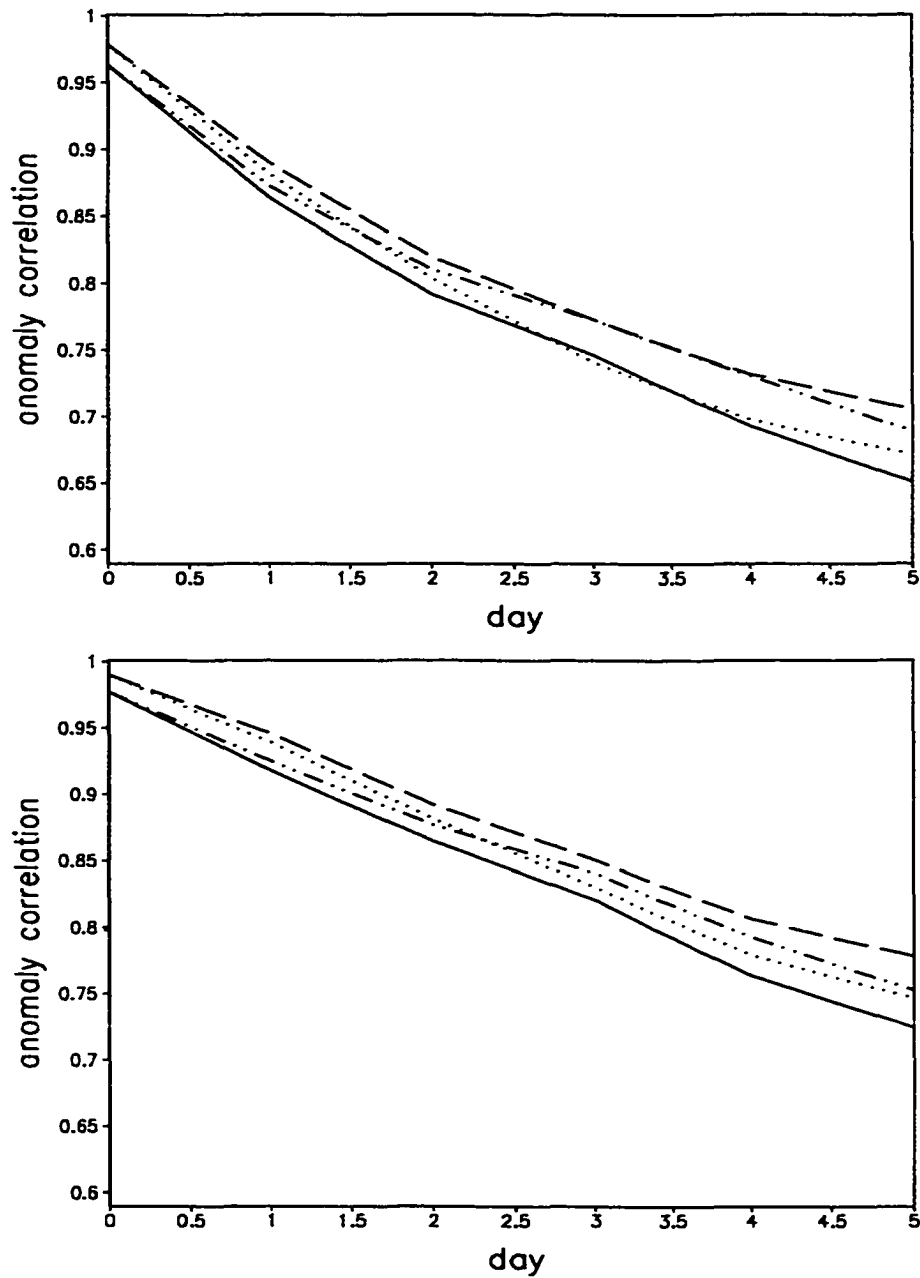


Figure 5.21: Anomaly correlation of the specific humidity forecasts at 850 hPa for the control experiments (solid line), “optimal parameter” experiments (dot dot dashed line), “optimal initial condition” experiments (dotted line), and the experiments using both the optimal initial conditions and optimally identified parameter values (dashed line). Upper panel: tropical belt; Lower panel: Northern Hemisphere.

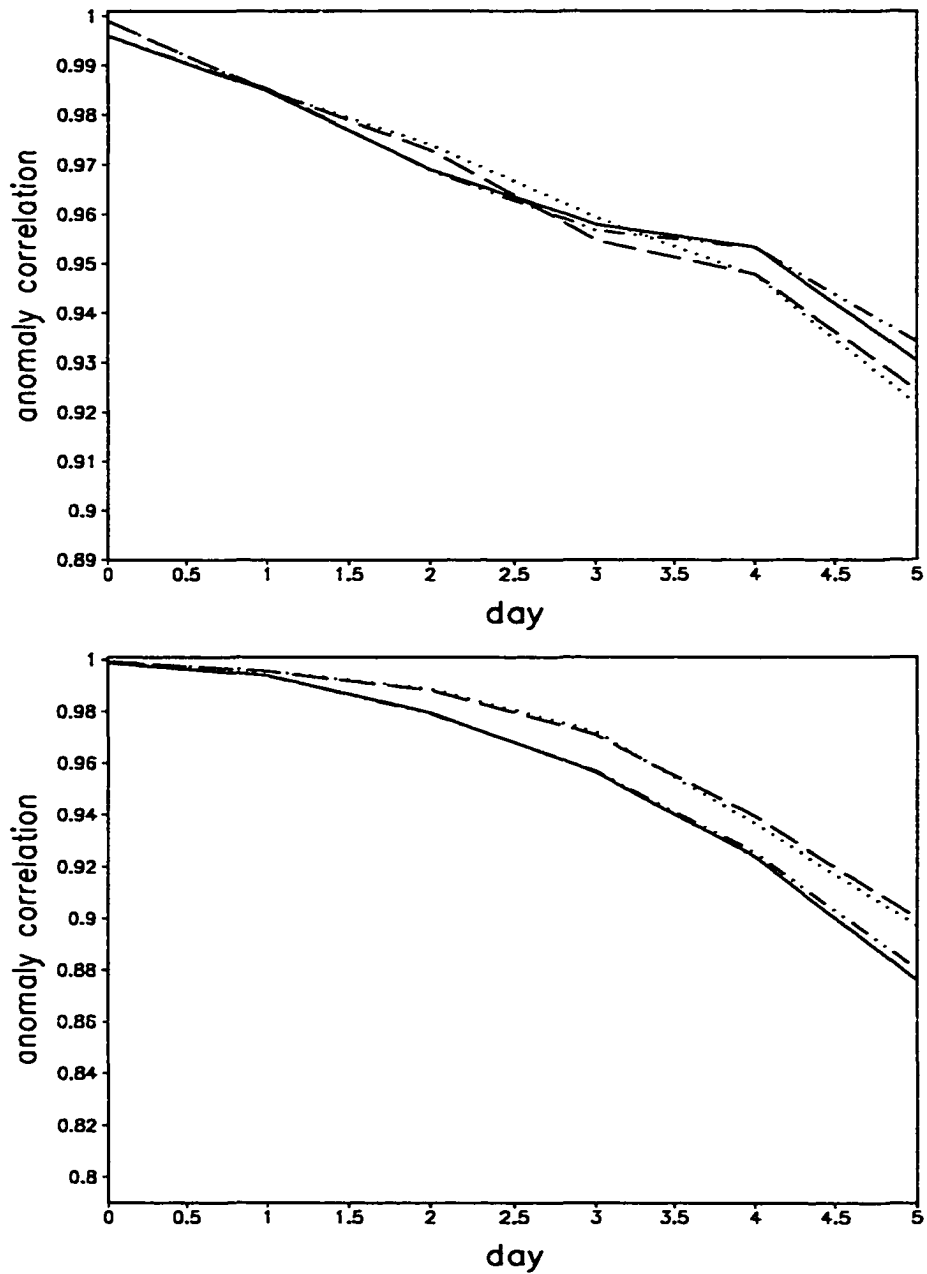


Figure 5.22: Anomaly correlation of the geopotential height forecasts at 500 hPa for the control experiments (solid line), “optimal parameter” experiments (dot dot dashed line), “optimal initial condition” experiments (dotted line), and the experiments using both the optimal initial conditions and optimally identified parameter values (dashed line). Upper panel: tropical belt; Lower panel: Northern Hemisphere.

integration period. The “optimal initial condition” technique appears to be more skillful than the “optimal parameter” method for the first 24h forecast in the tropical belt and for the first 48h forecasts in Northern Hemisphere. However, later in the forecast, for the period 48 - 120 h, the “optimal parameter” method yields better skill results than the “optimal initial condition” technique. The experiments using both the optimal initial conditions and optimally identified parameter values have the highest anomaly correlations, where for the 120h forecast, the anomaly correlation increases from 0.651 in the control experiment to 0.707 for the tropical belt and from 0.725 in the control experiment to 0.778 for the Northern Hemisphere. It is well-known that the anomaly correlation of the geopotential height forecasts at 500 hPa is a major index for the mid-latitude forecast. It is shown that the “optimal initial condition” technique is more skillful throughout the 5-day forecasts in the Northern Hemisphere in terms of the anomaly correlation of the geopotential height forecasts at 500 hPa. However, the “optimal parameter” experiments exhibit only a small improvement which becomes manifest for the 4-day and 5-day forecasts. The reasons for this might be that the three parameters were not very sensitive to the surface pressure and also due to the fact that the horizontal diffusion was not applied to the surface pressure. Nevertheless, the experiments using the optimal initial conditions and optimally identified parameter values simultaneously achieved satisfactory results over all of the Northern hemisphere and the tropical belt.

CHAPTER 6

AN APPLICATION OF SENSITIVITY OF THE MODEL FORECAST ERROR TO THE INITIAL CONDITIONS

The adjoint method is an efficient approach to carry out sensitivity analysis. This method allows us to calculate the gradients of any response (forecast aspect) with respect to all of the model input variables and parameters with only one integration of the forward nonlinear model and one backward integration of its adjoint model. The use of adjoint in sensitivity studies was initiated by the early work of Cacuci (1981a, b), who introduced a general sensitivity theory for nonlinear systems. Hall et al. (1982) applied the theory successfully to sensitivity of a climate radiative-convective model to some parameters. An in-depth review of the entire range of applications of sensitivity theory has been presented by Cacuci (1988). Later, Errico and Vukićević (1992) indicated that the adjoint fields quantify the previous conditions that most affect a specified forecast aspect. Rabier et al. (1992) used the adjoint of a global primitive equation model to investigate the following question: to which aspects of the initial conditions is cyclogenesis most sensitive in a simple idealized situation? Zou et al. (1993c) examined the sensitivity of a blocking index in a two-layer isentropic model using a response functional depending on both space and time.

One of the applications of adjoint sensitivity is to trace back the geographical regions where large forecast errors originate. Since the numerical weather prediction

model forecasts are generally sensitive to small errors in the initial conditions, the errors in analyses might amplify rapidly in model forecasts, leading to large forecast errors. Some studies have been carried out recently applying adjoint sensitivity to targeted or adaptive observations. For instance, Morss et al. (1998) examined adaptive observation strategies using a multilevel quasi-geostrophic channel model and a realistic data assimilation scheme. Pu et al. (1998) applied the quasi-inverse linear and adjoint methods to targeted observations during FASTEX. Both of their results indicated that the adjoint method was useful in determining the locations for adaptive observations.

In this study, sensitivity experiments using the adjoint method were carried out for a case on June 8, 1988 during the Indian summer monsoon. We will explore the sensitivity of the 1-day forecast error over a localized region of interest with respect to the initial conditions, which will be taken as a diagnostic tool to identify possible regions of analysis problems leading to large forecast errors, and expect that sensitivity analysis will provide us with an indication for the placement of adaptive observations in the locations where they are most needed, i.e., adding observations in the areas of large uncertainty (Lorenz and Emanuel, 1997).

6.1 Experimental setup

The model used in this study is a T42L12 version of the FSU GSM developed by Krishnamurti's lab, i.e., the horizontal resolution is of a triangular truncation type with total wavenumber of 42 and 12 levels in the vertical. The physical processes for both the forecast model and the adjoint model include planetary boundary layer

processes, vertical diffusion, dry adjustment, large-scale condensation and evaporation, deep cumulus condensation, horizontal diffusion and radiation processes. The adjoint integration was performed in the vicinity of a basic trajectory derived from the forward nonlinear FSU GSM starting from an ECMWF analysis valid 24 hours before the verification time. The gradients of the 1-day forecast error with respect to the initial conditions are called sensitivity patterns.

Let us denote by \mathbf{X} the state vector of the model at time t and $J(\mathbf{X}(t_1))$ the forecast aspect. Suppose the time evolution of the atmosphere is governed by the equation

$$\frac{d\mathbf{X}}{dt} = \mathbf{F}(\mathbf{X}) , \quad (6.1)$$

whose corresponding discretized tangent linear model is as follows

$$\delta\mathbf{X}(t_1) = \mathbf{P}(t_1, t_0) \delta\mathbf{X}(t_0) , \quad (6.2)$$

where t_0 and t_1 denote the initial time and verification time, respectively. The adjoint of the tangent linear model is

$$\mathbf{S}(t_0) = \mathbf{P}^T(t_1, t_0) \mathbf{S}(t_1) . \quad (6.3)$$

As shown in Rabier (1992) the gradient of J with respect to $\mathbf{X}(t_0)$ is equal to

$$\nabla_{\mathbf{X}(t_0)} J = \mathbf{P}^T(t_1, t_0) \nabla_{\mathbf{X}(t_1)} J , \quad (6.4)$$

where the operator \mathbf{P}^T is the adjoint of the tangent linear operator \mathbf{P} . Since the adjoint sensitivity in this study consists of the gradient of J with respect to the initial conditions, it can be computed by integrating the adjoint model backward in

time. A small perturbation or analysis error $\delta\mathbf{X}(t_0)$ in the initial conditions $\mathbf{X}(t_0)$ will result in a change in the forecast error J given by $\delta J = \langle \nabla_{\mathbf{X}(t_0)} J, \delta\mathbf{X}(t_0) \rangle$. Hence, in the geographical areas with a large (small) gradient value, a change in the initial conditions has a large (small) impact upon the forecast error.

We studied the sensitivity of 1-day forecast error integrated from 12UTC June 7, 1988 over a limited area, namely the Indian Monsoon area, with respect to the initial conditions. The forecast aspect is defined as the square norm of the differences between the model 1-day forecasts and the verifying analysis. The limited area or region of interest is defined to be the area between 60E and 100E, equator and 30N. On June 8, 1988, the Indian summer monsoon entered its active stage. A cross-equatorial flow set in, both the Arabian Sea and the Bay of Bengal branches were established, with depressions over the east central Arabian Sea and over the northern Bay of Bengal. Figures 6.1 and 6.2 display the geopotential height fields at 500 hPa at 12UTC June 7 and June 8, 1988 and the model 1-day forecast, respectively. The difference field of the geopotential height field at 500 hPa between the model 1-day forecast and the verifying analysis is displayed in Fig. 6.3. The differences are found to be rather large over the northern Bay of Bengal around 17.5N.

6.2 Results of the numerical experiment

The objective of this study is to find out the geographical areas to which the forecast aspect is the most sensitive. The gradient of J , i.e., the sensitivity pattern, is evaluated with respect to the model state variables.

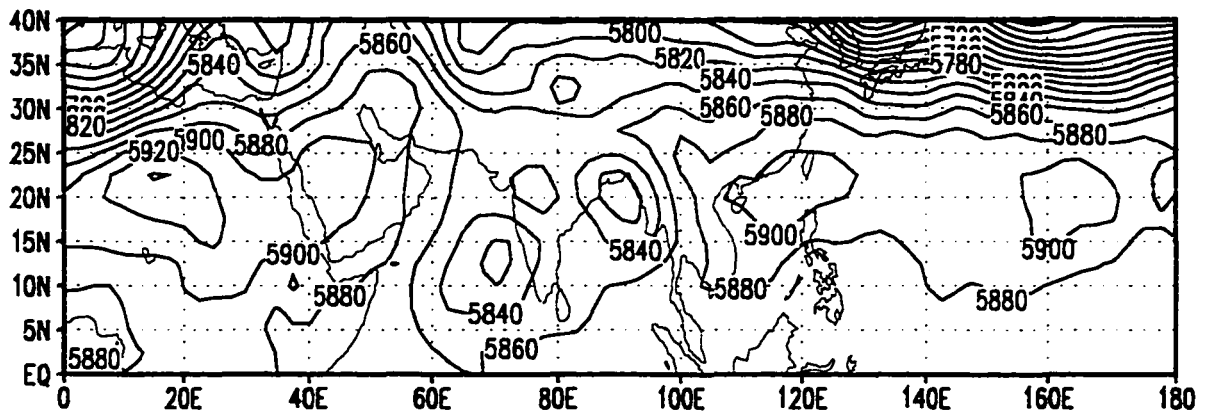
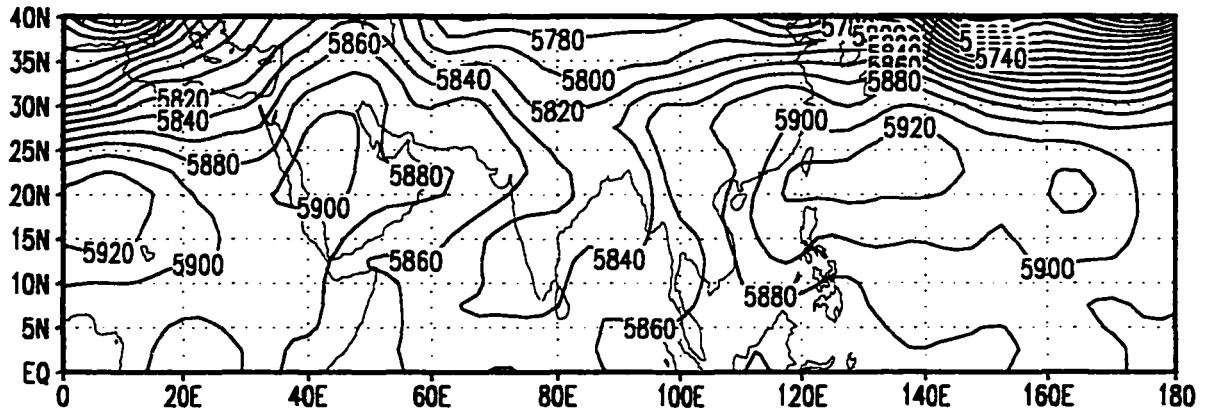


Figure 6.1: The geopotential height field at 500 hPa for 12UTC June 7 (upper panel) and June 8 (bottom panel), 1988.

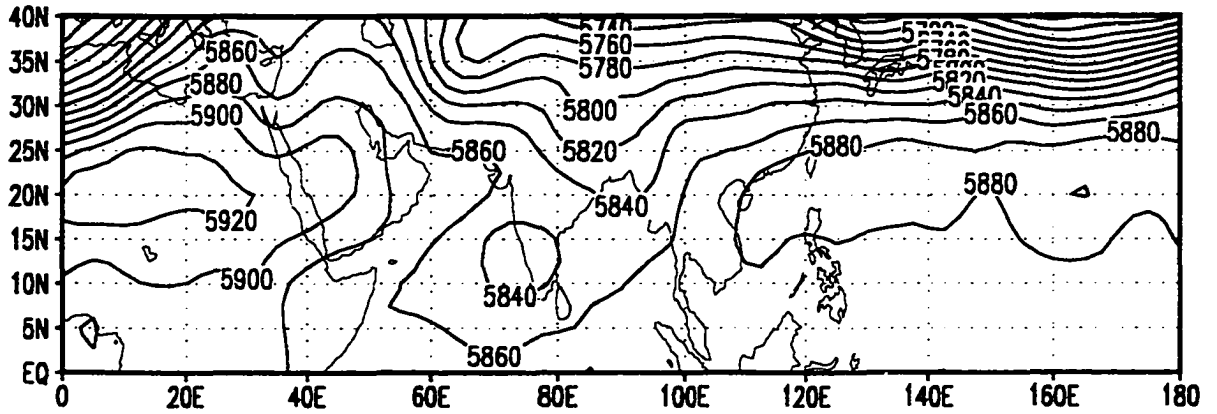


Figure 6.2: The geopotential height field at 500 hPa of the model 1-day forecast.

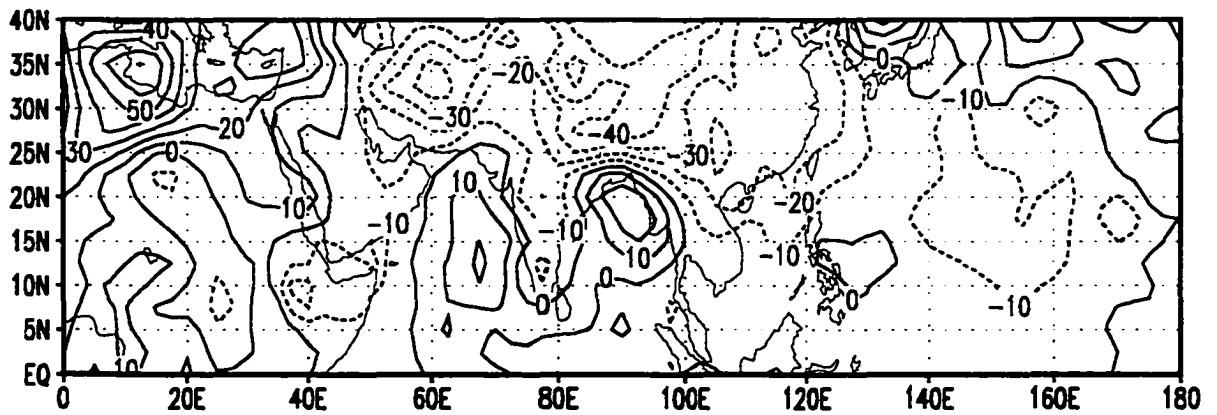


Figure 6.3: The difference field of the geopotential height field at 500 hPa between the model 1-day forecast and the verifying analysis.

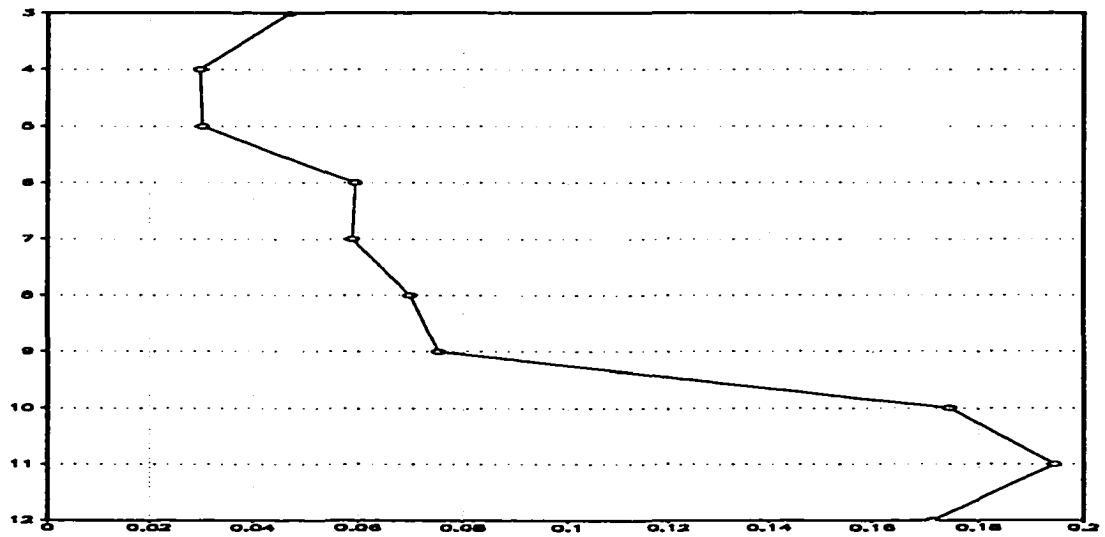


Figure 6.4: The squared sum of sensitivities with respect to the initial analysis of dewpoint depression for each model vertical level.

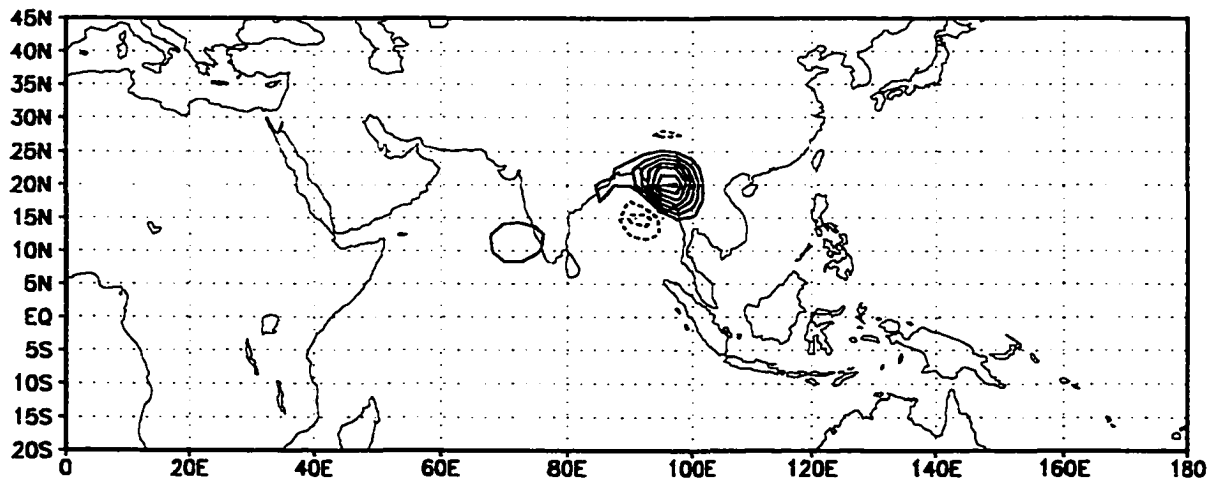


Figure 6.5: The sensitivities with respect to the dewpoint depression at the lowest model level. The contour interval is $1 K^{-1}$.

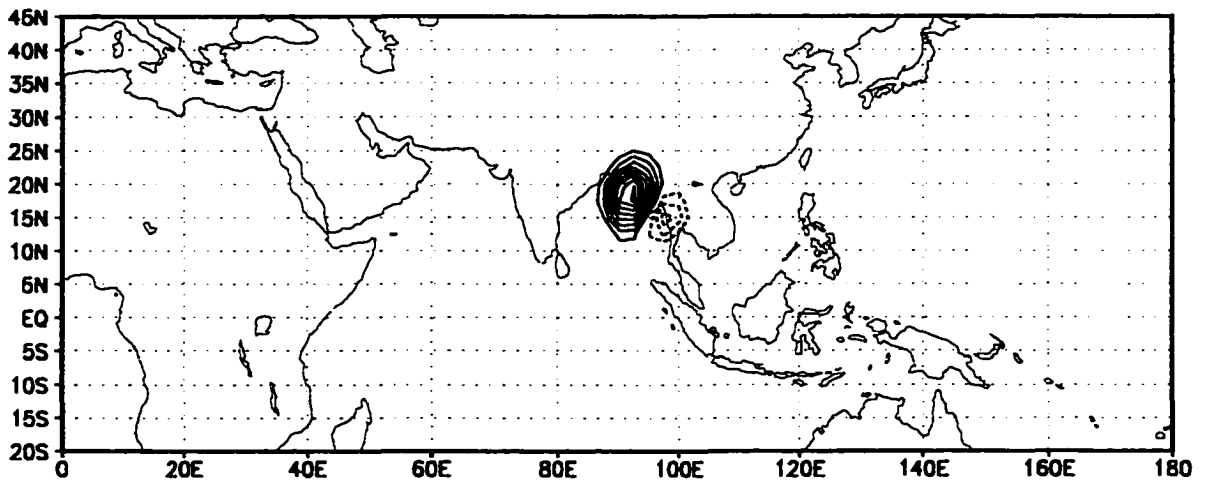


Figure 6.6: The sensitivities with respect to the initial analysis of dewpoint depression at the second lowest model level. The contour interval is $1 K^{-1}$.

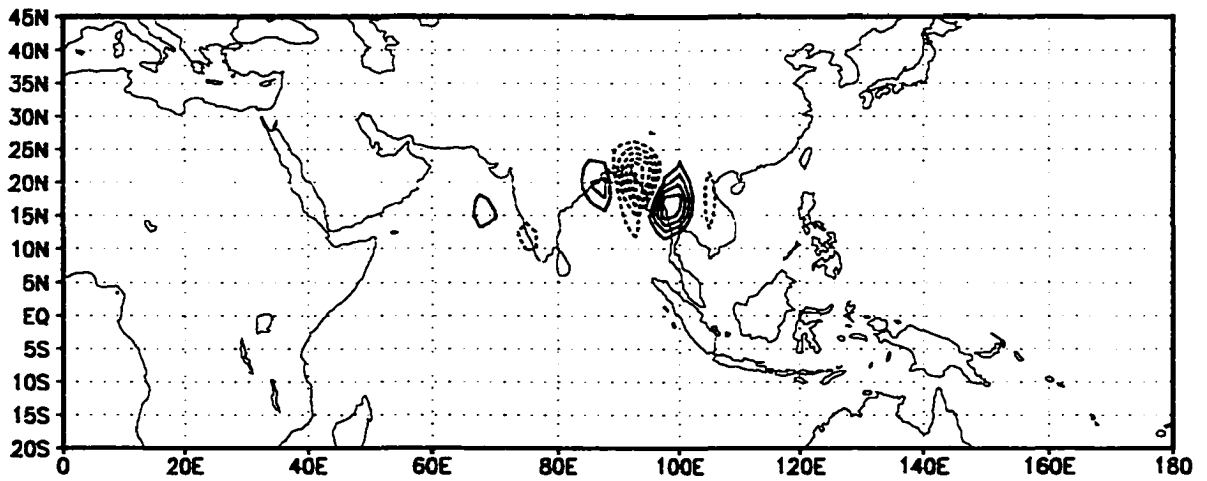


Figure 6.7: The sensitivities with respect to the initial analysis of dewpoint depression at the third lowest model level. The contour interval is $1 K^{-1}$.

It is known that the analysis of moisture field is usually unreliable over the tropics due to the lack of the observations, i.e., there is a large uncertainty in this analysis. Fig. 6.4 presents the squared sum of sensitivities with respect to the initial analysis of dewpoint depression for each model vertical level. The striking feature observed is that the forecast error is very sensitive to the initial analyses of dewpoint depression at the lowest three model vertical levels, while the sensitivities to the upper model levels are small. In order to provide a closer look at a single model vertical level, the sensitivity patterns with respect to the dewpoint depression at the lowest three model levels, i.e., model vertical levels 12, 11 and 10, are presented in Fig. 6.5 - Fig. 6.7, respectively. A large positive maximum center located at the upstream of the region with large forecast errors over the northern Bay of Bengal was observed for both of the two lowest model levels, but a large negative maximum center was more pronounced at the third lowest vertical level. The analyses of dewpoint depression at time t_0 were diagnosed to be too dry over the northern Bay of Bengal at the lowest two model vertical levels. The results obtained show that the model 1-day forecast error is most sensitive to the analysis errors in the dewpoint depression around 90E, 20N. Additional observations around this point are expected to improve the model 1-day forecast. The vertical cross-section at 20N for the sensitivity with respect to the dewpoint depression at time t_0 is displayed in Fig. 6.8. The pattern is tilted in the vertical to the west, which indicates that further growth of the depression is sensitive to baroclinic perturbations at the initial time.

The sensitivity patterns with respect to the initial analysis of virtual temperature at model vertical levels 12 and 10 (Figures. 6.9 and 6.10) also indicate the locations

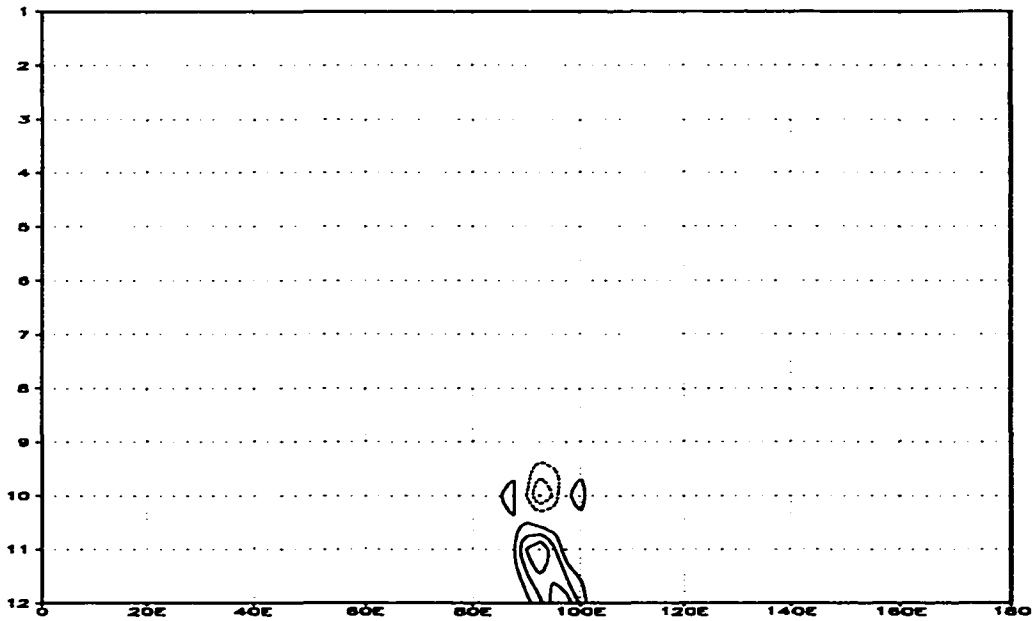


Figure 6.8: The vertical cross-section at 20N for the sensitivity with respect to the dewpoint depression at time t_0 . The contour interval is $2K^{-1}$.

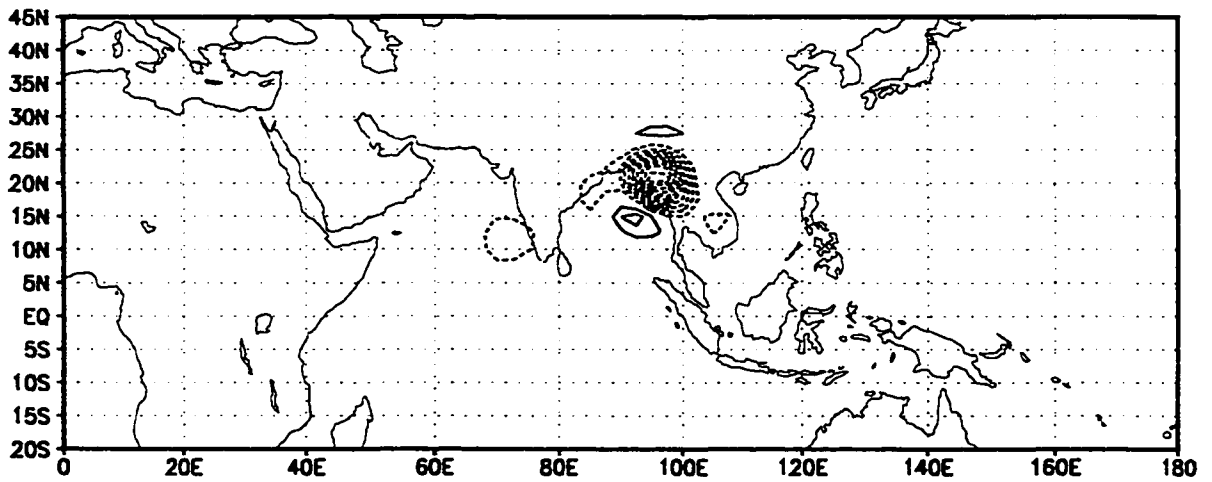


Figure 6.9: The sensitivity pattern with respect to the initial analysis of virtual temperature at model vertical level 12. The contour interval is $1 K^{-1}$.

of the geographical regions where the analysis problems lie in. The analyses of virtual temperature over the northern Bay of Bengal were diagnosed to be too low at model vertical level 12 and too high at model vertical level 10. The vertical cross-section at 20N is displayed in Fig. 6.11.

The calculation of the squared sum of sensitivities with respect to the initial analysis of vorticity for each model vertical level indicates that the model 1-day forecast error is sensitive to the uncertainties in the analysis at model vertical levels 11 and 7, which are approximately located near the surface and 700 hPa, respectively. For the initial analysis of divergence, the model 1-day forecast error is most sensitive to the errors at model vertical level 11. The sensitivity patterns with respect to the initial analyses of vorticity and divergence at model vertical level 11 are displayed in Fig. 6.12 and Fig. 6.13, respectively. Two important areas with opposite signs are observed for both the sensitivity patterns. The vertical cross-section at 20N for the sensitivity pattern with respect to vorticity at time t_0 (Fig. 6.15) exhibited two large centers with opposite signs, both of which were located in the lower troposphere around 90E, 20N. This indicated that the forecast error was very sensitive to the vorticity analysis uncertainties in the lower atmosphere. One maximum center, which is located at model vertical level 7, was also observed in the vertical cross-section at 10N for the sensitivity pattern with respect to the initial analysis of vorticity (Fig. 6.16), however, no westward-tilting of the vertical structure was observed. The results show that analysis uncertainties at model vertical level 7 are mainly distributed over the eastern Arabian Sea, while the analysis uncertainties at model vertical level 11 are mainly located around 90E, 20N.

The sensitivity signal is represented by the sum of the square of the sensitivity patterns throughout the whole range of vertical levels. The sensitivity signals for vorticity and dewpoint depression are displayed in Figures 6.17 and 6.18, respectively. It is apparent that the model 1-day forecast error is most sensitive to the analysis errors located around 90E, 20N over the northern Bay of Bengal.

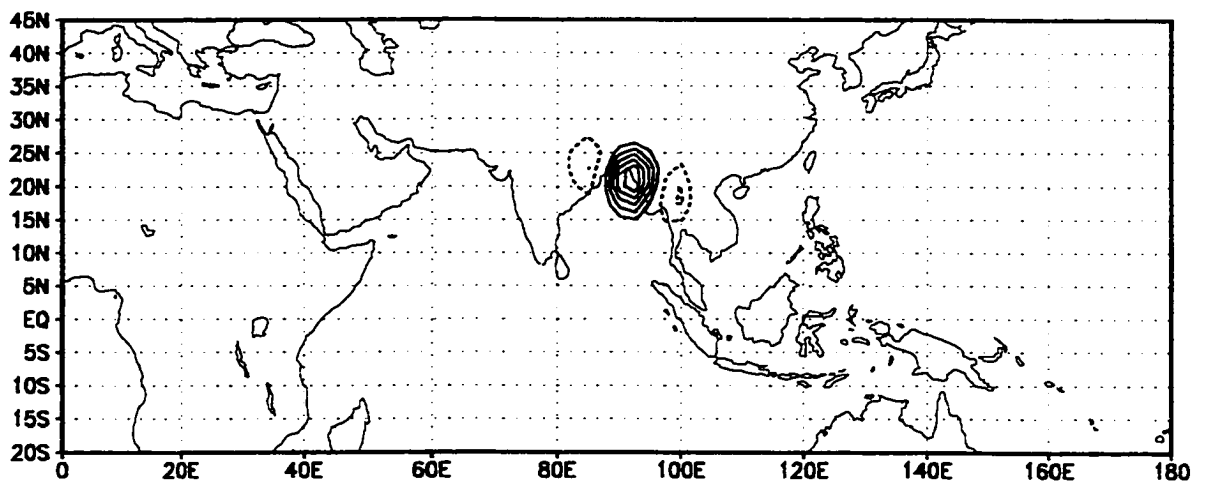


Figure 6.10: The sensitivity pattern with respect to the initial analysis of virtual temperature at model vertical level 10. The contour interval is $2 K^{-1}$.

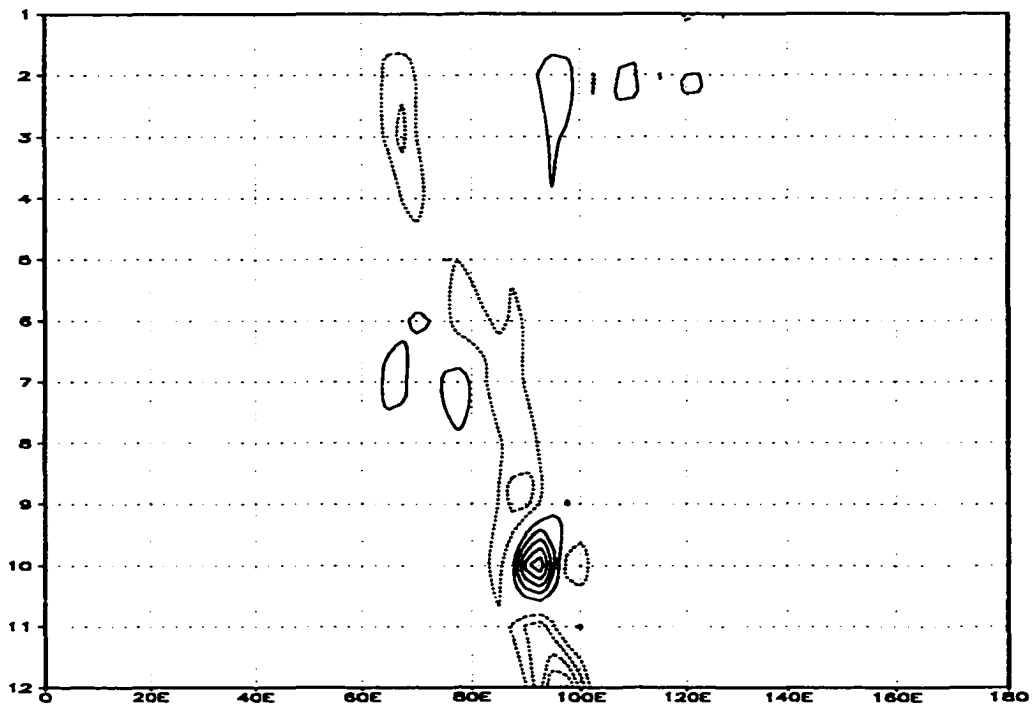


Figure 6.11: The vertical cross-section at 20N for the sensitivity pattern with respect to virtual temperature at time t_0 . The contour interval is $2 K^{-1}$.

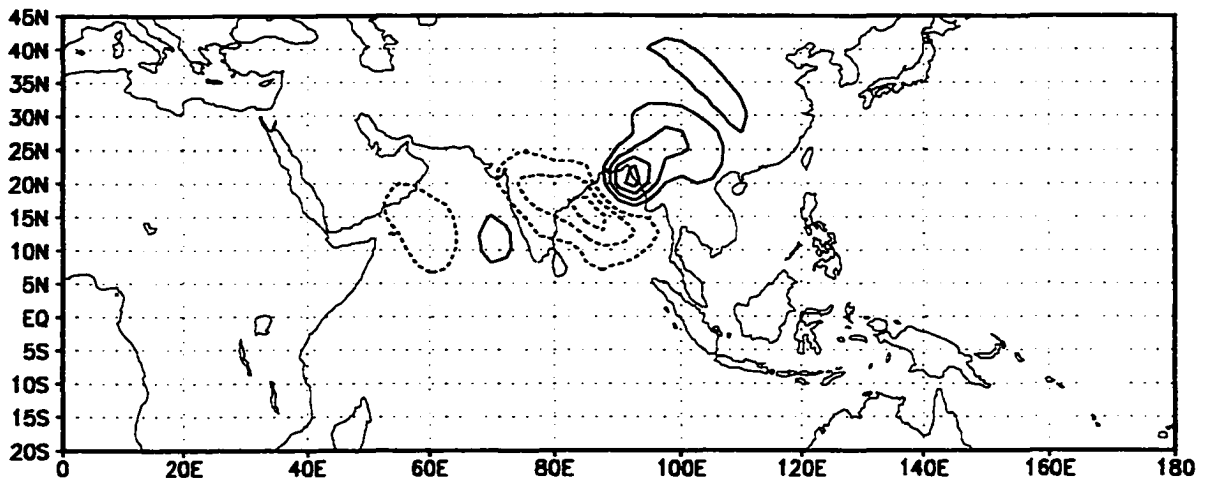


Figure 6.12: The sensitivity pattern with respect to the initial analysis of vorticity at model vertical level 11. The contour interval is 200000s.

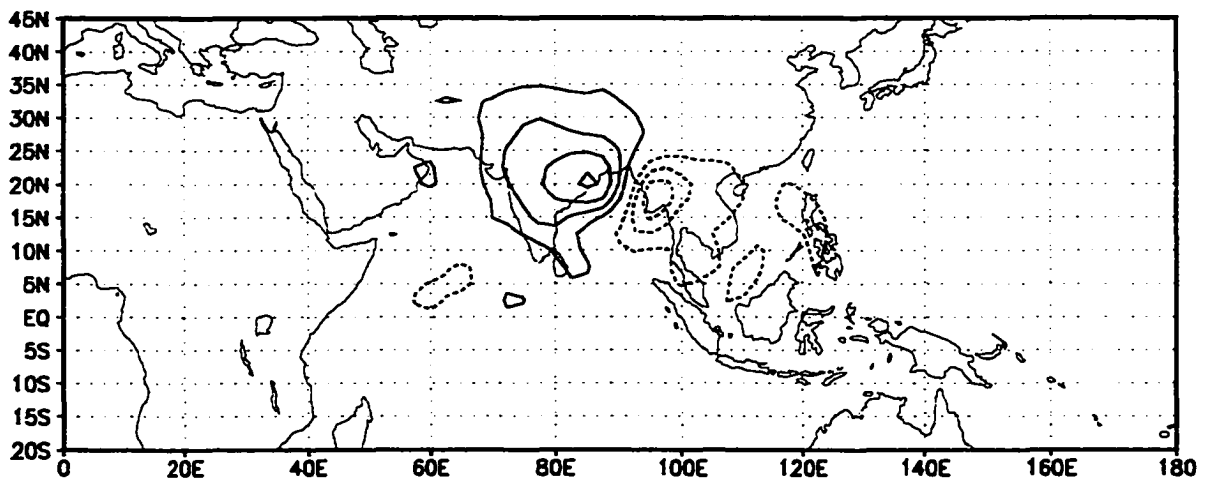


Figure 6.13: The sensitivity pattern with respect to the initial analysis of divergence at model vertical level 11. The contour interval is 200000s.

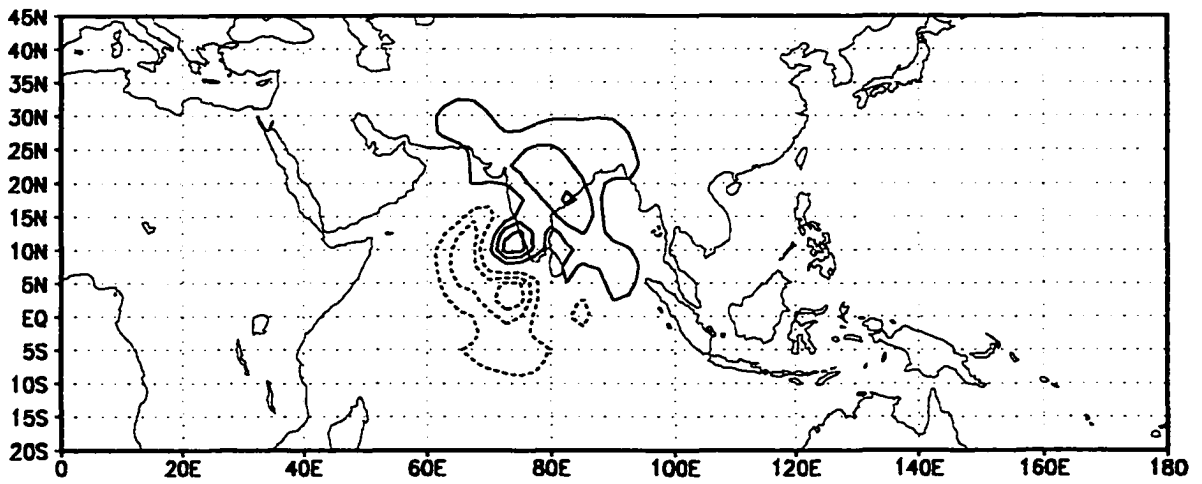


Figure 6.14: The sensitivity pattern with respect to the initial analysis of vorticity at model vertical level 7. The contour interval is 200000s.

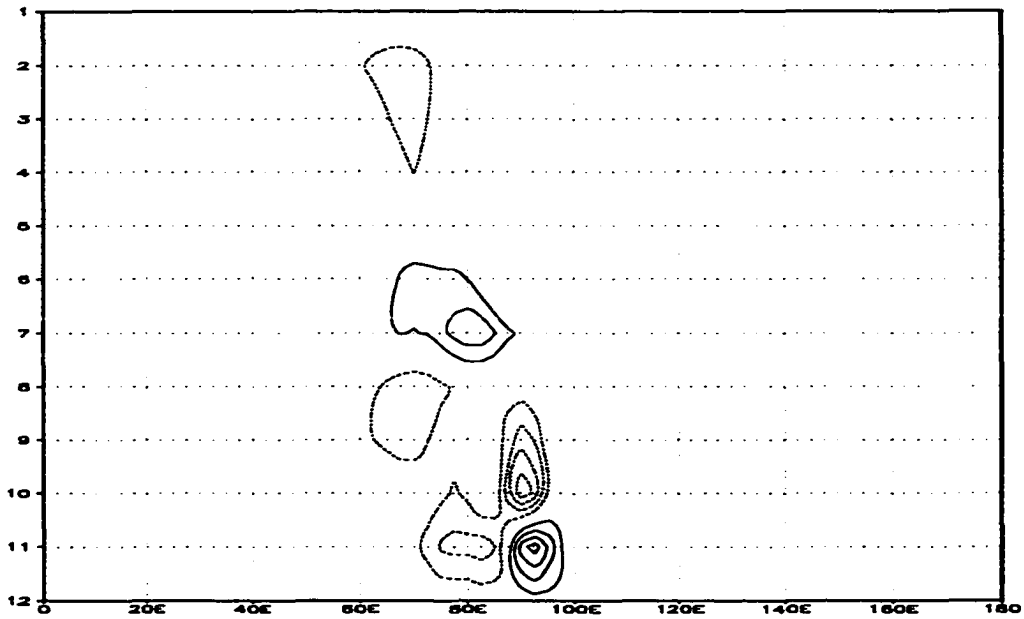


Figure 6.15: The vertical cross-section at 20N for the sensitivity pattern with respect to vorticity at time t_0 . The contour interval is 200000s.

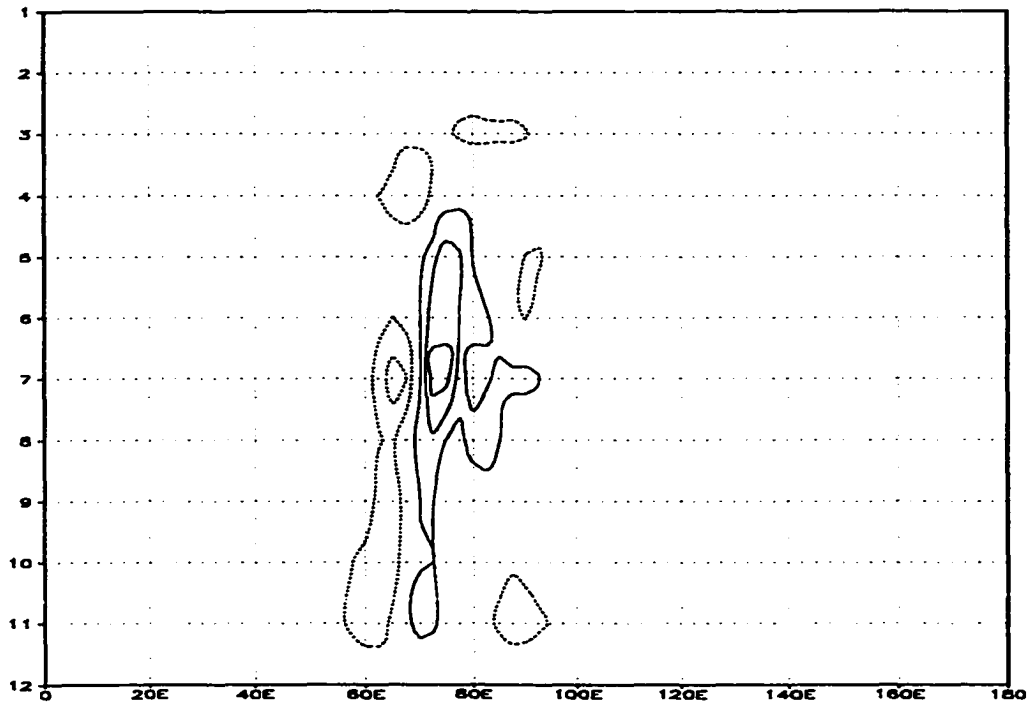


Figure 6.16: The vertical cross-section at 10N for the sensitivity pattern with respect to vorticity at time t_0 . The contour interval is $200000s$.

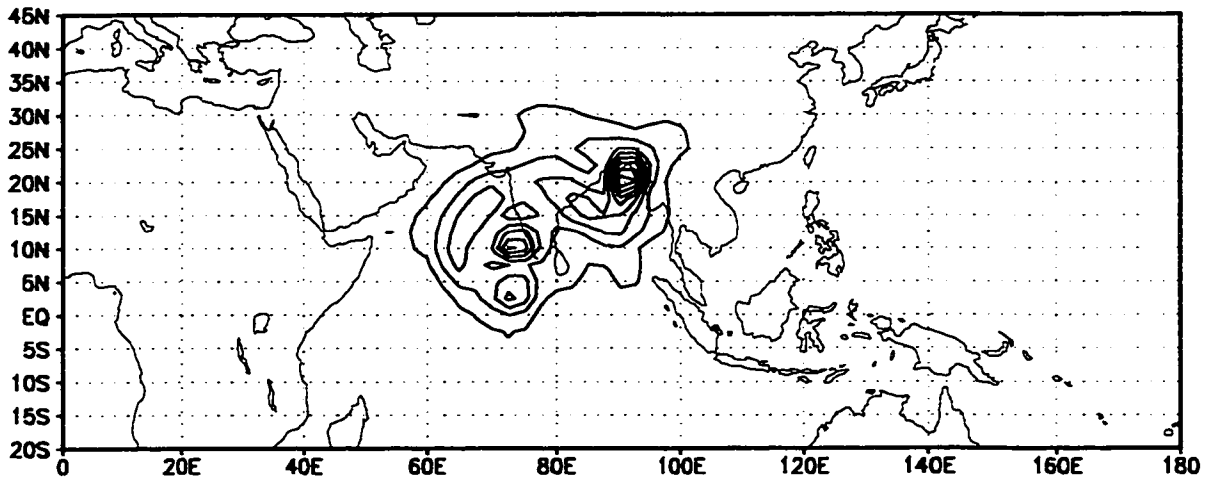


Figure 6.17: The sensitivity signal for vorticity at time t_0 .

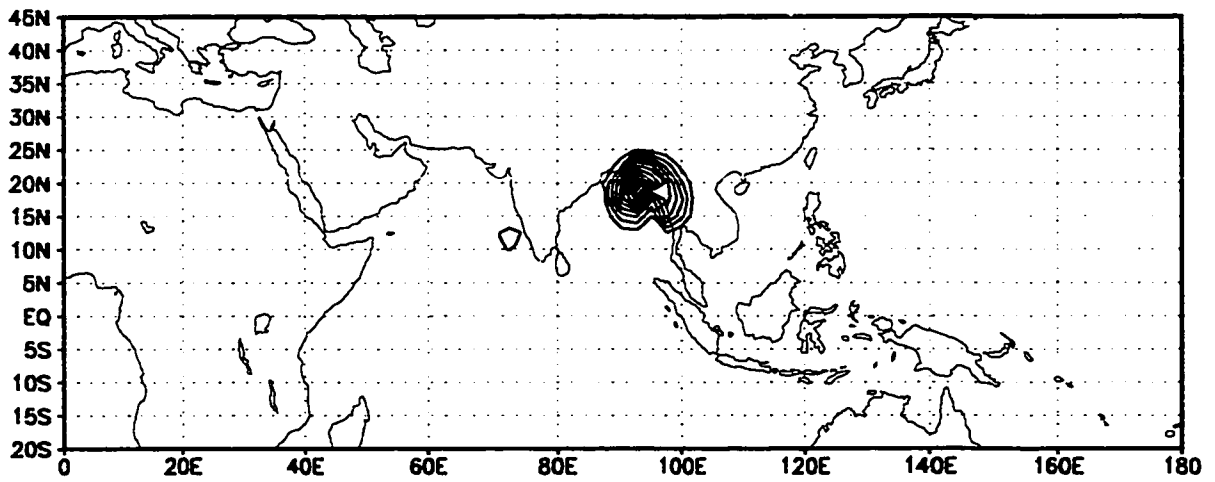


Figure 6.18: The sensitivity signal for dewpoint depression at time t_0 .

CHAPTER 7

SUMMARY AND FUTURE RESEARCH

In this study, we developed the tangent linear and adjoint codes for the radiation and the boundary layer process packages, removing the existing discontinuities in the physical processes which most affect the linear approximation and the behavior of the minimization convergence rate. This resulted in the completion of the full-physics adjoint model for the FSU GSM. With the availability of the FSU GSM and its full-physics adjoint model, we carried out a twin experiment to demonstrate the feasibility of 4-D VAR using the full-physics adjoint model, and closely examined the quality of the retrieved initial conditions. The results obtained were very encouraging. This effort was followed by numerical experiments of variational data assimilation and adjoint parameter estimation which were performed using the initialized ECMWF analysis data. Both optimal initial conditions and optimal values of three key parameters, i.e., the bi-harmonic horizontal diffusion coefficient, the Asselin filter coefficient and the ratio of the transfer coefficient of moisture to the transfer coefficient of sensible heat, were recovered using the full-physics adjoint of the FSU Global Spectral Model. The optimally identified value of the bi-harmonic horizontal diffusion coefficient was found to be almost twice the value used in the original forecast model, while the optimally identified value of Asselin filter coefficient was found to be very close to its original estimated value which indicated that

its estimation was fairly good. The optimal value for the parameter γ was found to be only half of the value used in the original forecast model.

We focused our investigation on the 6h forecast fields at the end of the assimilation window starting from the retrieved optimal initial conditions and the optimal parameter values, which are the fields at the latest analysis time. The results showed that these fields successfully captured the main features of the analysis fields. Although the impact of optimal initial conditions dominated that of the optimal parameter values at the early stages of the forecast, a positive impact due to each optimally estimated parameter value was observed. The ensuing 24h forecast experiments where only the optimal parameter values were used further showed the positive impact of using optimal parameter values. The optimally identified bi-harmonic horizontal diffusion coefficient improved vorticity and divergence fields as well as the fields of virtual temperature and dewpoint depression at the upper vertical levels. The ratio γ of the transfer coefficient of moisture to the transfer coefficient of sensible heat had a large positive impact on the lower vertical levels of the model, especially for the virtual temperature and the dewpoint depression fields. By combining the three optimally identified parameter values, we obtained the best forecast results. Further studies of ensuing forecasts using the optimally identified parameter values and the optimal initial condition respectively showed that the model tended to “forget” first the impact of the optimal initial condition while the impact of optimally identified parameter values persisted well beyond the range of 72 hours forecast. The optimally identified values of the bi-harmonic horizontal diffusion coefficient and the ratio of the transfer coefficient of the moisture to the transfer coefficient of the sen-

sible heat improved the performance of the corresponding physical parameterization scheme, therefore, the regions of the impacts resulting from variationally derived optimal initial conditions and from the optimally identified parameter values were quite different. The anomaly correlation results indicated that the experiments using simultaneously optimal initial conditions and optimally identified parameter values yielded the best performance.

However, we should be aware that these results were obtained for a single case study. Further studies should be conducted for different initial conditions in order to draw a more general conclusion. Moreover, the parameters studied in this paper were assumed to be constant in both time and space. In future research, we should address the issue of retrieving values of κ and γ that vary both in space and time. In particular, we would like to focus on the values of γ for different stages of a tropical system and for different regions, and study their impact on the forecasts, especially on the precipitation field. Additionally, for a parameter estimation to be properly specified, the parameter's seasonal variation should also be taken into account.

The three optimal parameter values were determined on the basis of one day on which these computations were carried out. When the number of parameters to be estimated is small, the parameter estimation process can provide us with both optimally determined parameters and initial conditions simultaneously for every case without involving significant additional computational burden. However, in as far as the operational forecast is concerned, it is not necessary and efficient to optimally identify parameter values in a daily manner. The parameter estimation procedure should be carried out over a period of many days (such as 30 days) so that a reliable

expected value for each parameter can be obtained. The issue of the period of validity of optimally estimated parameters and the frequency with which they should be refreshed in an operational model would necessitate further studies. Yet another question that deserves further study is the issue of the feedback between the effects of various optimally estimated parameters.

In this study, the nonlinear forecast model was assumed to be perfect, i.e., it was used as a strong constraint. Further studies should be conducted to take into account the model forecast error, i.e., the forecast model can be regarded as a weak constraint, and its effect on the retrieved initial conditions and optimal parameter values should be examined.

At the end of the study, a preliminary experiment was carried out for the the sensitivity of the model 1-day forecast error to the initial conditions for an Indian summer monsoon case. The results were applied to localize the regions with large analysis uncertainties where more observations were required in order to reduce the model forecast error. However, the sensitivity study was performed in “a posteriori” diagnostic way in this study. For a practical problem, large forecast uncertainties can be identified using the ensemble forecast system (Kalnay and Toth, 1996). The forecast difference may be obtained by subtracting one member of the ensemble from another, then the localized forecast errors may be applied to the adjoint model in order to obtain the adjoint sensitivity.

APPENDIX A

Sensitivity analysis

The most general and fundamental concept for the definition of the sensitivity of a response to variations in the system parameters is the Gateau differential. The G-differential $VR(e^0; h)$ of a specified response $\mathbf{R}(x)$ at e^0 with increment h , is defined as

$$\lim_{t \rightarrow 0} [\mathbf{R}(e^0 + th) - \mathbf{R}(e^0)]/t = VR(e^0; h) \quad (.1)$$

where all vectors $h = (h_x, h_\alpha)$. The G-differential $VR(e^0; h)$ is related to the total variation of \mathbf{R} at e^0 through the relationship

$$\mathbf{R}(e^0 + h) - \mathbf{R}(e^0) = VR(e^0; h) + \Delta(h)^2 \quad (.2)$$

where

$$\lim_{t \rightarrow 0} [\Delta(th)/t] = 0 \quad (.3)$$

Following Zou et al. (1993c) and Navon (1997), given a specific response $R(x, \alpha)$

$$R(x, \alpha) = \int_{t_0}^{t_R} r(t; x, \alpha) dt \quad (.4)$$

where α is a model parameter vector, x denotes the model variables, the G differential $VR(x^0, \alpha^0, h_x, h_\alpha)$ of R at the nominal values (x^0, α^0) , for increments (h_x, h_α) around (x^0, α^0) , is given by

$$VR(x^0, \alpha^0; h_x, h_\alpha) = \int_{t_0}^{t_R} r'_x \cdot h_x dt + \int_{t_0}^{t_R} r'_\alpha \cdot h_\alpha dt \quad (.5)$$

$$r'_x = \left[\left(\frac{\partial r}{\partial x_1}, \dots, \frac{\partial r}{\partial x_P} \right) \right]_{(x^0, \alpha^0)} \quad (.6)$$

$$r'_\alpha = \left[\left(\frac{\partial r}{\partial \alpha_1}, \dots, \frac{\partial r}{\partial \alpha_N} \right) \right]_{(x^0, \alpha^0)} \quad (.7)$$

N is the dimension of the vector of model parameters and P is the dimension of the model variable.

If a variation occurs solely in the n -th parameter, the corresponding variation h_{α}^n of the parameter vector is

$$h_{\alpha}^n = (0, \dots, h_{\alpha}^n, \dots, 0)^T$$

and the corresponding sensitivity is VR^n . The relative sensitivity S_n is defined as the dimensionless quantity

$$S_n = \frac{VR^n}{R} \left(\frac{h_{\alpha}^n}{\alpha_n^0} \right)^{-1} \quad (.8)$$

The larger the relative sensitivity, the more important the parameter. Hence, sensitivity analysis can also be utilized as a tool in choosing the subset of the parameters for the parameter estimation by ranking their relative sensitivities to model responses.

APPENDIX B

An example for deriving tangent linear and adjoint codes

1. The original nonlinear codes

```

SUBROUTINE SFLX(U1,U2,T1,T2,Q1,Q2,Z1,Z2,NTYPES,II,JJ,RIB,
+             FSX,FLT,FM,RHO,GW)
PARAMETER (ILEVV=12,ILEV1V=ILEVV+1)
C
C  SUBROUTINE RETURNS SURFACE SENSIBLE (SEN) AND LATENT (CON)
C  HEAT FLUXES VIA STABILITY DEPENDENT BULK AERODYNAMIC
C  FORMULATION
C
C  INPUT PARAMETERS:
C
C  NTYPES - TYPE OF SURFACE
C
C             -1 ==> LAND
C             0  ==> OCEAN
C             1  ==> LAND WITH SNOW
C             2  ==> OCEAN WITH ICE
C
C  XHT1  - TERRAIN HEIGHT IN METERS
C  U1,U2 - WINDS IN M/S      AT LEVEL 1 & 2
C  T1,T2 - POTENTIAL TEMP.  AT LEVEL 1 & 2
C  Q1,Q2 - SPECIFIC HUMIDITY AT LEVEL 1 & 2
C
COMMON /RHH9/ RH(ILEVV),DQQ(ILEVV)
COMMON /EXTRA9/ RB,USTR,OL,CD,CH,CQ,X7,X8,SIGZ2,ZV,ZT
C
DATA G,VKC,ALPHA,CP/9.81,.35,.04,1004.5/
C
INDX = 0
CHP  = 0.
CQP  = 0.
```

```

C
  IF (NTYPES .NE. 0) GOTO 15
C
  Z2 = ZT
C
C   COMPUTE CD OVER OCEAN AS A FUNCTION OF WIND SPEED
C
  CD = 0.0011
C
C   IF LAND POINT , COMPUTE ZO FROM TERRAIN HEIGHT FORMULATION
C   WITHIN SUBROUTINE TG
C   IF OCEAN POINT, COMPUTE ZO FROM ITERATIVE CHARNOCK METHOD
C
  USTRSQ = CD*(U2**2)
  ZO = ALPHA*USTRSQ/G
C
  IF (ZO .LT. 1.0E-4) ZO = 1.0E-4
C
  Z1 = ZO
C
  IF (Z1 .GE. Z2) Z2 = Z2+Z1
C
  DO 35 I=1,3
  U2DUM = U2*ALOG(Z2/Z1)/ALOG(ZV/Z1)
  CALL SFXPAR(U1,U2DUM,T1,T2,Z1,Z2,USTR,TSTR,RIB,OL,
+ CD,CH,CQ,II,JJ,KT,CHP,CQP,INDX)
C
  ZO = ALPHA*(USTR**2)/G
  IF (ZO .LT. 1.0E-4) ZO = 1.0E-4
  Z1 = ZO
C
  IF (Z1 .GE. Z2) Z2 = Z2+Z1
C
35 CONTINUE
C
  CHMAX = -2.0E-03
  CDMAX = 2.0E-03
  GOTO 25

```



```

15  U2DUM = U2*ALOG(Z2/Z1)/ALOG(ZV/Z1)
C
    CHMAX = -5.0E-03
    CDMAX =  5.0E-03
25  CALL SFXPAR(U1,U2DUM,T1,T2,Z1,Z2,USTR,TSTR,RIB,OL,
+ CD,CH,CQ,II,JJ,KT,CHP,CQP,INDX)
C
    CD = AMIN1(CD,CDMAX)
    CH = AMAX1(CH,CHMAX)
    CQ = CH
C
    U22 = U2DUM
    U22 = AMAX1(5.0,U22)
    FSX = RHO*CH*CP*U22*(T2-T1)
    FLT = RHO*CQ*U22*GW*(Q2-Q1)
    FM  = RHO*CD*U22*U22
C
    RETURN
    END

```

2. The tangent linear codes

```

SUBROUTINE TANSFLX(U1,U2,T1,T2,Q1,Q2,Z1,Z2,NTYPES,II,JJ,RIB,
.           FSX,FLT,FM,RHO,GW,U19,U29,T19,T29,Q19,Q29,
.           Z19,Z29,CD99,CH99,CQ99)
C
C   input: U19,U29,T19,T29,Q19,Q29,Z19,Z29,CD99,CH99,CQ99
C           U1,U2,T1,T2,Q1,Q2,Z1,Z2,ZV,ZT,RHO
C   output: FSX,FLT,FM,Z1,T1
C
C   PARAMETER (ILEVV=12,ILEV1V=ILEVV+1)
C
C   SUBROUTINE RETURNS SURFACE SENSIBLE (SEN) AND LATENT (CON)
C   HEAT FLUXES VIA STABILITY DEPENDENT BULK AERODYNAMIC
C   FORMULATION
C
C   COMMON /RHH/ RH(ILEVV),DQQ(ILEVV)

```

```

COMMON /EXTRA/ RB,USTR,OL,CD,CH,CQ,X7,X8,SIGZ2,ZV,ZT
C
COMMON /EXTRA9/ RB9,USTR9,OL9,CD9,CH9,CQ9,X79,X89,SIGZ29,ZV9,ZT9
COMMON /DENSITY9/ RH09
C
DIMENSION ZS19(4),ZS29(4),ZUSTR9(4),ZU2DUM8(4)
DIMENSION ZZ18(4),ZZ28(4)
C
DATA G,VKC,ALPHA,CP/9.81,.35,.04,1004.5/
C
INDX = 0
CHP = 0.
CQP = 0.
C
IF (NTYPES .NE. 0) THEN
C
    CHMAX = -5.0E-03
    CDMAX = 5.0E-03
    U2DUM9 = U29*ALOG(Z29/Z19)/ALOG(ZV9/Z19)
C
ELSE
C
    CHMAX = -2.0E-03
    CDMAX = 2.0E-03
C
    ZZ29 = ZT9
    CCD90 = 0.0011
    USTRSQ9 = CCD90*(U29**2)
    ZZ09 = ALPHA*USTRSQ9/G
    IF (ZZ09 .LT. 1.0E-4) ZZ09 = 1.0E-4
    ZZ19 = ZZ09
    ZZ18(1) = ZZ09
    ZZ28(1) = ZZ29
    IF (ZZ19 .GE. ZZ29) ZZ29 = ZZ29+ZZ19
    ZUSTR9(1) = USTRSQ9
    ZS19(1) = ZZ19
    ZS29(1) = ZZ29
C

```

```

DO 35 I=1,3
U2DUM8 = U29*ALOG(ZZ29/ZZ19)/ALOG(ZV9/ZZ19)
CALL SFYPAR(U19,U2DUM8,T19,T29,ZZ19,ZZ29,UUSTR9,TSTR9,RRIB9,
           00L9,CCD9,CCH9,CCQ9,II, JJ,KT,CHP,CQP,INDX)
ZZ09   = ALPHA*(UUSTR9**2)/G
IF (ZZ09 .LT. 1.0E-4) ZZ09 = 1.0E-4
ZZ19   = ZZ09
C
ZZ18(I+1) = ZZ09
ZZ28(I+1) = ZZ29
IF (ZZ19 .GE. ZZ29) ZZ29 = ZZ29+ZZ19
C
ZU2DUM8(I) = U2DUM8
ZUUSTR9(I+1) = UUSTR9
ZS19(I+1) = ZZ19
ZS29(I+1) = ZZ29
C
35 CONTINUE
C
Z19 = ZZ19
Z29 = ZZ29
U2DUM9 = U2DUM8
C
END IF
C
U229 = U2DUM9
U229 = AMAX1(5.0,U229)
C
IF (NTYPES .NE. 0) THEN
C
U2DUM = U2*ALOG(Z29/Z19)/ALOG(ZV9/Z19)
      +U29*Z2/(Z29*ALOG(ZV9/Z19))
      -U29*ALOG(Z29/Z19)*ZV/(ZV9*(ALOG(ZV9/Z19))**2)
C
ELSE
C
CCD = 0.
USTRSQ = 2.*CCD90*U29*U2

```

```

ZZO      = ALPHA*USTRSQ/G
IF (ZZ18(1) .LE. 1.0E-4) ZZO = 0.
C
ZZ1      = ZZO
C
ZZ2      = ZT
IF (ZZ18(1) .GE. ZZ28(1)) ZZ2 = ZZ2+ZZ1
C
DO 36 I=1,3
U2DUMM = U2*ALOG(ZS29(I)/ZS19(I))/ALOG(ZV9/ZS19(I))
.         +U29*(ZZ2/ZS29(I)-ZZ1/ZS19(I))/ALOG(ZV9/ZS19(I))
.         -U29*ALOG(ZS29(I)/ZS19(I))*(ZV/ZV9-ZZ1/ZS19(I))
.         /(ALOG(ZV9/ZS19(I))**2)
CALL TANSFXPAR(U1,U2DUMM,T1,T2,ZZ1,ZZ2,UUSTR,TSTR,RRIB,OOL,
.             CCD,CCH,CCQ,II,JJ,KT,CHP,CQP,INDX,U19,ZU2DUM8(I),T19,
.             T29,ZS19(I),ZS29(I),UUSTR9,1,0)
C
ZZO      = 2.*ALPHA*ZUUSTR9(I+1)*UUSTR/G
IF (ZZ18(I+1) .LE. 1.0E-4) ZZO = 0.
ZZ1      = ZZO
C
IF (ZZ18(I+1) .GE. ZZ28(I+1)) ZZ2 = ZZ2+ZZ1
C
36      CONTINUE
Z1      = ZZ1
Z2      = ZZ2
U2DUM   = U2DUMM
C
END IF
C
CALL TANSFXPAR(U1,U2DUM,T1,T2,Z1,Z2,USTR,TSTR,RIB,OL,
.             CD,CH,CQ,II,JJ,KT,CHP,CQP,INDX,U19,U2DUM9,T19,
.             T29,Z19,Z29,USTR9,0,1)
C
IF(CD99 .GE. CDMAX) CD = 0.
IF(CH99 .LE. CEMAX) CH = 0.
CQ = CH

```

```

C
  U22 = U2DUM
  IF(U2DUM9 .LT. 5.) U22 = 0.
C
  FSX = RHO*CH99*CP*U229*(T29-T19)+RH09*CH*CP*U229*(T29-T19)
      +RH09*CH99*CP*U22*(T29-T19)+RH09*CH99*CP*U229*(T2-T1)
  FLT = RHO*CQ99*U229*GW*(Q29-Q19)+RH09*CQ*U229*GW*(Q29-Q19)
      +RH09*CQ99*U22*GW*(Q29-Q19)+RH09*CQ99*U229*GW*(Q2-Q1)
  FM  = RHO*CD99*U229**2+RH09*CD*U229**2+2.*RH09*CD99*U229*U22
C
  RETURN
  END

```

3. The adjoint codes

```

      SUBROUTINE ADJSFLX(U1,U2,T1,T2,Q1,Q2,Z1,Z2,NTYPES,II,JJ,RIB,
      .
      .
      .
      FSX,FLT,FM,RHO,GW,U19,U29,T19,T29,Q19,Q29,
      .
      .
      Z19,Z29,CD99,CH99,CQ99)
C
C   input: U19,U29,T19,T29,Q19,Q29,Z19,Z29,CD99,CH99,CQ99
C           FSX,FLT,FM,Z1,T1
C   output: U1,U2,T1,T2,Q1,Q2,Z1,Z2,ZV,ZT,RHO
C
C   PARAMETER (ILEVV=12,ILEV1V=ILEVV+1)
C
C   SUBROUTINE RETURNS SURFACE SENSIBLE (SEN) AND LATENT (CON)
C   HEAT FLUXES VIA STABILITY DEPENDENT BULK AERODYNAMIC
C   FORMULATION
C
C   COMMON /RHH/ RH(ILEVV),DQQ(ILEVV)
C   COMMON /EXTRA/ RB,USTR,OL,CD,CH,CQ,X7,X8,SIGZ2,ZV,ZT
C
C   COMMON /EXTRA9/ RB9,USTR9,OL9,CD9,CH9,CQ9,X79,X89,SIGZ29,ZV9,ZT9
C   COMMON /DENSITY9/ RH09
C
C   DIMENSION ZS19(4),ZS29(4),ZUSTR9(4),ZU2DUM8(4)
C   DIMENSION ZZ18(4),ZZ28(4)

```

```

C
DATA G,VKC,ALPHA,CP/9.81,.35,.04,1004.5/
C
INDX = 0
CHP = 0.
CQP = 0.
C
IF (NTYPES .NE. 0) THEN
C
    CEMAX = -5.0E-03
    CDMAX = 5.0E-03
    U2DUM9 = U29*ALOG(Z29/Z19)/ALOG(ZV9/Z19)
C
ELSE
C
    CEMAX = -2.0E-03
    CDMAX = 2.0E-03
C
    ZZ29 = ZT9
    CCD90 = 0.0011
    USTRSQ9 = CCD90*(U29**2)
    ZZ09 = ALPHA*USTRSQ9/G
    IF (ZZ09 .LT. 1.0E-4) ZZ09 = 1.0E-4
    ZZ19 = ZZ09
    ZZ18(1) = ZZ09
    ZZ28(1) = ZZ29
    IF (ZZ19 .GE. ZZ29) ZZ29 = ZZ29+ZZ19
    ZUSTR9(1) = USTRSQ9
    ZS19(1) = ZZ19
    ZS29(1) = ZZ29
C
    DO 35 I=1,3
    U2DUM8 = U29*ALOG(ZZ29/ZZ19)/ALOG(ZV9/ZZ19)
    CALL SFXPAR(U19,U2DUM8,T19,T29,ZZ19,ZZ29,USTR9,TSTR9,RRIB9,
    .           OOL9,CCD9,CCH9,CCQ9,II,JJ,KT,CHP,CQP,INDX)
    ZZ09 = ALPHA*(USTR9**2)/G
    IF (ZZ09 .LT. 1.0E-4) ZZ09 = 1.0E-4
    ZZ19 = ZZ09

```

```

C
    ZZ18(I+1) = ZZ09
    ZZ28(I+1) = ZZ29
    IF (ZZ19 .GE. ZZ29) ZZ29 = ZZ29+ZZ19
C
    ZU2DUM8(I) = U2DUM8
    ZUSTR9(I+1) = USTR9
    ZS19(I+1) = ZZ19
    ZS29(I+1) = ZZ29
C
35    CONTINUE
C
    Z19 = ZZ19
    Z29 = ZZ29
    U2DUM9 = U2DUM8
C
    END IF
C
    U229 = U2DUM9
    U229 = AMAX1(5.0,U229)
C
    RH0 = RH0+FM*CD99*U229**2
    CD = RH09*FM*U229**2
    U22 = 2.*RH09*CD99*U229*FM
    RH0 = RH0+FLT*CQ99*U229*GW*(Q29-Q19)
    CQ = RH09*FLT*U229*GW*(Q29-Q19)
    U22 = U22+RH09*CQ99*FLT*GW*(Q29-Q19)
    Q2 = RH09*CQ99*U229*GW*FLT
    Q1 = -RH09*CQ99*U229*GW*FLT
    RH0 = RH0+FSX*CH99*CP*U229*(T29-T19)
    CH = RH09*FSX*CP*U229*(T29-T19)
    U22 = U22+RH09*CH99*CP*FSX*(T29-T19)
    T2 = RH09*CH99*CP*U229*FSX
    T1 = T1-RH09*CH99*CP*U229*FSX
C
    IF(U2DUM9 .LT. 5.) U22 = 0.
    U2DUM = U22
C

```

```

      CH = CH+CQ
      IF(CD99 .GE. CDMAX) CD = 0.
      IF(CH99 .LE. CHMAX) CH = 0.
C
C      Z2 = 0.
      U1 = 0.
C
      USTR = 0.
C      OL = 0.
      CALL ADJSFXPAR(U1,U2DUM,T1,T2,Z1,Z2,USTR,TSTR,RIB,OL,
.           CD,CH,CQ,II, JJ,KT,CHP,CQP,INDX,U19,U2DUM9,T19,
.           T29,Z19,Z29,USTR9,0,1)
C
      U2 = 0.
C      ZV = 0.
      IF (NTYPES .NE. 0) THEN
C
      U2 = U2+U2DUM*ALOG(Z29/Z19)/ALOG(ZV9/Z19)
      Z2 = Z2+U29*U2DUM/(Z29*ALOG(ZV9/Z19))
      ZV = ZV-U29*ALOG(Z29/Z19)*U2DUM/(ZV9*(ALOG(ZV9/Z19))**2)
C
      ELSE
C
      U2DUMM = U2DUM
      ZZ2 = Z2
      ZZ1 = Z1
C
      ZT = 0.
C
      DO 36 I=3,1,-1
C
      IF (ZZ18(I+1) .GE. ZZ28(I+1)) ZZ1=ZZ1+ZZ2
      ZZO = ZZ1
      IF (ZZ18(I+1) .LE. 1.0E-4) ZZO = 0.
      USTR = 2.*ALPHA*ZUSTR9(I+1)*ZZO/G
      ZZ1 = 0.
      IF(I.NE.3) U2DUMM = 0.

```



```

      CCD = 0.
      CCH = 0.
      OOL = 0.
      CALL ADJSFXPAR(U1,U2DUMM,T1,T2,ZZ1,ZZ2,UOSTR,TSTR,RRIB,OOL,
.          CCD,CCH,CCQ,II,JJ,KT,CHP,CQP,INDX,U19,ZU2DUM8(I),T19,
.          T29,ZS19(I),ZS29(I),UOSTR9,1,0)
      U2 = U2+U2DUMM*ALOG(ZS29(I)/ZS19(I))/ALOG(ZV9/ZS19(I))
      ZZ2 = ZZ2+U29*U2DUMM/ZS29(I)/ALOG(ZV9/ZS19(I))
      ZZ1 = ZZ1-U29*U2DUMM/ZS19(I)/ALOG(ZV9/ZS19(I))
      ZV = ZV-U29*U2DUMM*ALOG(ZS29(I)/ZS19(I))
.          /(ZV9*ALOG(ZV9/ZS19(I))**2)
      ZZ1 = ZZ1+U29*U2DUMM*ALOG(ZS29(I)/ZS19(I))/(ZS19(I)*
.          ALOG(ZV9/ZS19(I))**2)
C
C 36 CONTINUE
C
      IF (ZZ18(1) .GE. ZZ28(1)) ZZ1=ZZ1+ZZ2
      ZT = ZT+ZZ2
C
      ZZO = ZZ1
C
      IF (ZZ18(1) .LE. 1.0E-4) ZZO = 0.
      USTRSQ = ALPHA*ZZO/G
      U2 = U2+2.*CCD90*U29*USTRSQ
      CCD = 0.
      END IF
C
      RETURN
      END

```

REFERENCES

- [1] Asselin, R., 1972: Frequency filter for time integrations. *Mon. Wea. Rev.*, **100**, 487-490.
- [2] Axelsson, O., 1994: *Iterative Solution Methods*. Cambridge University Press, 654 pp.
- [3] Bao J.W. and Warner, T.T., 1993: Treatment of on/off switches in the adjoint method: FDDA experiments with a simple model. *Tellus*, **45A**, 525-538.
- [4] Bao Jian-Wen and Ying-Hwa Kuo, 1995: On-off switches in the adjoint method: step functions. *Mon. Wea. Rev.*, **123**, 1589-1594.
- [5] Businger, J. A., J.C. Wyngaard, Y. Izumi and E.F. Bradley, 1971: Flux-profile relationships in the atmospheric surface layer. *J. Atmos. Sci.*, **28**, 181-189.
- [6] Cacuci, D. G., 1981a: Sensitivity theory for nonlinear systems. I: Nonlinear functional analysis approach. *J. Math. Phys.*, **22**, 2794-2802.
- [7] Cacuci, D. G., 1981b: Sensitivity theory for nonlinear systems. II: Extension to additional classes of responses. *J. Math. Phys.*, **22**, 2803-2812.
- [8] Cacuci, D. G., 1988: The forward and adjoint methods of sensitivity analysis. *Uncertainty Analysis*, Yigal Ronen, Ed., CRC Press, Inc., 71-144.
- [9] Carrera, J., and S.P. Neumann, 1986a: Estimation of aquifer parameters under transient and steady state conditions: 1. Maximum likelihood method incorporating prior information, *Water Resources Research*, **22**, No. 2, 199-210.
- [10] Carrera, J., and S.P. Neumann, 1986b: Estimation of aquifer parameters under transient and steady state conditions: 2. Uniqueness, stability and solution algorithms, *Water Resources Research*, **22**, No. 2, 211-227.
- [11] Carrera, J., and S.P. Neumann, 1986c: Estimation of aquifer parameters under transient and steady state conditions: 3. Application to synthetic and field data, *Water Resources Research*, **22**, No. 2, 228-242.
- [12] Chang C. B., 1980: On the influences of solar radiation and diurnal variation of surface temperatures on African disturbances. *Ph. D. Dissertation*, Dept. of Meteorology, College of Arts and Sciences, Florida State University, p157.

- [13] Chavent, G., 1974: Identification of functional parameters in partial differential equations. In *Identification of parameters in distributed systems, ASME conference on Automatic Control*, Austin, Texas, June 17-21, 1974. Goodson R.E. and Polis M. Eds., 31-48.
- [14] Courtier, P., 1984: Présentation d'une méthode variationnelle d'assimilation dynamique de données meteorologique réparties dans l'espace et le temps. *Note E.E.R.M.*, **101**, 21.
- [15] Courtier, P. and O. Talagrand, 1990: Variational assimilation of meteorological observations with the direct and adjoint shallow-water equations. *Tellus*, **42A**, 531-549.
- [16] Courtier, P., J.-N. Thepaut and A. Hollingsworth, 1994: A strategy operational implementation of 4-D VAR using an incremental approach. *Q. J. R. Meteorol. Soc.*, **120**, 1367-1387.
- [17] Danard, M., 1969: A simple method of including long-wave radiation in a tropospheric numerical prediction model. *Mon. Wea. Rev.*, **97**, 77-85.
- [18] Deardorff, J.W., 1968: Dependence of air-sea transfer coefficients on bulk stability. *J. Geophys. Res.*, **73**, 2549-2557.
- [19] Derber, J.C., 1985: The variational 4-D assimilation of analysis using filtered models as constraints. Ph.D. thesis, University of Wisconsin-Madison, 142pp.
- [20] Dyer, A.J., 1967: The turbulent transport of heat and water vapor in an unstable atmosphere. *Q. J. R. Meteorol. Soc.*, **93**, 501-508.
- [21] Errico, R.M. and T. Vukićević, 1992: A sensitivity analysis using an adjoint of the PSU-NCAR Mesoscale Model. *Mon. Wea. Rev.*, **120**, 1644-1660.
- [22] Errico, R.M., T. Vukićević, and K. Raeder, 1993: Comparison of initial and lateral boundary condition sensitivity for a limited area model. *Tellus*, **45A**, 539-557.
- [23] Ghil, M. and P. Malanotte-Rizzoli, 1991: Data assimilation in meteorology and oceanography. in *Advances in Geophysics*, B. Saltzman editor, Academic Press, **33**, 141-266.
- [24] Giering, Ralf and Thomas Kaminski, Recipes for adjoint code construction. *Max-Planck-Institut fur Meteorologie*.
- [25] Gill P.E., Walter Murray and Margaret H. Wright, 1981: Practical Optimization. *Academic Press*, London, 401pp.

- [26] Gordon, C.T. and Stern, W.F., 1982: A description of the GFDL global spectral model. *Mon. Wea. Rev.*, **110**, 625–644.
- [27] Gustafsson, N. and Lönnberg P., 1995: Data assimilation for high resolution limited area models. *The Geophysical Magazine*, series 2, Special Issue, collection of lecture notes presented at *The WMO 2nd International Symposium on Assimilation of observations in meteorology and oceanography*, 13–17, March 1995, Tokyo, Japan, V-i-1-V-i-20.
- [28] Hall, M. C. G., D. G. Cacuci and M. E. Shlesinger, 1982: Sensitivity analysis of a radiative-convective model by the adjoint method. *J. Atmos. Sci.*, **39**, 2038–2050.
- [29] Haltiner George J. and Roger Terry Williams, 1980: Numerical prediction and dynamic meteorology. *John Wiley & Sons, Inc., Second Edition*, 477pp.
- [30] Hamming, R. W., 1973: Numerical methods for scientists and engineers. 2nd ed., *McGraw-Hill*, New York, 505pp.
- [31] Hoskins, B.J., 1982: The mathematical theory of frontogenesis. *Annual Review of Fluid Mechanics*, **14**, 131–151. Annual Review Inc..
- [32] Kalnay, E and Z. Toth, 1996: Ensemble prediction at NCEP. Preprints of 11th Conference on Numerical Weather Prediction, August 19-23, 1996, Norfolk, VA, ppJ19–J20.
- [33] Kanamitsu M., K. Tada, T. Kudo, N. Sato and S. Isa, 1983: Description of JMA Operational Spectral Model. *J. Meteorol. Sci. of Japan*, **61**, 812-827.
- [34] Kanamitsu Masao, 1989: Description of the NMC Global Data Assimilation and Forecast System. *Weather and Forecasting*, **4**, 335–342.
- [35] Kanamitsu M., J.C. Alpert, K.A. Campana, P.M. Caplan, D.G. Deaven, M.Iredell, B. Katz, H.-L. Pan, J. Sela and G.H. White, 1991: Recent changes implemented into the global forecast system at NMC. *Weather and Forecasting*, **6**, 425-435.
- [36] Krishnamurti, T.N. and Nancy Dignon, 1988: The FSU global spectral model. *Dept. of Meteorology, Florida State University*.
- [37] Krishnamurti, T.N., X Jishan, H.S. Bedi, K. Ingles and D. Osterhof, 1991: Physical initialization for numerical weather prediction over tropics. *Tellus*, **43A**, 53–81.

- [38] Krishnamurti, T.N., H.S. Bedi, K. Ingles, 1993: Physical initialization using SSM/I rainfall rates. *Tellus*, **45A**, 247–269.
- [39] Kuhn, P.M., 1963: Radiometersonde observations of infrared flux emissivity of water vapor. *J. Appl. Meteor.*, **2**, 368–378.
- [40] Le Dimet F. X., 1980: une etude generale d'analyse objective variationnelle des champs meteorologiques. Rapport Scientifique NM-0 28, laboratoire Associe de Meteorologie Physique, Universite Blaise Pascal, 63170 AUBIER, France.
- [41] Le Dimet F. X., 1982: A general formalism of variational analysis. Report CIMMS - 73091 - 22 - 1, University of Oklahoma, Norman, OK.
- [42] Le Dimet F. X., Y. K. Sasaki and L. White, 1983a: Dynamic initialization with filtering of gravity waves. CIMMS report and Contribution NM-04, University of Oklahoma, Norman, OK.
- [43] Le Dimet F. X., 1983b: Slow manifold and initialization. CIMMS report and Contribution NM-09, University of Oklahoma, Norman, OK.
- [44] Le Dimet F. X. and Talagrand, O., 1986: Variational algorithms for analysis and assimilation of meteorological observations: Theoretical aspects. *Tellus*, **38A**, 97–110.
- [45] Le Dimet F. X. and I. M. Navon, 1988: Variational and optimization methods in meteorology: A review. Technical Report - SCRI - 144. Supercomputer Computations Research Institute, Florida State University. Tallahassee, FL 32306, 83pp.
- [46] Leith, C. E., 1965: Numerical simulation of the earth's atmosphere. *Math. in Comp. Physics*, **4**, New York, Academic Press.
- [47] Leith, C. E., 1971: Atmospheric predictability and two-dimensional turbulence. *J. Atmos. Sci.*, **28**, 145-161.
- [48] Lewis, J.M. and J.C. Derber, 1985: The use of adjoint equations to solve a variational adjustment problem with advective constraints. *Tellus*, **37A**, 309–322.
- [49] Lilly, D. K., 1965: On the computational stability of numerical solutions of time dependent non-linear geostrophical fluid dynamics problem. *Mon. Wea. Rev.*, **93**, 11-26.
- [50] Li, Y. and K. K. Droegemeier, 1993: The influence of diffusion error on variational data retrieval using adjoint technique. *Tellus*, **45A**, 435-448.

- [51] Liou Kuo-Nan, 1980: An introduction to atmospheric radiation. *Academic Press, Inc.*, p392.
- [52] Liu, D.C. and J. Nocedal, 1989: On the limited memory BFGS method for large scale optimization. *Math. Prog.*, **45**, 503–528.
- [53] Lorenc A.C., 1986: Analysis methods for numerical weather prediction. *Quart. J. R. Met. Soc.*, **112**, 1177–1194.
- [54] Louis, J.F., 1979: A parametric model of vertical eddy fluxes in the atmosphere. *Bound. Layer Meteor.*, **17**, 187–202.
- [55] Lorenz, E. N. and K. A. Emanuel, 1997: Optimal sites for supplementary weather observations: simulations with a small model. *J. Atmos. Sci.*, (under review).
- [56] MacVEAN, M.K., 1983: The effects of horizontal diffusion on baroclinic development in a spectral model. *Q. J. R. Meteorol. Soc.*, **109**, 771–783.
- [57] Morss R. E., K. A. Emanuel and C. Snyder, 1998: Adaptive observations in a quasi-geostrophic model. *12th Conference on Numerical Weather Prediction*, 11-16 January 1998, Phoenix, Arizona, 10–11.
- [58] Nash, S. G. and A. Sofer, 1996: Linear and nonlinear programming. *McGraw Hill Series on Industrial and Management Science*, 692pp.
- [59] Navon, I. M., 1969: Inclusion of lateral viscosity and the application of a Matsuno scheme in a two level model of the general circulation of the atmosphere. *M.Sc. Thesis*, Dept. of Meteorology, Hebrew University, Jerusalem, 77pp plus 40 figures.
- [60] Navon, I.M. and D.M. Legler, 1987: Conjugate-Gradient methods for large-scale minimization in meteorology. *Mon. Wea. Rev.*, **115**, 1479–1502.
- [61] Navon, I.M., X. Zou, M. Berger, P.K.H. Phua, T. Schlick and F.X. Le Dimet, 1992a: Numerical experience with Limited Memory Quasi-Newton and truncated Newton Methods. *Optimization Techniques and Applications*. Vol 1, Edited by K.H. Phua et al., World Scientific Publishing Co., 33–48.
- [62] Navon, I.M., X. Zou, M. Berger, P.K.H. Phua, T. Schlick and F.X. Le Dimet, 1992b: Testing for Reliability and Robustness of Optimization Codes for Large Scale Optimization Problems. *Optimization Techniques and Applications*. Vol 1, Edited by K.H. Phua et al., World Scientific Publishing Co., 445–480.

- [63] Navon, I.M., X. Zou, J. Derber, and J. Sela, 1992c: Variational data assimilation with an adiabatic version of the NMC spectral model. *Mon. Wea. Rev.*, **120**, 1433–1446.
- [64] Navon, I.M., 1996: Large-scale unconstrained and constrained optimization methods and their applications. *Tech. Report*, FSU-SCRI.
- [65] Navon, I.M., 1997: Practical and theoretical aspects of adjoint parameter estimation and identifiability in meteorology and oceanography. In *Special Issue of Dynamics of Atmosphere and Ocean in honor of Prof. Richard Pfeffer*. 747pp.
- [66] Nickerson, E.C. and V.E. Smiley, 1975: Surface layer and energy budget parameterizations for mesoscale models. *J. Appl. Meteor.*, **14**, 297–300.
- [67] Panchang, V. G. and J. J. O'Brien, 1989: On the determination of hydraulic model parameters using the strong constraint formulation. *Modeling Marine Systems, I*, Editor: A. M. Davies, CRC Press, Inc., 5-18.
- [68] Parrish David F. and John C. Derber, 1992: The national meteorological Center's spectral statistical-interpolation analysis system. *Mon. Wea. Rev.*, **120**, 1747–1764.
- [69] Phillips, N.A., 1956: The general circulation of the atmosphere: a numerical experiment. *Q. J. R. Meteorol. Soc.*, **82**, 123-164.
- [70] Phillips, N.A., 1959: An example of non-linear computational instability. *The atmosphere and the sea in motion*. Ed. Bert Bolin, The Rockefeller Institute Press, New York, 501–504.
- [71] Pu Z. X., Eugenia Kalnay, John C. Derber and Joseph G. Sela, 1997: Using forecast sensitivity patterns to improve future forecast skill. *Q. J. R. Meteorol. Soc.*, **123**, 1035–1053.
- [72] Pu Z. X., Eugenia Kalnay and Zoltan Toth, 1998: Application of the quasi-inverse linear and adjoint NCEP global models to targeted observations during FASTEX. *12th Conference on Numerical Weather Prediction*, 11-16 January 1998, Phoenix, Arizona, 8–9.
- [73] Rabier, F. and P. Courtier, 1992: Four-dimensional assimilation in the presence of baroclinic instability. *Q. J. R. Meteorol. Soc.*, **118**, 649–672.
- [74] Rabier, F., P. Courtier and O. Talagrand, 1992: An application of adjoint models to sensitivity analysis. *Beitr. Phys. Atmosph.*, **65**, 177–192.

- [75] Restrepo, J.M., Gary K. Leaf and Andreas Griewank, 1998: Circumventing storage limitations in variational data assimilation studies. *to be accepted by SIAM J. Sci. Comput.*
- [76] Richard, J. R. and K.E. German, 1965: A contribution to the problem of stratospheric diffusion by large-scale mixing. *Mon. Wea. Rev.*, **93**, 313–321.
- [77] Robert, A.J., 1966: The integration of a low order spectral form of the primitive meteorological equations. *J. Meteor. Sci. of Japan*, **44**, 237–245.
- [78] Sela, J.G., 1980: Spectral modeling at the National Meteorological Center. *Mon. Wea. Rev.*, **108**, 1279–1292.
- [79] Smagorinsky, J., S. Manabe, and J. L. Holloway, 1965: Numerical results from a nine-level general circulation model of the atmosphere. *Mon. Wea. Rev.*, **93**, 727–768.
- [80] Smagorinsky, J., 1971: Large-scale atmospheric circulation. In *Man's Impact on the Climate*, Cambridge, MA: The MIT Press, 200–204.
- [81] Smestad, O.M. and O'Brien, J.J., 1991: Variational data assimilation parameter estimation in an equatorial Pacific Ocean model. *Prog. Oceanog.*, **26**, 179–241.
- [82] Shannon, D.F. and K.H. Phua, 1980: Remark on algorithm 500 - A variable method subroutine for unconstrained nonlinear minimization. *ACM Trans. Math. Software*, **6**, 618–622.
- [83] Stephens, J.J., 1996: Objective Analysis. *Dept. of Meteorology, Florida State University*.
- [84] Talagrand, O. and P. Courtier, 1987: Variational assimilation of meteorological observations with the adjoint vorticity equation - Part I: Theory. *Q. J. R. Meteorol. Soc.*, **113**, 1311–1328.
- [85] Thépaut Jean-Noël and Philippe Courtier, 1991: Four-dimensional variational data assimilation using the adjoint of a multilevel primitive-equation model. *Q. J. R. Meteorol. Soc.*, **117**, 1225–1254.
- [86] Thépaut Jean-Noël, Philippe Courtier, Gilles Belaud and Gwendal Lemaitre, 1996: Dynamical structure functions in a four-dimensional variational assimilation: a case study. *Q. J. R. Meteorol. Soc.*, **122**, 535–561.
- [87] Tichonov, A.N. and V. Y. Arsenin, 1977: Solutions of ill-posed problems. Halsted Press, New York, 258pp.

- [88] Tsuyuki Tadashi, 1996a: Variational data assimilation in the tropics using precipitation data. Part I: Column model. *Meteor. Atmos. Phys.*, **60**, 87–104.
- [89] Tsuyuki Tadashi, 1996b: Variational data assimilation in the tropics using precipitation data. Part II: 3-D model. *Mon. Wea. Rev.*, **124**, 2545–2561.
- [90] Tsuyuki Tadashi, 1997: Variational data assimilation in the tropics using precipitation data. Part III: Assimilation of SSM/I precipitation rates. *Mon. Wea. Rev.*, **125**, 1447–1464.
- [91] Vukićević, T. and R.M. Errico, 1993: Linearization and adjoint of parameterized moist diabatic processes. *Tellus*, **45A**, 493–510.
- [92] Wergen, W., 1992: The effect of model errors in variational assimilation. *Tellus*, **44A**, 297–313.
- [93] Wang, Zhi, 1993: Variational Data Assimilation with 2-D Shallow Water Equations and 3-D FSU Global Spectral Models, *Ph. D. Dissertation*, Department of Mathematics, College of Arts and Sciences, The Florida State University, 235 pp.
- [94] Wang, Zhi, I.M.Navon ,X. Zou and F.X. Le Dimet, 1995: A truncated-Newton optimization algorithm in meteorology applications with analytic Hessian/vector products. *Computational Optimization and Applications*, **4**, 241–262.
- [95] Wang, Zhi, Kelvin K. Droegemeier, L. White and I.M.Navon, 1997: Application of a New Adjoint Newton Algorithm to the 3-D ARPS Storm Scale Model Using Simulated Data. *Mon. Wea. Rev.*, **125**, 2460–2478.
- [96] Yang, Weiyu, I.M. Navon and P. Courtier, 1996: A New Hessian Preconditioning Method Applied to Variational Data Assimilation Experiments Using NASA General Circulation Models. *Mon. Wea. Rev.*, **124**, 1000–1017.
- [97] Yu, L. and J. J. O'Brien, 1991: Variational estimation of the wind stress drag coefficient and the oceanic eddy viscosity profile. *J. Phys. Oceanogr.*, **21**, 709–719.
- [98] Zhu, Yanqiu and I. Michael Navon, 1997: Documentation of the Tangent-Linear and Adjoint Models of the radiation and boundary layer parameterization packages of the FSU Global Spectral Model T42L12. *Tech. Report*, FSU-SCRI-97-98.
- [99] Zou, X., Navon, I.M. and Le Dimet, F.X., 1992: An optimal nudging data assimilation scheme using parameter estimation. *Q. J. of Roy. Met. Soc.*, **118**, 1163–1186.

- [100] Zou, X., I.M. Navon, M. Berger, M.K. Phua, T. Schlick, and F. X. LeDimet, 1993a: Numerical Experience with Limited-Memory, Quasi-Newton Methods for Large-Scale Unconstrained Nonlinear Minimization, *SIAM Journal on Optimization*, **3**, No 3, 582–608.
- [101] Zou, X., Navon, I.M. and Sela, J.G., 1993b: Variational data assimilation with moist threshold processes using the NMC spectral model. *Tellus*, **45A**, 370–387.
- [102] Zou, X., A Barcion, I. M. Navon, J. Whitaker and D. G. Cacuci, 1993c: An adjoint sensitivity study of blocking in a two-layer isentropic model. *Mon. Wea. Rev.*, **121**, 2833–2857.
- [103] Zou X., 1996: Tangent linear and adjoint of 'on-off' processes and their feasibility for use in four-dimensional variational data assimilation. *Tellus*, **49**, 3–31.
- [104] Zupanski, M., 1993a: A preconditioning algorithm for large scale minimization problems, *Tellus*, **45A**, 478–492.
- [105] Zupanski, M., 1993b: Regional four-dimensional variational data assimilation in a quasi-operational forecasting environment. *Mon. Wea. Rev.*, **121**, 2396–2408.
- [106] Zupanski, Dusanka, 1993c: The Effects of Discontinuities in the Betts-Miller Cumulus Convection Scheme on Four-Dimensional Variational Data Assimilation. *Tellus*, **45A**, 511–524
- [107] Zupanski, M., 1996: A Preconditioning Algorithm for Four-Dimensional Variational Data Assimilation. *Mon. Wea. Rev.*, **124**, 2562–2573.
- [108] Zupanski, Dusanka, 1997: A general weak constraint applicable to operational 4DVAR data assimilation systems. *Mon. Wea. Rev.*, **125**, 2274–2292.

BIOGRAPHICAL SKETCH

Yanqiu Zhu

Education

- **Florida State University** - Ph.D. graduate student in Geophysical Fluid Dynamics (May 1994 - April 1998)
Ph.D. expected: April, 1998
- **Chinese Academy of Meteorological Sciences** - M.S. in Numerical Weather Prediction (September, 1987 - July, 1990)
- **Peking University** - B.S. in Meteorology (September, 1983 - July, 1987)

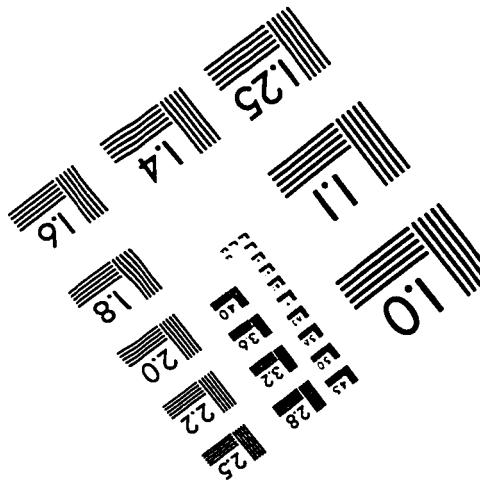
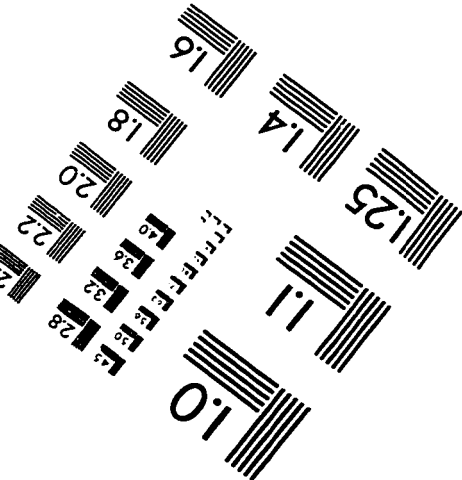
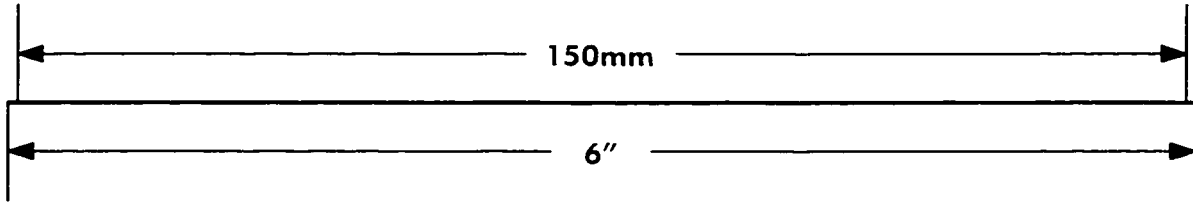
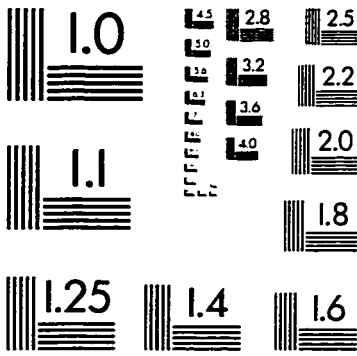
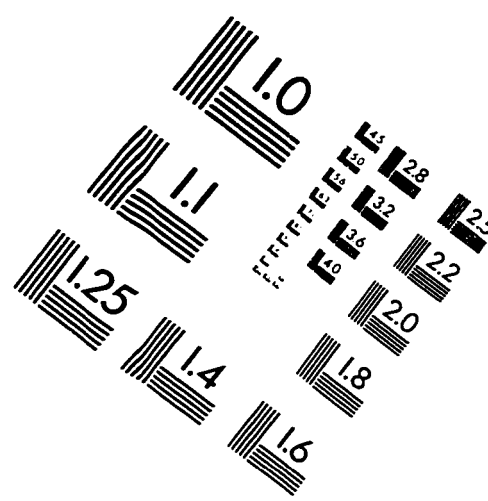
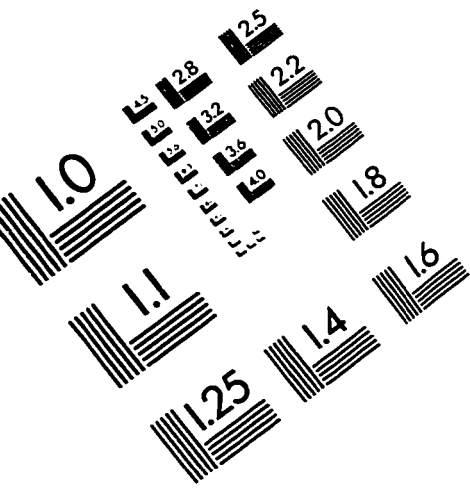
Research Experience

- **Ph.D. Graduate Research Assistant**
Geophysical Fluid Dynamics Institute, Florida State University (May, 1994 -).
- **Research Engineer**
Numerical Weather Prediction Division, National Meteorological Center, Beijing, China (July, 1990 - April, 1994).
- **Graduate Research Assistant**
Chinese Academy of Meteorological Sciences (September, 1988 - July, 1990).

- **Undergraduate Research Assistant**

Peking University (September, 1982 - July, 1983).

IMAGE EVALUATION TEST TARGET (QA-3)



APPLIED IMAGE, Inc
1653 East Main Street
Rochester, NY 14609 USA
Phone: 716/482-0300
Fax: 716/288-5989

© 1993, Applied Image, Inc.. All Rights Reserved